Modeling, Machine Vision Sensing and Material Flow System Definition of Braiding Point Motion

by

Guangli Ma

A dissertation submitted to the Graduate Faculty of
Auburn University
in partial fulfillment of the
requirements for the Degree of
Doctor of Philosophy

Auburn, Alabama
May 09, 2010

Keywords: braiding, material flow system,
machine vision sensing, PI controller

Approved by

David G. Beale, Chair, Professor of Mechanical Engineering
David Bevly, Philpot-WestPoint Stevens Associate Professor of Mechanical Engineering
George Flowers, Professor of Mechanical Engineering and Dean of Graduate School
Roy Broughton Jr., Professor Emeritus of Polymer and Fiber Engineering

Abstract

This dissertation is focused on the modeling of one kind of braiding machine and its key part, the carrier. The carrier is a small mass-spring-damping tensioning system, which defines the characteristics and response of the braiding point on an operating braiding machine. The yarn tension from a carrier versus displacement characteristic is first derived, and experimentally verified. Based on this result, the braiding point motion envelop is investigated in order to determine and explain the expected range of small braid point motion and oscillation that occur about the steady state. A material flow system model is derived for the braiding process at the braiding point. Three mathematical models are created and combined to form an integrated model of the entire braiding process. Using machine vision routines developed in this dissertation, a control program was used to monitor and record the braiding point motion and compare it with analytical results. A new noninvasive machine vision sensor was developed, for use with a piecewise PI controller on a separate take up motor using the position data acquired from a machine vision sensing loop. Correlated experiment and simulation response validate the mathematical model, which is similar to a first order liquid level system.

Braiding is a manufacturing process for making tubular products. A yarn or tow tensioning system, a carrier, is required that consists of two small pulleys, two springs and a ratchet with the ratchet gear on the spool with wound yarn. The tension coming from a single carrier is nearly constant, varying within an acceptable range during braided

product formation and releasing a discrete amount of material from a spool when an upper limit on the tension is reached. The releasing frequency depends on the towed speed of the yarn. A mathematical model of tension versus yarn displacement of a standard package tensioning system is presented. The response before ratchet release is a series of piecewise linear kinematic regions that include two separate spring preload regions, a single spring tensioning region, and a two spring tensioning regions. During the ratchet releasing, the system is modeled as two regions of a single degree-of-freedom dynamic model, releasing region and impact region. Ratchet reengagement that incorporated impact with an elastic yarn was required to improve model accuracy of response.

The 32-carrier braiding machine used in this dissertation included a braiding motor, a take up motor and 32 carriers with corresponding yarns. The tension coming from single yarn is nearly constant, especially, when compared with the tension of the rope towed by the take up motor during the braiding process. The length of material releasing from the carriers affects the motion of braiding point. The tension of a single yarn changes because of yarn releasing. The releasing materials and releasing tension of the yarn cause the oscillation of the braiding point. A mathematical model of the braiding process close to the braiding point region is presented as a quasistatic process. The response after ratchet release is shown to be the reason for oscillation of the braiding point in the steady state. The amount released determines the maximum range of the locus of the braiding point. And the releasing frequency determines the frequency of oscillation. The locus of the braiding point moves on an “ellipsoidal cap”. Since the

releasing of yarn is almost instantaneous, the motion of braiding point rapidly jumps from one point to another.

Controlling braiding angle is important for controlling the quality of braiding products. Controlling the position of the braiding point also controls the braiding angle. In practice, it takes a long time for a braiding point to find its steady state position after startup (if the two motor keep a constant speed). This can lead to a large amount of wasted material and lost production. The braiding point pattern includes 32 yarns, rope and the convergent zone. This machine vision pattern, viewed with a USB camera, changes from moment to moment during braiding process. Setting up the corresponding threshold for pattern change is important, and is based on the color of yarn and lighting condition (illumination) of the background. The machine vision algorithm senses the braiding point using the geometric pattern matching method in Labview. The PI controller is designed to drive the take up motor in order to reduce the settling time of the braiding point, using a feedback position signal from the machine vision system. Experimental results confirms this technique to substantially reduce the amount of material waste.

Acknowledgements

The author would like to express his special gratitude to his major professor Dr. David G. Beale most deeply for his guidance during the whole period of this study. Also, special appreciation is expressed to Drs. David M. Bevly, George. T. Flowers, and Roy M. Broughton Jr. for their service on his advisory committee. I would like to specially thank Dr. Broughton and Polymer and Fiber department for all his help insight and use of equipment for tensile testing and braiding. Special appreciation is expressed to David J. Branscomb for his introduction of braiding machine operation. Special thanks to outsider reader Dr. Peter Schwartz for his review of this study. Also thanks to Jeff Thompson for his providing tools and guidance for operating braiding machine. Thanks to Dr. John Hung for his guidance on controlling principle. Thanks to Dr. Wenhua Zhu in Chemical Department for him lending me measuring tools.

Jiping Ma and Fengrong Zhu, my wonderful parents, have been always a constant source of encouragement and support even though my father passed away at the beginning of this study. My wonderful wife, Dr. Chunying Yang, always believes in me and supports me in every time of struggle. Special appreciation for her love, encourage and sacrifice. She also help me to take care of our two year old son, Henry Yuhang Ma, who is so handsome, smart and make me happy every day during this study. Also thanks my sisters, Guangxia, Hongxia, and Xiuqing, for their supports.

Table of Contents

List of Tables

List of Figures

List of Abbreviations

θ_{spool}	Rotation angle of spool
θ_{pawl}	Rotation angle of pawl
k_1	Spring1 spring constant
k_2	Spring2 spring constant
δ, δ_1,δ_2, δ_3	Pulley2/plate displacements
h	The height for tooth of ratchet
B	Spool diameter
c	Takeup speed of yarn
E	Young's modulus of yarn
f	Friction force of pulley2/plate on shaft
F_{s1}	Spring1 force
F_{s2}	Spring2 force
g	Acceleration of gravity
I_{pawl}	Pawl moment of inertia
$I_{pulley1}$	Pulley1 moment of inertia
$I_{pulley2}$	Pulley2 moment of inertia
k_{1y}	Axial stiffness of left side yarn in Figure 9,
k_{2y}	Axial stiffness of right side yarn in Figure 9,
k_y	Equivalent yarn stiffness

d	The diameter of spool on carrier
l_1, l_2	Length of left arm and right arm of pawl, respectively
L_1,L_2	Length of yarn on left side and right side in Figure 2.8, respectively
m_{pawl}	Mass of pawl
$m_{pawllift}$	Mass of pawl lift
$m_{pulley1}$	Mass of pulley1 (=m_{pulley})
$m_{pulley2}$	Mass of pulley2 (=m_{pulley})
m_{plate}	Mass of plate
$m_{spring1}$	Mass of spring1
$m_{spring2}$	Mass of spring2
P	Spring preload of spring
P1	Preload of spring1
P2	Preload of spring2
r	Radius of pulley1 or pulley2
s_1	Axial stretch of left side yarn in Figure 9
s_2	Axial stretch of right side yarn in Figure 9
t	Time
T, T_1, T_2, T_3, T_4, T_5, T_{d1}, T_{d2}	Tension forces of single yarn
x	Length of material removed from tensioning system
θ	Braiding angle(˚)
r_{rope}	The radius of rope (m)
ω	Braiding machine angular velocity(rpm)
ω_{lc}	Angular velocity of load shaft of take up motor (rpm)

r_{lc}	The radius of load shaft of Servo Motor
V	Take up speed, constant (m/s)
Kt	Torque constant of motor(N-m/A)
J_m	Moment of inertia of motor(kg-m^2)
K_b	Motor voltage constant(V-rad/s)
J_l	Moment of inertia of load shaft(kg-m^2)
b_m	Damping of motor(N-m/rad/s)
R_m	Motor terminal resistance(ohm)
n	The ration of gearhead
b_{lc}	Damping of load shaft(N-m/rad/s)
K	The spring constant (N/m)
m_e	The equivalent mass of moving of entire spool
θ_l	Angular displacement of load capstan of actuator load (radian)
T_{rope}	Tension of rope (N)
H (H_0)	The distance between braiding point and braiding plane(in steady state), (m)
L_{yarn}	The length of single yarn from braiding point to braiding plane (m)
L	The length of rope from braiding point to tangent point of capstan (m)
r_{sc}	Base radius of spherical cap(m)
h_{sc}	Height of the spherical cap(m)
$\alpha_{OO'}, \alpha_{O'O'_1}$	Angular acceleration of braiding point at oo_1 and $o'o'_1$ location (rad/s^2)
α	Rotating angle of rope(radian)
l	Length of single yarn between braiding plane and braiding point(m)

R_c	Radius for the base circle of pathtrack of carriers (m)
A_p	Amplitude of path track of carrier.
w_i	The bias of tension in single yarn relative to T_0
R	The resistance of material flow system, m^3/s
Q	Steady state material flow rate
C	Capacitance of MFS, m^2
A	Cross section area of material Flow, m^2
q_i	Small displacement of inflow rate from its steady state in x direction, m^3/s
q_o	Small displacement of outflow rate from its steady state in x direction, m^3/s
A_{yarn}	Cross section area of single yarn, m^2
A_{rope}	Cross section area of rope
Q_{in}	Inflow rate
K_I	Integration gain
K_p	Proportional gain
T_{time}	The period time of tension between releasing region and rebuilding region
L_{rl}	The length of release material
V_{sytk}	The take up speed of single yarn

1 Introduction and Literature Review

Braiding is a textile-manufacturing process, which is most commonly used to manufacture textile, fabric, wire or composite preform tubes [1]. With the invention of new material and the increasing performance requirement of engineered materials technology, braiding technology is now an interest in modern manufacturing. Advanced automated technology is now being used in braiding manufacture. Motion control and machine vision sensing are some of the new advanced technologies, which could eventually be used in braiding field. Other software and hardware based on the personal computer could also be useful in the braiding field.

1.1 Basic Concept of Braiding

Braiding is a long-established textile manufacturing process. Braiding was originally a manual process. A plait of human hair is a very good example, which has uniform shape for personal adornment [2]. This originally hand braiding process has evolved into an industry machine with the development of modern braiding machines. Even if the fundamental operation is mostly unchanged, the advanced braiding machines of today improve on the efficiency and precision. They are the important industrial machines with a long and interesting history. In 1748, Thomas Walford applied for the first patent for a braiding machine in the world. In 1767, the first working braiding machine was built by Mr. Bockmühl in German [3]. Even though it was created more than two hundred years ago, the most common braiding machine is still the maypole

braider (Figure 1.1). The maypole path track has remained since it was first invented. The carriers' support system has been improved significantly to decrease wear and increase machine speed. There may be many horn gears assembled in the braiding machine. Two sets of carriers move on a circular track with a nearly sinusoidal oscillation, one set moving clockwise and the other rotating counterclockwise, and driven by the circular horn gear train. The yarns are deflected and interlaced to form tubular products. The formed tubular products are pulled and rolled onto a motor driven reel rotating and pulling the rope off at the "take up speed".

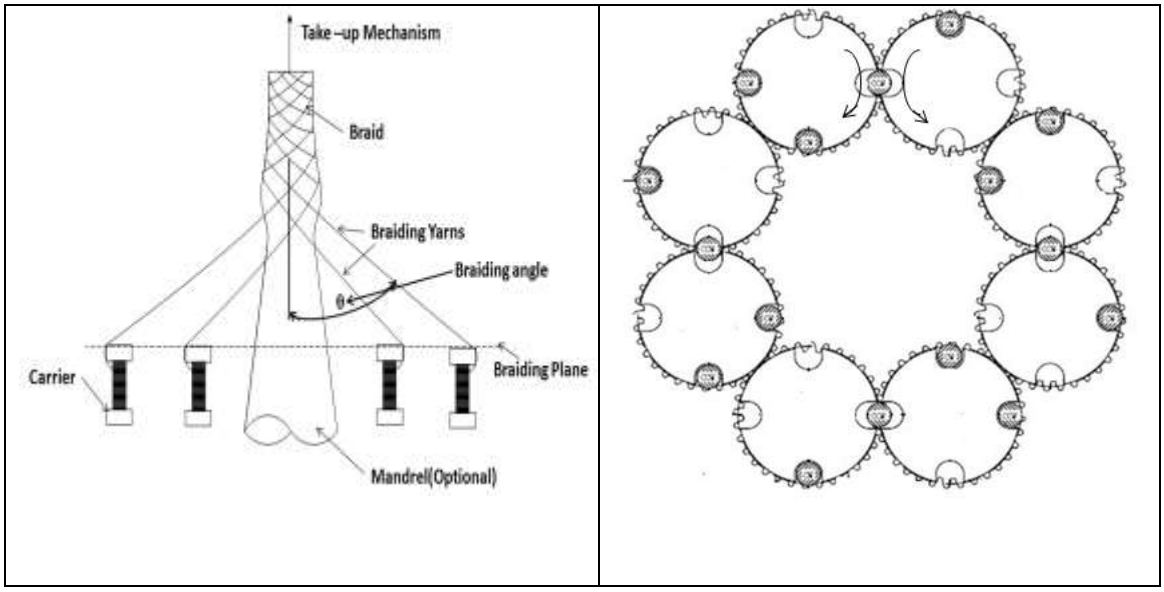

Figure 1.1 Left: Braiding machine showing spools and yarns that are transported on carriers on a horizontal track surface (not shown) to form a yarn. Right: Circular spur gear train. Each spur gear has a slotted horn gear plate rigidly attached. The figure shows how carriers with end stubs (represented a dark circles in the slots) are passed from one gear to the next via attached and slotted horn gears.

Braiding machines have been created with as few as three carriers and over a thousand carriers. Although the basic technology is ancient, it is still commonly in use, and new products and new materials continue to be developed. These create new and

challenging requirements that sometimes stimulate braiding machine innovations and design improvements. The scope of materials is enlarged by the use of polymers, metals and even ceramics. Many braided products exist, including reinforcement for hydraulic hoses, electromagnetic shielding, tether, cord, laces, whips, shoelaces, sutures, fish net, mountain climbing ropes, yarns of resorbable materials for medical applications, tethers for offshore oil platforms, airbeams for tents and composite performs for bicycle frames, skis, skateboards and hockey sticks. New braided products from high strength synthetic fibers including Vectran™, Zylon™, Carbon, Spectra™, and Kevlar™ have led to greater demands on braiding equipment in order to meet product quality requirements. With the development of more and more new materials, braiding will have larger application in the future. Variations on the classic maypole braiding machine that can create nontubular forms include the flat braider, the solid braider, soutache braider, 3-D braider, and the lace braider.

Many intricate fabric forming machines can be modified and hence become applicable for composite forming processes [4]. There are several classifications of braiding, including two dimensional braiding and three dimensional [5]. Circular (tubular) type is two dimensional braiding. Circular braids typically include three structures: Diamond, Regular and Hercules [6]. These structures improve the tension stability and damage resistance [5].

1.2 Overview of Braiding Machinery

Since the maypole braider was invented, many improvements have been made to increase the speed and efficiency of braiding machines. There have been many patents for

the designs of braiding machines or braiding mechanisms. J. Lundgren patented a braiding machine design with two additional sets of thread supplying devices in 1903[7]. Since the two sets of devices are stationary, the braiding products have additional straight longitudinal threads interwoven with the braided threads. In 1912, S. W. Wardwell invented his famous braiding machine, which was later called the Wardwell braider [8]. The machine drives one set of carriers in one direction by a rotating plate and the other package of carriers in the opposite direction by a two driving bars for each carrier. The driving bars were set in a cam profile. This improvement simplified the old high speed braiders by replacing the plurality of gears with the same cam mechanism. The machine speed and efficiency was increased. Some later patents were based on the similar braiding machine design [9] [10]. Fisher invented an apparatus and method to control speed, especially, operating speed, which improve the efficiency of the braiding machine [11].

1.3 Literature Review

1.3.1 Yarn Wind and Unwind on Spool

Numerous studies have been published in the literature on the dynamics of yarns, and other applications in the broad class of axially moving materials. Padfield [12] studied tensions and shape in a flexible string that is unwound longitudinally from a stationary package, forming a balloon shape, while including the effect of air resistance. Recently, Ghosh, Batra and Murthy [13] performed parametric studies and calculated balloon shape and unwinding tension as functions of unwinding direction, wind angle, residual tension, and a yarn-package drag coefficient. Review articles [14~15] focused on the vibration and resonance in band saws, cable driven and other axially moving material

systems. Predoi, Motomancea and Bugaru [16] developed expressions and computed the axial stretch for dynamic cable and pulley lifting mechanisms like elevators. Murakami et al [17] found that the calculated dynamic tension fluctuations in the yarn with different transporting speed adversely affected yarns as they were unwound from a roller; it was suggested that the braking system operation is critical to limiting yarn damage.

The weight-and-lever method of applying tension that changes between full and empty diameters of a beam [18], electromagnetic tensioners [19], commercially-available magnetic brake and clutches [20], and dancer rolls which can be actively or passively controlled. For example, Ludwicki and Unnikrishnan [21] investigated a dancer roll with an actively controlled unwind roll for unwind tension in a film finishing application. They used two motors and focused on design of a control system. Song and Sul [22] have demonstrated inertia-induced tension increase from unwind roll startup, and developed a control law to depress the tension increase. Lin *et al.* [23] proposed a tension observer able to estimate the tension increase evolving from accelerations.

1.3.2 Modeling of the Braiding Process

Compared with the research for tension control and process analysis of filament, circular braiding technology has little attention in the literature for the past several decades. Few publications can be found regarding braiding process analysis and braiding process control. The braiding process is the process of yarns interlaced by the machine operation, with material flow. The modeling of the braiding process is rather difficult and complicated since the process involves highly flexible material and yarns interlacing. In order to achieve high production rates and high quality products, some improvements and

new developments were needed. G. W. Du and P. Popper mathematically modeled the circular braiding process by a kinematic analysis [24]. They consider the braiding point as a convergent zone. The mathematical model was derived to describe this process and an experiment was also built to measure responding parameters to confirm the mathematical model. They developed models to predict braiding angle changes in convergent zone. They did not discuss variable mandrel linear speed, different carrier rotational speeds and so forth. Pastore and Ko used the similar equations as Du and Popper to develop a computer integrated manufacturing (CIM) system to design, analyze, and manufacture braided preforms for advanced composites [25]. They integrated the manufacturing system in a CAM environment to bridge the communication gap between composite structural design and composite preform manufacturing. These two papers neglect the tension interactions in the braiding point area.

1.3.3 Tension Control Application on Yarn/Web Rolling

Tension control is concerned with axial moving materials such as the filament, web and tape. One key research issue is how to use a dancer roll or arm to measure tension. Ebler, N. A., Arnason, R., and Michaelis, G [26] studied the use of load cells with a dancer roller inside the control loop. McDow, B., and Rahn, C. [27] proposes an adaptive web-tension controller that uses dancer arm position, take-up roller velocity sensors and a supply-roller torque actuator. The controller learns and cancels the effects of dancer arm weight, supply-roller friction, upstream tension, and dancer-arm and supply-roller inertia. Nagarkatti and Zhang [28] designed a full order controller to regulate speed and tension of a web using tension sensors and speed sensors. Tension

sensors were used in a dancer arm mechanism. Accurate speed and tension control are essential during continuous manufacture of axially moving materials such as fiber, paper, foil, and film. These mechanisms are all combined inside the system. In order to control the system, all yarns must have sufficient tension in order that the control architecture works well [29]. These tensions and speeds are directly dependent on the motors. In [29], the displacement of the braiding point is independent of the tension control loop, and does not follow or respond to the motion of the motors.

The structure of the braided product is important because of the challenges of near-net shape manufacturing of high damage tolerant structural composites [3]. Tension control is important since it can help to form a high quality structure. Controlling braiding angle is a direct method to control the braided structure and its quality.

1.3.4 Position Control and Machine Vision Sensing

If the position of the braiding point can be controlled, the braiding angle can be controlled. In the braiding field, there are a few publications concerning the control of the braiding process. David Branscomb [30] implemented a constant velocity using a separate, machine-independent take up motor. P. Potluri discussed how to move a mandrel to get the different layers and structures by changing take-up speed [31]. These researches were not focus on the braiding process, nor did they present mathematic models for braiding process except that they were focused on the operation of a braiding machine. Also they were unable to automatically control the take up motor or mandrel in real time, with the moving of braiding point.

Since braiding process depends on motion parameters (carrier rotating speed and take up speed) and braiding geometry parameters (the radii of braiding machine and tubular products), it would be excellent if a method was available for tracking the braiding point that is independent of the braiding process. In this case, not only the position of braiding point can be tracked directly, but also the error or noise caused by the motion loop could be prevented. A machine vision measuring algorithm is a noncontact measurement principle, which is important in cases where it is difficult to perform contact measurements. Vision measuring and tracking systems are a good option since braiding point is a structural pattern which can be discerned by machine vision technology. And machine vision has been successful in many other fields. The detecting, locating, and tracking of people in a dynamic environment are important aspects in the video analysis and a popular topic in machine vision as well. Honglian Ma studied an effective people detection algorithm based on the bi-directional projection histogram of grayscale two-frame differencing images [32]. Andriluka used a simple method to track people using an articulation and limb-based detection approach [33]. The extracting structure of the object is very useful in vision system. Andrew I. Comport [34] try to use a joint configuration modeled by Pfaffian velocity constraints to track of articulated non-rigid objects in 3D. The configuration and location of general mechanical joints was then used to build a general Jacobian Matrix which relates individual rigid body velocities (twists) to an underlying minimal subspace. The background subtraction is used to extract the object from the images. First, a present image is pulled from the background image and the object is extracted. The image that extracted the object is binarized. The centroid of the object is detected by using histogram matching method [35]. Some optical sensors

were assembled with the object; some are not [36]. These are considered as human eyes, which were used as a gaze control mechanism. The gaze control mechanism is absolutely indispensable for some vision systems, although visual information, in particular, plays an important role in order to realize "admirable intelligence". In fact, there are many difficulties of both aspects of restrictive hardware resources for a machine vision and real-time image processing for motor control.

1.4 Objective and Organization

The braiding process based on a maypole braiding machine without mandrels. It focuses on studying and modeling a carrier of a braiding machine, studying and modeling the braiding process based on braiding point motion and design of controllers to control take up motor using feedback position signal coming from a machine vision sensing loop.

1.4.1 Modeling of the Tensioning System on a Braiding Machine Carrier

The tensioning system, the carrier, is the key part in braiding process. Its properties mostly affect the performance of the braiding process. It must also allow a sufficient buildup of tension in order that yarns are able to slide and interlace to form the braid, and release a limited amount of yarn as needed. An ideal tensioning system would release material yet keep the tension within a small range about the desired tension level. There is an optimum tension level for a specific product. In order to check and improve the performance of current carriers, the static, kinetic and dynamic models are investigated in this dissertation.

1.4.2 Modeling of Braiding Process based on Braiding Point

The braiding process is a force interaction process. This dissertation concentrates on the braiding point pattern, which include 32 yarns, and the convergent zone and rope.

The tension coming from yarns is a piecewise releasing tension, which will affect the performance of the braiding point. How the tension coming from carriers affects motion of braiding point will be studied here using a mathematical model of the braiding point based on braiding machine motion and parameters.

1.4.3 Material Flow System Definition and Position Control of the Braiding Point Motion

The braiding angle is key factor for getting high quality of braided products. The velocities ratios are determines by the braiding angle. If braiding point motion can be controlled automatically, it will save material and improve the quality of braided products.

Chapter 1 introduces the basic understanding of braiding and reviews the development of braiding technology, including historical background, application of braiding, the new technologies that could be transferred to braiding field and summarizes some relevant literature. Chapter 2 is written to study the mathematical model of the carrier on a braiding machine. It is a detailed study for the static, kinetic and part-dynamic model of a carrier, which is shown how the tension inside a carrier changes when yarn is towed. It is an overall study for a key component of a braiding machine. Chapter 3 is developed a static and dynamical model of braiding point motion. Why oscillation of the braiding point is present during the braiding process is discussed. Chapter 4 first defines a material flow system model of the braiding process. A PI controller is designed to control the take up motor based on the material flow model. Also, machine vision sensing algorithm and corresponding control program are presented in this chapter. Using this control program, the position of the braiding point can be

controlled automatically, which is also very useful for anyone wishing to control braiding, and using motion control and machine vision research. In chapter 2, 3 and 4, the corresponding experimental results will be discussed and correlated to validate the mathematical modeling.

1.5 List of References

[1] Lee, S. M., Braiding, *International Encyclopedia of Composites*. VCH Publishers, New York, 1990, 130-147.

[2] Irene Emery, *Primary Structure of Fabrics*, (1966) 66-69.

[3] J. Lundgren, "Braiding Machine," US Patent #887,257, 1903.

[4] Frank K. Ko, "Braiding," in *Engineered Materials Handbook,* ASM International, Metals Park, OH, 1987, pp. 519-528.

[5] Pastore, C., "Opportunities and Challenges for Textile Reinforced Composites," *Mechanics of Composite Materials,* Vol. 36, No.2, 2000.

[6] Barmer, "General Developments in Braiding Machinery," *Textile Institute and Industry*, October, 1974.

[7] S. W. Wardwell, "Braiding Machine", US Patent #1, 032, 870, 1912.

[8] S. W. Wardwell, "Braiding Machine", US Patent #1, 197, 692, 1916.

[9] V.G. Sokol, "Braiding Machine", US Patent #2, 64, 899, 1949.

[10] Fischer, Thomas A., "Speed control apparatus and method for braiding machine," *http://www.patentstorm.us/patents/4716807/description.html*, Issued on January 5, 1988, US Patent 4716807

[11]L. Vincent A Haehnel, Rudolf H, "Braiding machine," US Patent # 4,765,220, 1988.

[12] Padfield, D. G., The motion and tension of an unwinding thread, I, *Proceedings of the Royal Society of London, Series A, Mathematical and Physical Sciences*, 245 (1958), 382-407.

[13] Ghosh,T.K., Batra,S.K., Murthy, A.S., "Dynamic analysis of yarn unwinding from cylindrical packages--part I: Parametric studies of the two-region problem." *Textile Research Journal*. 71 (2001), 771-778.

[14] Ulsoy, A.G., Mote, C.D. Szymani, R., "Principal developments in band saw vibration and stability research," *Holz als Roh und Werkstoff* 36 (1978), 273-280.

[15] Wickert, J.A., Mote, C.D., "Current research on the vibration and stability of axially moving material," *Shock and Vibration Digest* 20 (1988), 3-13.

[16] Predoi, M.V., Motomancea, A., Bugaru, M., "Dynamics of cables for lifting mechanisms," *The eight IFToMM international symposium on theory of machines and mechanisms*, (2001), 267-272.

[17] Murakami, F., Watanabe, T., Tazaki, H., and Goto, H., "Dynamic tension on yarns being unwound from a beam," *Journal of the Textile Machinery Society of Japan*, 31(1978), 60-66.

[18] R. Marks and A.T.C. Robinson, "Principles of Weaving," *The Textile Institute, Manchester*, UK, 1986.

[19] Podsiedlik,W., Wojtysiak, J., "Multi-Barrier Electromagnetic Tensioner for Control of Yarn Tension in Processing," *Fibres & textiles in Eastern Europe*, 14(2006), 125-128.

[20] http://www.warnernet.com/PDF/P-771-WE_pg098-105.pdf.

[21] Ludwicki, J.E., Unnikrishnan, R., "Automatic control of unwind tensioning film finishing application," *Industrial Electronics Conference*, 1995. 774-779.

[22] S. H. Song and S. K. Sul, "A new tension controller for continuous strip processing line," *in IEEE Ind. Applicat. Conf.*, 3(1998), 2225–2230.

[23] K. C. Lin, M. C. Tsai, and Z. W. Wang, "Observer-based web tension control with inertia compensation," *Proc. 1998 Int. Conf. Metratronic Technology, Hsinchu, Taiwan,* R.O.C., 1998, pp. 355–360. C.

[24] G. W. Du, P. Popper and T. W. Chou, *in 'Proceeding of Symposium on Processing of Polymers and Polymeric Composites', ASME Winter Annual Meeting , Dallas, TX,* U.S.A, 199, P11.

[25] C. Pastore and F. Ko, "CIM of Braided Preforms for Composties", *Computer Aided Design in Composite Material Technology, Proceedings of the International Conference, Southampton,* 1988, pp.135-155.

[26]Similarly, Ebler, N. A., Arnason, R., and Michaelis, G., 1993, "Tension Control: Dancer Rolls or Load Cells," *IEEE Trans. Ind. Appl.*, 29, No. 4, pp. 727–739.

[27]McDow, B., and Rahn, C., 1998, "Adaptive Web Tension Control Using Dancer Arms," *Tappi J.*, 81, No. 10, pp. 197–205.

[28]Siddharth P. Nagarkatti, Fumin Zhang, Christopher D. Rahn, Darren M. Dawson, "Tension and Speed Regulation for Axially Moving Materials," *Journal of Dynamic Systems, Measurement, and Control* ,September 2000 -- Volume 122, Issue 3, 445 (9 pages) doi:10.1115/1.1286270.

[29] Robert L. Williams II [1 *], Paolo Gallina [2], Jigar Vadia [3] "Planar Translational Cable-Direct- Driven Robots," *Journal of Robotic Systems* V. 20 Issue 3, Pages 107 – 120.

[30] David Branscomb, Thesis, *A machine vision and sensing system for yarn defect detection, diagnosis and prevention during manufacture*.

[31] P. Potluri, A. Rawal, M. Rivaldi, I. Porat, "Geometrical modelling and control of a triaxial braiding machine for producing 3D performs, Composites Part A:" *Applied Science and Manufacturing* Volume 34, Issue 6, June 2003, Pages 481-492.

[32] Honglian Ma, Huchuan Lu, Mingxiu Zhang, "A real-time effective system for tracking passing people using a single camera," *Intelligent Control and Automation*, 2008. WCICA 2008. 7th World Congress on, pp 6173 - 6177.

[33]Andriluka, Mykhaylo, Roth, Stefan, Schiele, Bernt Source, "People-tracking-by-detection and people-detection-by-tracking," *26th IEEE Conference on Computer Vision and Pattern Recognition*, CVPR, 2008.

[34]Andrew I. Comport, Eric Marchanda and Franc¸ois Chaumette, "Kinematic sets for real-time robust articulated object tracking," *Image and Vision Computing* 25, 2007, pp.374-391.

[35]Mitsuhiro Kimura, Masami Konishi and Jun Imai, "Image processing system for work position control of master slave 2-dof Manipulators," *Proceeing of the 2009 IEEE international conference on Networking, Sensing and Control, Okayama, Japan,* March 26-29, 2009.

[36]Ushida, S., Yoshimi, K., Okatani, T., Deguchi, K., "The Importance of Gaze Control Mechanism on Vision-based Motion Control of a Biped Robot," *Intelligent Robots and Systems*, 2006 IEEE/RSJ International Conference on pp: 4447 – 4452.

2 Modeling of the Tensioning System on a Braiding Machine Carrier

The tensioning system of Figure 2.1 consists of two pulleys, two springs, and a ratchet with the ratchet gear on the spool. The tension coming from each single carrier is nearly constant, varying within an acceptable range during braid formation and releasing a discrete amount of material from a spool when an upper limit on the tension is reached. A mathematical model of tension versus yarn displacement of a standard package tensioning system is presented. The response before ratchet release is a series of piecewise linear kinematic regions that include spring 1 preload region, the tension of spring 1 tensioning with yarn be towed, spring 2 preload region, and two spring tensioning region. During ratchet release, the system is modeled as two regions of a single degree-of-freedom dynamic model, releasing region and impact region. Ratchet reengagement that incorporated impact with an elastic yarn was required to improve model accuracy of response. All the expressions of the tension T versus displacement of yarn are derived in all these regions. Correlated experiment and simulation response validate the mathematical model, for use as a designer's tool.

2.1. Introduction

Braiding is a fabric-forming process that is most commonly used to form textile products, braided wire or composite preform tubes [1]. Braids are created on braiding machines, which are important industrial machine with a long and interesting history. The most common braiding machine is a maypole braider (Figure 1.1), where two sets of

packages (spools) on carriers move on a circular track with a nearly sinusoidal oscillation, one set moving clockwise and the other counterclockwise, and driven by a circular spur gear train.

Of particular importance to the braiding process is the yarn tensioning system. The payout of yarn or tow from a spool requires a tensioning system attached to and moving with the spool and on the carrier. It must allow a sufficient buildup of tension so that yarns are able to slide and cone-in on each other to form the braid [2], and release a limited amount of yarn when a desired maximum tension level is exceeded [3]. An ideal tensioning system would release material yet keep the tension within a small range about the desired tension level. There is an optimum tension level for a specific product. Bull et al invented a new carrier for a strand supply bobbin, which provide instantaneous braking action as well accurate tension setting and minimum variations in tension during strand release. Unfortunately, this new carrier is too complex in structure to be used in industry [4].

In order to get perfect performance on tension buildup and material pay out, many people modified or invented many kinds of spindle carriers. Simon A invented a strand carrier to make braiding machine operate at greater speed and with fewer and shorter interruptions by tension change [5]. The carriers used in this paper are most like the molded elastomeric braiding machine bobbin carrier, which was invented in 1973 by Joseph E. Stahl [6]. The noise produced by this carrier is greatly reduced.

The focus of this chapter is the passive tensioning system found on the carrier, Wardwell BX-26C, seen in Figure 2.1 and modeled in Figure 2.2. This tensioning system is typical of what is widely available throughout the industry. In this analysis a yarn from

the carrier passes over a translationally-fixed pulley 1, under pulley 2, through a fixed circular guide (not shown) and to a large reel driven by a motor. The plate is constrained to only slide upward; pulley 2 rotates on the plate and translates with it. The motor is constrained to rotate at a constant speed and so $\dot{\mathbf{x}}$ is a constant. Starting from zero tension and the ratchet-locked spool, the pulley 2/plate combination will translate upward and the plate will compress spring1 while yarn rolls on pulley1 and pulley 2. Later the pulley 2/plate reaches the second spring, lifting the pawl lift which rotates the pawl. As the pawl rotates the end of the pawl slides down one tooth of ratchet and eventually gets off it. When the tooth of the ratchet gear on the spool, it unlocks the spool. Yarn pays off the spool as it rotates while the springs are releasing and lengthening, driving pulley 2/plate and pawl lift downward until the pawl reengages the ratchet at the next tooth, stopping the spool. With the spool stopped the cycle of yarn tensioning, ratchet release and spool rotation repeats.

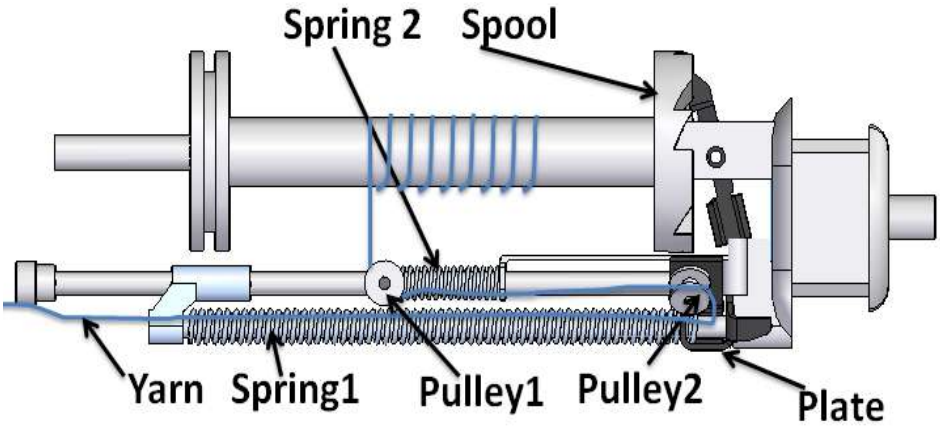

Figure 2.1 Wardwell BX-26C Carriers with Tensioning System

The tension level affects the quality of the final braided products, but the tension release is not ideal. Material does not come off the spool continuously, but in discrete

lengths. Large tensions possibly damage brittle yarns like carbon fiber and other high strength synthetic fibers as they bend and abrade on small radius pulleys or sliding through guides. Excessive tension variations can also adversely affect the final braid structure. The purpose of this effort here is to investigate the mechanics of this passive tension control system deeply, by creating a mathematical model in order to allow analysis of the response and to optimize its performance.

2.2 Kinematic Regions

There are two preloaded compression springs at work in Figure 2.2. Spring 1, the longer of the two, is always active on the pulley2/plate. Spring 2 is not compressed beyond preload until the plate of pulley2 contacts the pawl lift. Spring stiffnesses, preloads (P_1 and P_2) and preload deflection were as measured in Table 2.1.

Spring 1(k_1)			Spring 2(k_2)		
Spring stiffness (Color: Blue)	Preload Deflection	Preload	Spring stiffness (Color: Gray)	Preload Deflection	Preload
0.07355N /mm	27mm	1.9859N	0.1422N /mm	12mm	1.7064N

Table 2.1 Spring stiffnesses and preloads

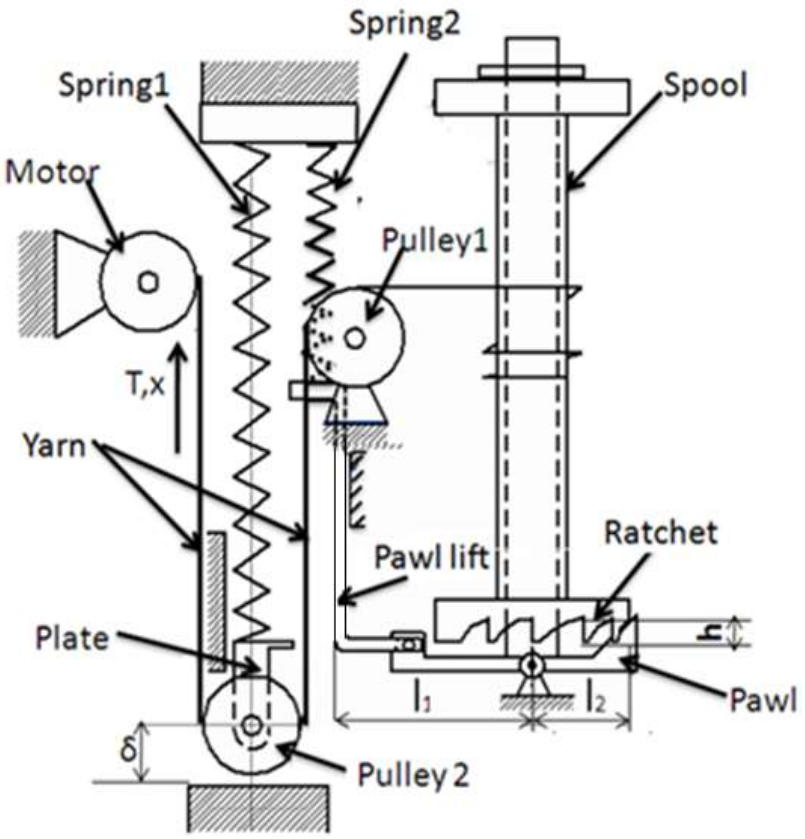

Figure 2.2 Tensioning System Model

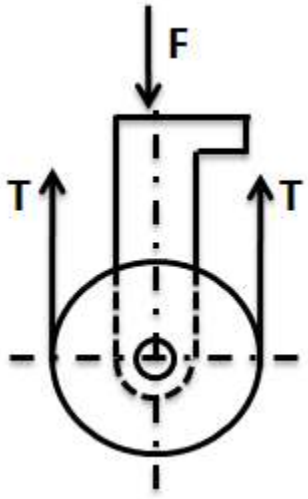

Figure 2.3 Free body diagram of pulley2/plate

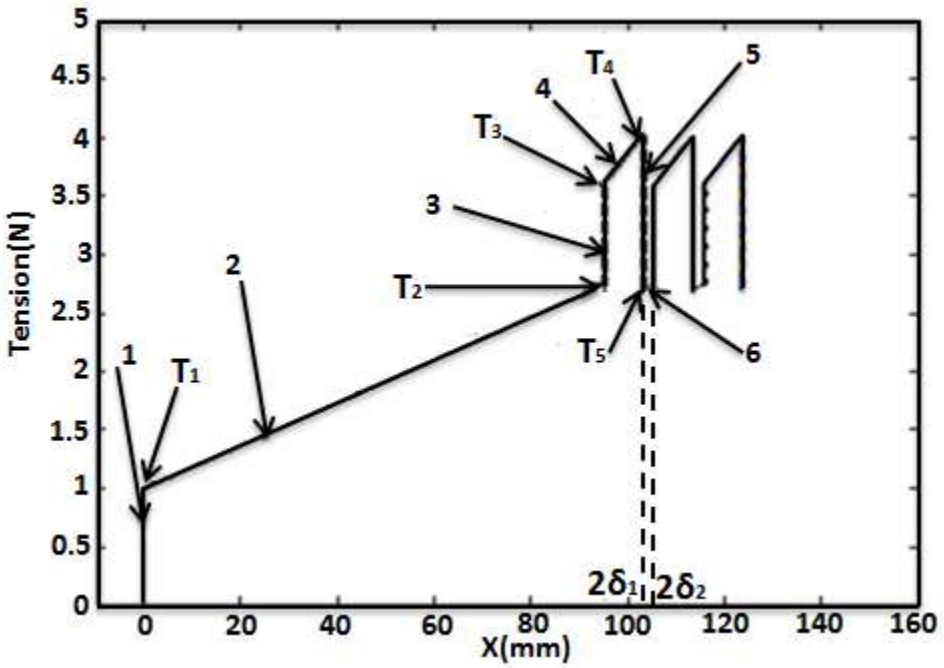

Figure 2.4 Kinematic simulation of pulling the yarn of single spool, including every region.

2.2.1 Region 1- Tensioning of Spring1 to Preload

A free body diagram of pulley2/plate is shown in Figure 2.3, where F is the total spring force. Spring1 is installed with preload P1, forcing the pulley2/plate against a bottom stop. Tension T increases without displacement x until the preload is met; no material is taken off the spool since it is locked, nor does the pulley2/plate move from its bottomed out (i.e. $\delta=0$) preloaded condition. In region 1 shown in Figure 2.4,

$$x=0,\ \delta=0, \qquad 0< T < \tfrac{1}{2} P_1 \tag{1}$$

At the point of impending payout of material, T reaches T_1 in Figure 2.4, and

$$x=0 \text{ and } \delta=0, \quad T_1 = \tfrac{1}{2} P_1 \tag{2}$$

2.2.2 Region 2- Spring1 Compressing

The motor pull now starts to slide pulley2/plate and compress spring1, while the spool remains locked by a pawl and engaged ratchet tooth. x increases as material pays out of the tensioning system. This is region 2 in Figure 2.4, and is described by

$$\text{For } 0 < x \leq 2\delta_1^-, \quad T = \frac{1}{2}P_1 + \frac{1}{4}k_1 x \tag{3}$$

When the plate reaches the pawl lift, then

$$x = 2\delta_1^-, \qquad T_2 = \frac{1}{2}P_1 + \frac{1}{2}k_1\delta_1 \tag{4}$$

2.2.3 Region 3- Spring1 Compressed, While Loading Spring2 up to Preload

When x equals $2\delta_1^+$, T has jumped to T_3 in Figure 2.4, and the arm of the plate pinned to pulley2 contacts the pawl lift, which is in contact with spring2. Tension is increased without payout further increasing x due to the preload force of the second spring.

$$\text{For } x = 2\delta_1^+ \quad T_2 \leq T \leq T_3 \tag{5}$$

$$\text{Where:} \qquad T_3 = \frac{1}{2}(P_1 + P_2) + \frac{1}{2}k_1\delta_1 \tag{6}$$

2.2.4 Region 4 – Spring1 and Spring2 Compressing

As the tension increases beyond T3 the pawl starts to slide down the ratchet tooth face of height h in region 4. Both springs exert a downward force on pulley2/plate. In this region the increase in x displacement, Δx, is constrained by the relationship $h = \frac{\Delta x}{2} = \delta 2 - \delta 1$ (since l1=l2 here for the geometry of this particular tensioning system).

$$\text{For } 2\delta_1 < x < 2\delta_2 \quad T = \frac{1}{2}(P_1 + P_2) + \frac{1}{2}k_1\delta_1 + \frac{1}{4}(k_1 + k_2)(x - 2\delta_1) \tag{7}$$

$$\text{For } x = 2\delta_2 \qquad T_4 = \frac{1}{2}(P_1 + P_2) + \frac{1}{2}k_1\delta_2 + \frac{1}{2}k_2(\delta_2 - \delta_1) \tag{8}$$

2.2.5 Region 5 – Simplified Modeling of Release

When δ is equal to δ_2 and x is equal to $2\delta_2$, T equals T_4, at which time the pawl slides off the tooth and the spool is no longer locked but is free to rotate in response to the yarn tension. Spool rotation is now a degree of freedom, and the response in region 5 is a dynamic event. Yarn tension is created by the released springs which apply downward force on pulley2/plate with yarn, which accelerate the spool rotation. The springs quickly forces pulley2/plate downward below δ_2 and the pawl reengages on a new tooth, but not until an amount of material has unspool. All the while x remains nearly constant given that the event is very rapid compared to the slower takeup speed $\dot{x} = c$, so in this region $x=ct \cong 2\delta_2$. The ratchet mechanism limits the spool rotation; here we assume an optimally maintained tensioning system that will rotate the spool and engage the next tooth, and not skip teeth before engaging.

This region ends when a new tooth is engaged and $\delta = \delta_3 = \delta_2 - \Delta\delta$. With 8 teeth on the gear of the ratchet (Figure 2.2), the nearly instantaneous yarn payout from the spool rotation is $\pi d/8$, where d is the plastic spool diameter including the diameter added by the yarn previously wrapped on the spool. Hence $\Delta\delta$, the total amount δ drops during release, is:

$$\Delta\delta = \frac{1}{2} * \frac{\pi}{8} d \tag{9}$$

And the amount of yarn removed from this spool at each release is therefore

$$2 * \Delta\delta = 2(\delta_2 - \delta_3) \tag{10}$$

In a simplified model x is kept constant at $x = 2\boldsymbol{\delta}_2$ (because the release is much faster than motor speed), the spool stops instantaneously, and the mass of the

pulley2/plate is assumed small. At onset of release T =T_4, which drops abruptly to T= T_5 on line "5" in Figure 2.4, which can be expressed as:

$$T_5 = P_1 + k_1\delta_3 \quad (11)$$

When the assumptions of this region are relaxed, a dynamic analysis will improve the correlation with the experiment. However this idealized release analysis may be useful to designers who may only need simplified and approximate expressions.

2.2.6 Region 6 – Tension Buildup

After the release region, the yarn continues to load onto the motorized spool at a constant rate $\dot{x} = c$, and yarn tension builds once again, from T_5. The computed tensions for all regions are presented in Table 2.2 and this explains the numerical values presented in Figure 2.4; region 6 is shown as the line labeled 6 in Figure 2.4. Line 6 has the same slope as line 2 because only the first spring is once again acting on pulley2/plate. In Figure 2.5 the pulley2/plate displacement δ and tension T always repeats the cycle of tension buildup to release at T_4 at δ_2, and dropping to T_5 at δ_3, followed by another buildup to release at T_4 at δ_2, etc.

	T_1 (N)	T_2 (N)	T_3 (N)	T_4 (N)	T_5 (N)	T_{d1} (N)	δ_1 (mm)	δ_2 (mm)	δ_3 (mm)	D (mm)
value	0.993	2.74	3.60	4.02	2.70	2.35	47.5	51.5	46.4	26

Table 2.2. Tension values for Figure 2.4

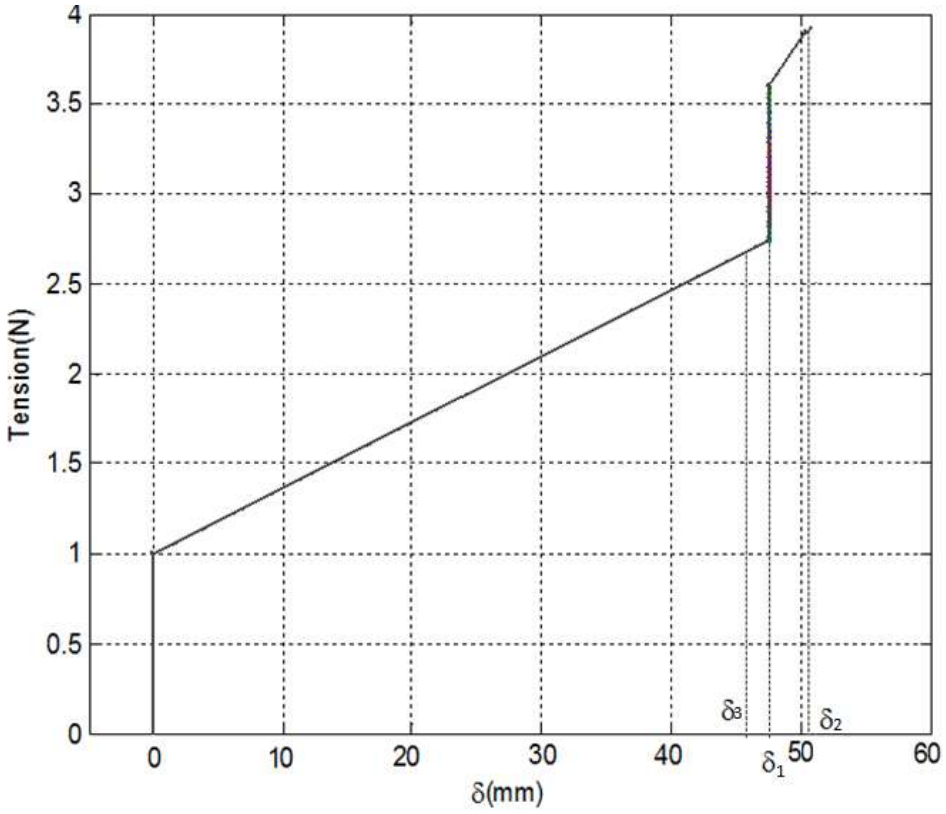

Figure 2.5 Simulation of tension vs. pulley2/plate displacement δ

2.3 Dynamic Analysis

The release period analysis of Region 5 idealized spool rotation as happening instantaneously. Improved correlation of experiment and analysis was found to be achieved when Region 5 is treated dynamically in Section 2.3.1, by including spool rotation as a degree of freedom and hence replacing a kinematic analysis with a dynamic one. It is assumed that the yarn is massless, flexible in bending with no bending stiffness, and axially rigid so it will not stretch. There is friction between the shaft and spool. A second dynamic region occurs when yarn stretch is accounted for, due to pulley2/plate impact on the yarn; equations for this region are developed in Section 2.3.2.

2.3.1 Dynamic Analysis during Release

At the start of the dynamic release period both springs are acting on the linkage consisting of pulley2/plate, pawl lift and pawl. The yarn is rapidly forced downward by the pulley2/plate, causing the spool to rotate. The pawl is approximated as a rod for determination of the moment of inertia.

$$I_{pawl} = m_{pawl}\frac{1}{12}(4l_1^2)$$

And $I_{pulley1} = I_{pulley2} = \frac{1}{2}m_{pulley}r^2$

The equivalent mass [16] of the linkage is

$$m_{e1} = \frac{m_{pawl}}{3} + m_{pawllift} + m_{plate} + 5m_{pulley} + \frac{m_{spring1}}{3} + \frac{m_{spring2}}{3} \qquad (12)$$

During the second dynamic release period the pawl lift and pawl are stopped, but pulley2/plate continues downward. The equivalent mass becomes

$$m_{e2} = m_{plate} + 4m_{pulley} + \frac{m_{spring1}}{3} \qquad (13)$$

For numerical simulation m_{e1} =30.5 gram and m_{e2} =18.4 gram from experimental measures. Based on the system of Figure 2.2 the equations of motion for pulley2/plate are

$$m_{e1}\ddot{\delta} + (k_1 + k_2)\delta = k_2\delta_1 - P_1 - P_2 + 2T + f \qquad \delta_2 \geq \delta \geq \delta_1 \quad (14)$$

$$m_{e2}\ddot{\delta} + k_1\delta = -P_1 + 2T + f \qquad \delta < \delta_1$$

where $f = \mu m_{pulley/plate}g$ and $\mu = 0.15$(steel on steel, degreased). The equation of motion for the spool is

$$I\ddot{\theta} = \frac{B}{2}T \qquad (15)$$

With the following constraints relationship between δ and θ,

$$\delta = \delta_2 - \frac{B}{4}\theta \qquad (16)$$

Differentiate equation (16) twice to obtain,

$$\ddot{\delta} = \frac{B}{4}\ddot{\theta} \tag{17}$$

Combining equation (14), (15) and (17), $\ddot{\delta}$ expression (18) and $\ddot{\theta}$ expression (19) can be obtained.

$$\ddot{\delta} = \begin{cases} -\frac{B^2}{16I+m_{e1}B^2}\left((k_1+k_2)\delta + P_1 + P_2 + f - k_2\delta_1\right), & \delta_1 \le \delta \le \delta_2 \\ -\frac{B^2}{16I+m_{e2}B^2}(k_1\delta + P_1 + f), & \delta < \delta_1 \end{cases} \tag{18}$$

$$\ddot{\theta} = \begin{cases} \frac{4B}{16I+m_{e1}B^2}\left((k_1+k_2)\delta + P_1 + P_2 + f - k_2\delta_1\right), & \delta \ge \delta_1 \\ \frac{4B}{16I+m_{e2}B^2}(k_1\delta + P_1 + f), & \delta < \delta_1 \end{cases} \tag{19}$$

Using MATLAB Runge-Kutta routine ODE45, equation (18) is integrated for responses $\delta, \dot{\delta}, \ddot{\delta}$ versus time (Figure 2.6) and tension T versus time (Figure 2.7). For $\delta_1 \le \delta \le \delta_2$ the initial conditions are:

$$\delta(0) = \delta_2, \qquad \dot{\delta}(0) = 0$$

The drop in tension in Figure 2.7 is obtained by combining equations 15, 17 and 18. Substituting $\delta = \delta_1$ to two parts of equation (18), the tension drop is

$$-\frac{B^2}{16I + m_{e1}B^2}(k_1\delta_1 + P_1 + P_2 + f) + \frac{B^2}{16I + m_{e2}B^2}(k_1\delta_1 + P_1 + f)$$

Integration proceeds until the spool has rotated 1/8 of a complete rotation, since there are 8 ratchet teeth on the spool; at that instant the integration of the release (dynamic region 1) is stopped, and δ and $\dot{\delta}$ are recorded and used as initial conditions for dynamic region 2. For this simulation, both springs are active until:

$t = 0.0127s,\ \delta(0.0127) = \delta_2 - 4 = 47.5\ \text{mm},\ \dot{\delta}(0.0127) = -614.1\ \text{mm/s}$

Afterwards only one spring is active until the spool is stopped. The total time the spool rotates, and the final position and velocity of pulley2/plate are:

$t = 0.0145s,\ \delta(0.0145) = \delta_2 - \frac{\pi D}{16} = 46.4\ \text{mm},\ \dot{\delta}(0.0145) = -687.2\ \text{mm/s}$. There is an acceleration jump at t=.0127 due to preload P_2. The final tension of yarn was calculated to be 2.3493N before collision (Figure 2.7).

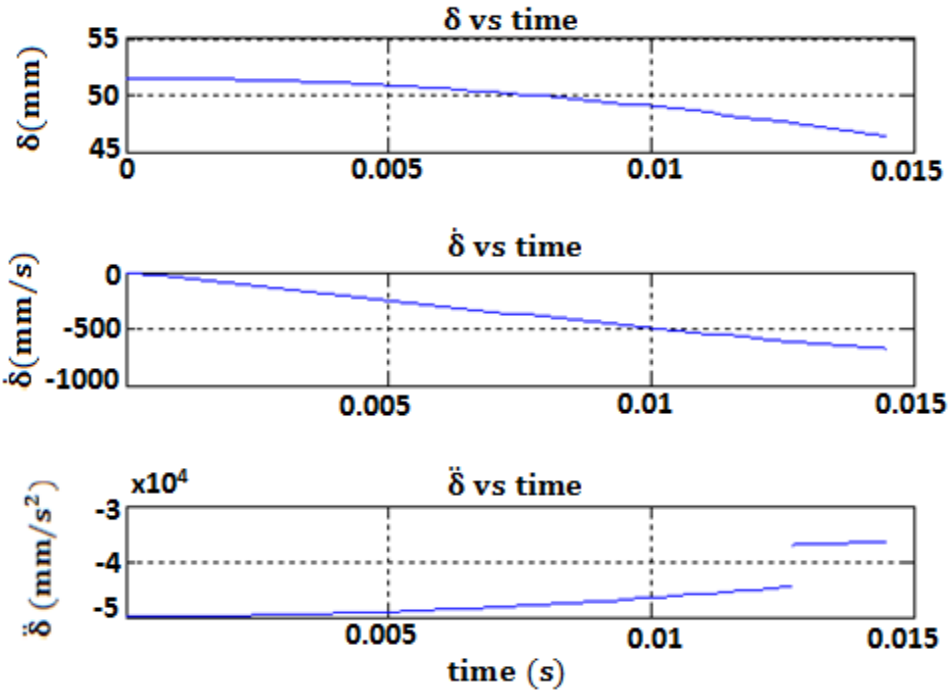

Figure 2.6 Simulation of $\delta, \dot{\delta}, \ddot{\delta}$ versus time

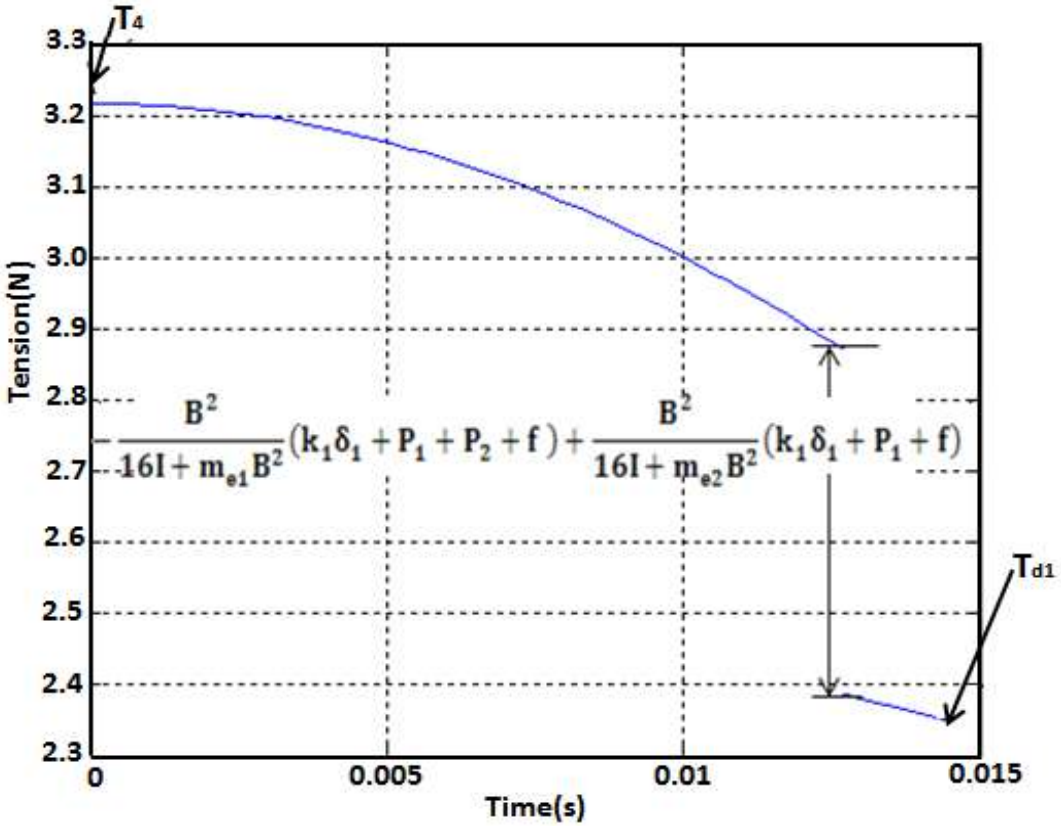

Figure 2.7. Tension versus time in releasing period

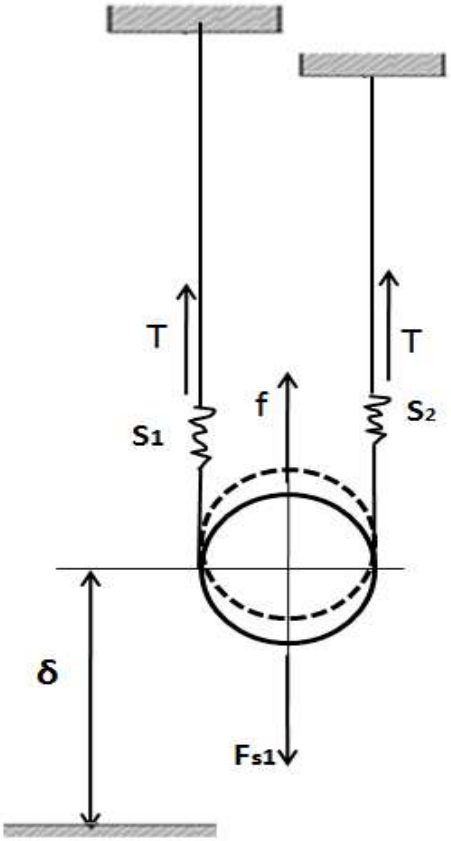

Figure 2.8 Free body diagram of pulley2 during impact

2.3.2 Dynamic Analysis during Pulley2/Plate Impact on Yarn

Although the spool stops suddenly, experimental results revealed that the tension did not suddenly plateau. We conjecture this as indicative of pulley2/plate impacting and stretching yarn, causing a rapid increase in yarn stretch. So from Figure 2.8:

$$2T + f - F_{s1} = m_{e2}\ddot{\delta} \tag{20}$$

$$T_1 = k_{1y}s_1 \tag{21}$$

$$T_2 = k_{2y}s_2. \tag{22}$$

With $T_1 = T_2 = T$, yarn stretch s_1 (left side of pulley) and s_2 (right side) are:

$$s_1 = T/k_{1y} \tag{23}$$

$$s_2 = T/k_{2y} \tag{24}$$

Yarn stretch at the end of the release region and the start of the impact region are matched by setting the displacement of the spring to an initial δ_0. The following relationships can also be derived:

$$\delta - \delta_0 = -(s_1 + s_2)/2 \tag{25}$$

$$\delta = \delta_0 - \left(\frac{T}{k_{1y}} + \frac{T}{k_{2y}}\right)/2 \tag{26}$$

$$T = -2\frac{k_{1y}k_{2y}}{k_{1y}+k_{2y}}(\delta - \delta_0) \tag{27}$$

$$s_1 = -2(\delta - \delta_0) - s_2 = -2(\delta - \delta_0) - T/k_{2y} \tag{28}$$

$$s_2 = -2(\delta - \delta_0) - s_1 = -2(\delta - \delta_0) - T/k_{1y} \tag{29}$$

Substitute equation (29) to equation (22),

$$-4\frac{k_{1y}k_{2y}}{k_{1y}+k_{2y}}(\delta - \delta_0) + f - F_{s1} = m_{e2}\ddot{\delta} \tag{30}$$

Then,
$$\ddot{\delta} = \frac{-\left(4\frac{k_{1y}k_{2y}}{k_{1y}+k_{2y}} + k_1\right)\delta + f - 4\frac{k_{1y}k_{2y}}{k_{1y}+k_{2y}}\delta_0 - P_1}{m_{e2}} \tag{31}$$

If $k_{1y} = k_{2y} = k_y$, then the equation (30) becomes:

$$-4k_y(\delta - \delta_0) + f - F_{s1} = m_{e2}\ddot{\delta}, \tag{32}$$

For polyester yarn ($A = 0.3mm^2$, $L_{1\_y} = 260mm$, $L_{2\_y} = 80mm$). the yarn stiffness was measured to be $K_{yarn} = 4273N/m$ for 50mm of polyester monofilament, from which the other stiffnesses are determined as $k_{1y} = 821.73N/m$, and $k_{2y} = 2670.625N/m$. Using MATLAB code ODE45, equation (31) is integrated for the response δ, $\dot{\delta}$ and $\ddot{\delta}$ in Figure 2.9 and tension in Figure 2.10, with both dynamic regions shown.

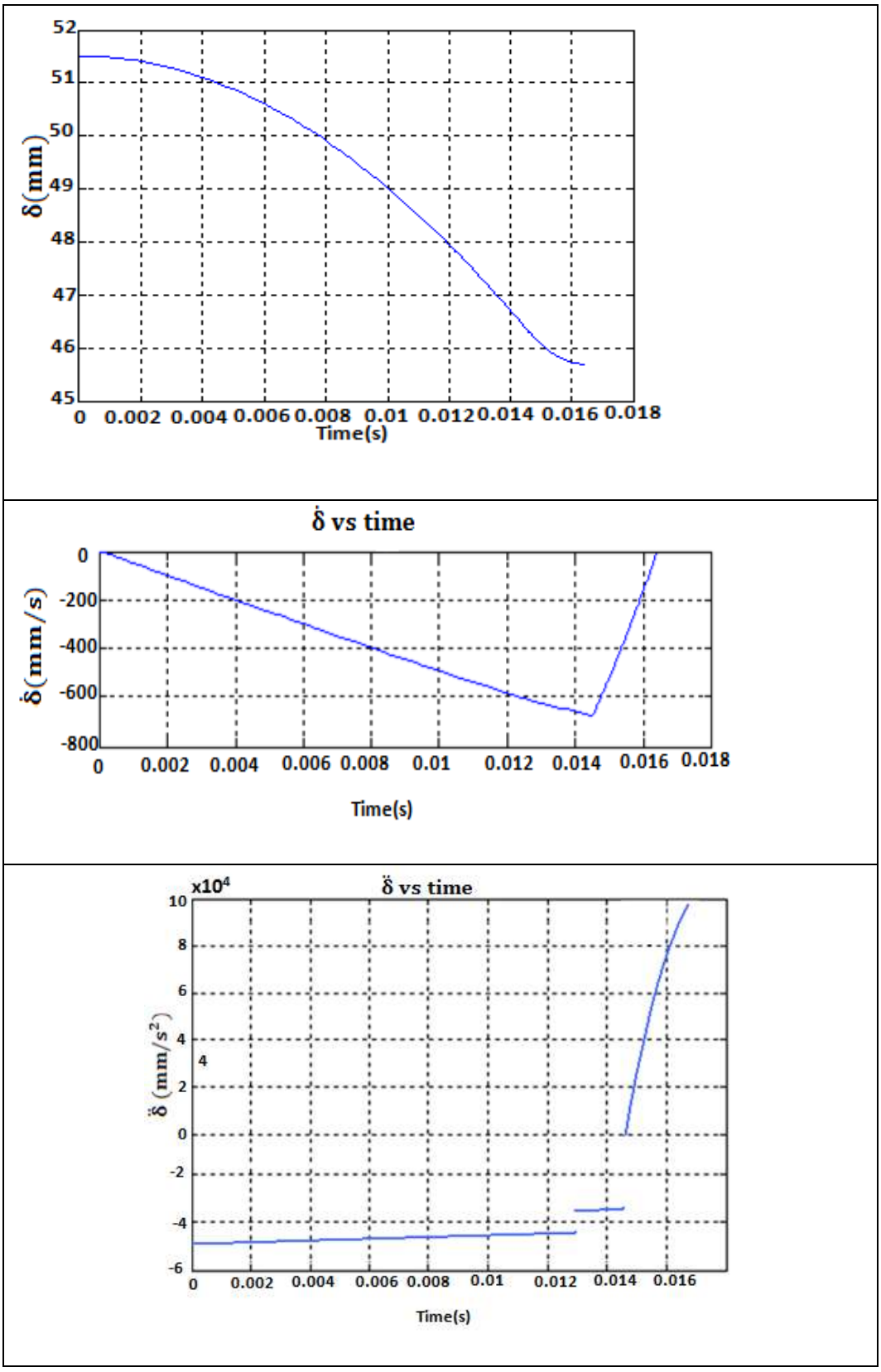

Figure 2.9 Simulation of $\delta, \dot{\delta}, \ddot{\delta}$ as function of time for dynamic regions 1 and 2

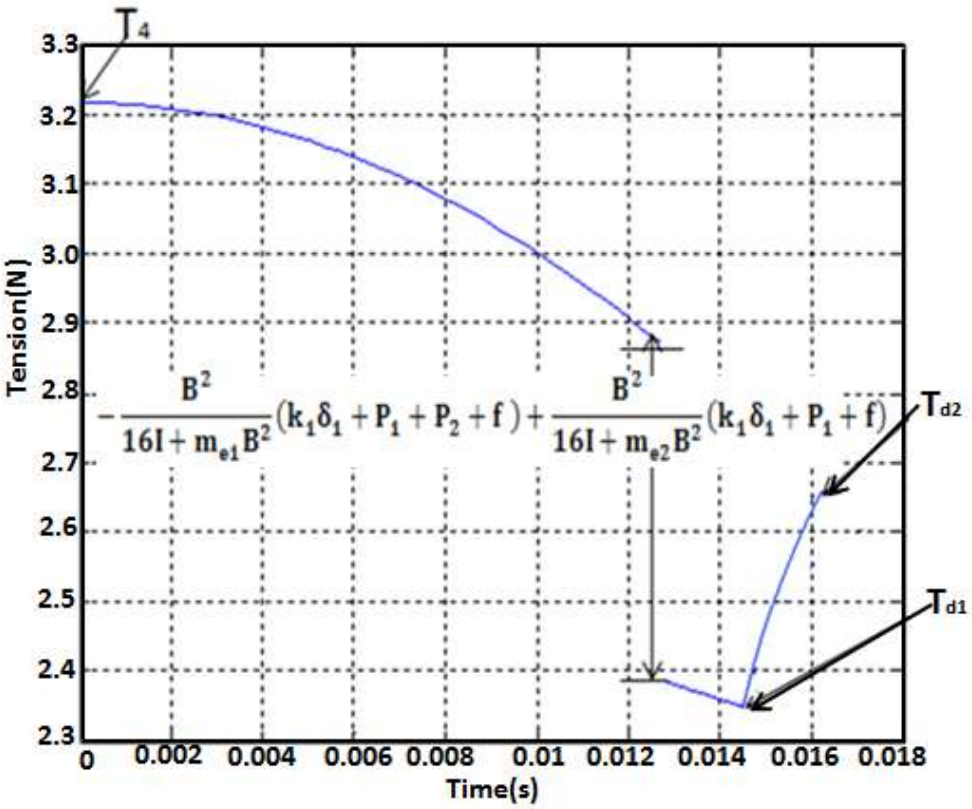

Figure 2.10 Dynamic tensions as a function of time for both dynamic regions, from Equations 31 and 18

In Figure 2.10, the yarn for a period of time stretches, which is attributed in part to impact of pulley2/plate inducing a tension increase $T_{d2} - T_{d1}$ =2.6786-2.3493N=0.329N. Figure 2.10 shows that tension rises from T_{d1} to T_{d2} at the maximum amount of stretch; stretch is induced here not only from pulley2/plate impacting on the yarn (0.2128N), but also the contributing effect (0.116N) due to a constant takeup speed of 100 mm/min. Combining the static simulation in Figure 2.4 with the dynamic regions, the graph of tension as a function of yarn displacement is completed in Figure 2.11.

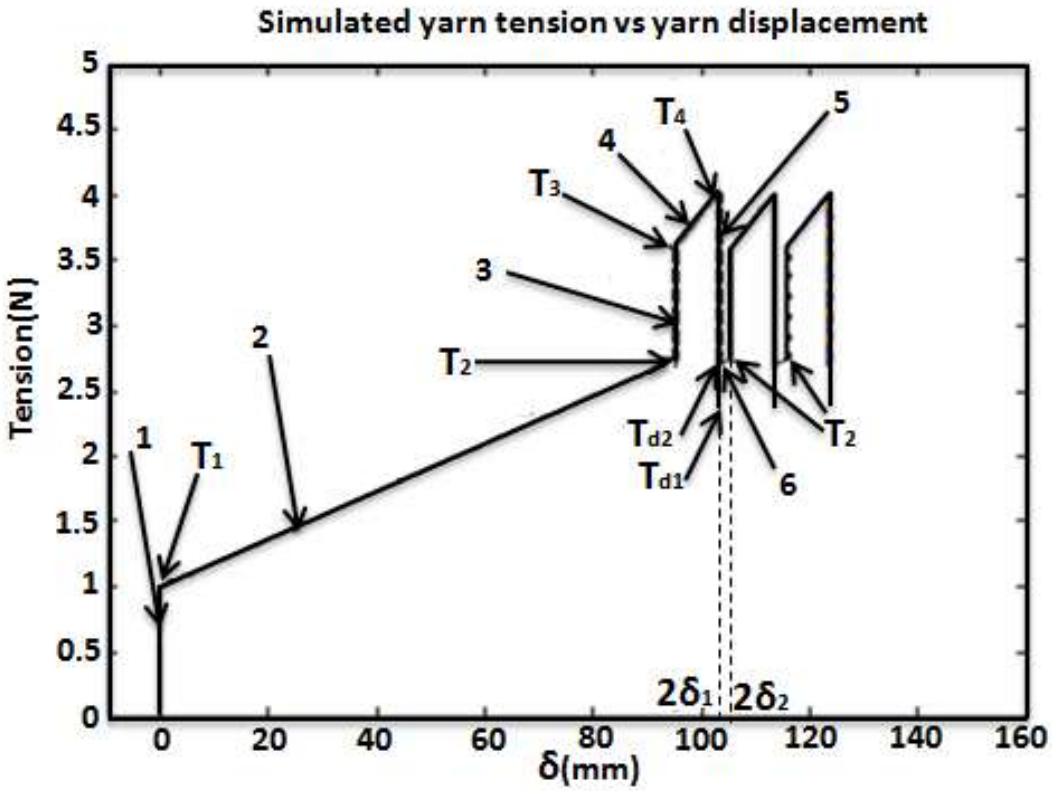

Figure 2.11 Simulated yarn tension versus displacement as yarn is pulled from the spool

Fig #	Parameter Value				T_1(N),	$T_{2(}$N)	T_3 (N)	T_4(N)	T_5(N)	T_{d1}(N)
	k_1(N/mm)	k_2(N/mm)	δ_1 (mm)	$\delta_2 - \delta_1$ (mm)						
5,12	0.0736	0.142	47.5	4	0.993	2.74	3.59	4.02	2.70	2.35
13	0.0736	0.108	47.5	4	0.993	2.74	3.39	3.75	2.70	2.33
14	0.0736	0.049	47.5	4	0.993	2.74	3.03	3.28	2.70	2.32
15	0.049	0.142	47.5	4	0.662	1.83	2.68	3.06	1.80	1.72
16	0.147	0.142	47.5	4	1.99	5.48	6.33	6.91	5.40	4.99
17	0.0736	0.142	47.5	2	0.993	2.74	3.59	3.81	2.63	2.10
18	0.0736	0.142	40	4	0.993	2.46	3.32	3.75	2.42	2.046

Table 2.3 Simulated data

Simulations with varied parameter values were performed to determine their effect on response, and presented in Table 2.3. First the effect of dropping k_2 to 0.1079 and 0.049 is shown in Figure 2.12 and 2.13, respectively. In these plots to Figures 2.4 and 2.11, the

preload force of the second spring drops, and also the slope between T_3 and T_4. Figures 2.15 and 2.16 show the effect of keeping the stiffness k_2 constant and changing k_1, showing that the first spring strongly effects the overall tension level during operation.

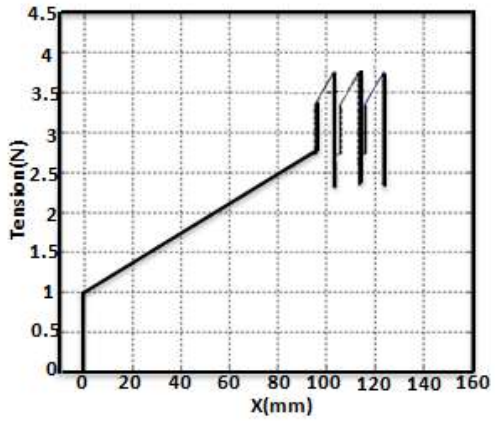

Figure 2.12 Simulated tension versus displacement, k1= 0.0735 N/mm, k2= 0.1079 N /mm

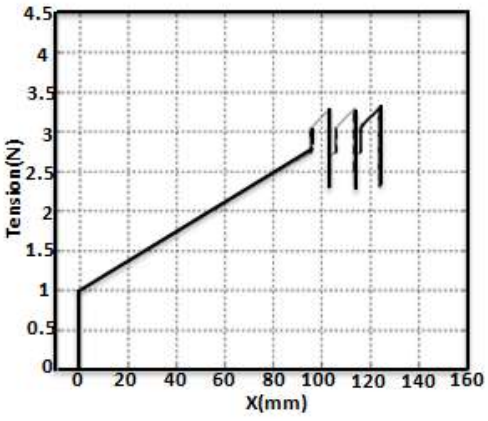

Figure 2.13 Simulated tension versus displacement, k1= .0735 N/mm, k2= 0. 049 N/mm

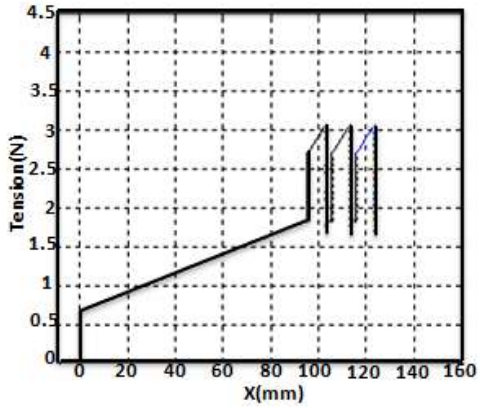

Figure 2.14 Simulated tension versus displacement, k_1=0.049 N/mm, k_2= 0.1422 N/mm

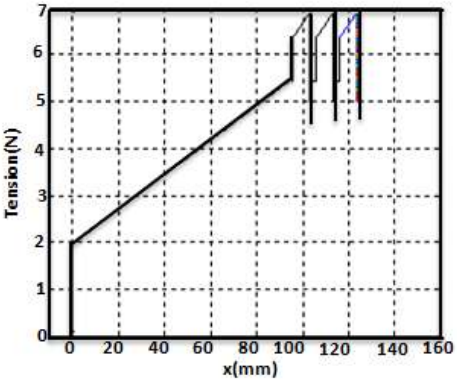

Figure 2.15 Simulated tension versus displacement, k_1=0.1471 N/mm, k_2= 0 .1422 N/mm

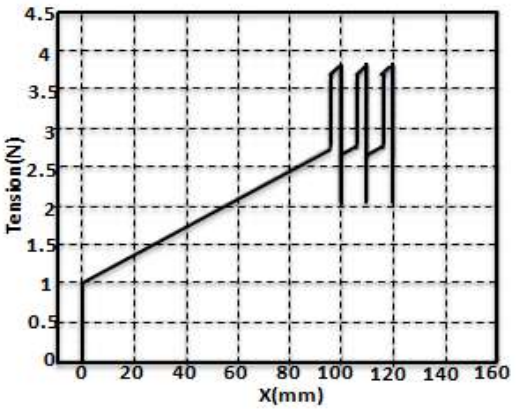

Figure 2.16 Simulated tension versus displacement ($\delta_2 - \delta_1 = 2$mm)

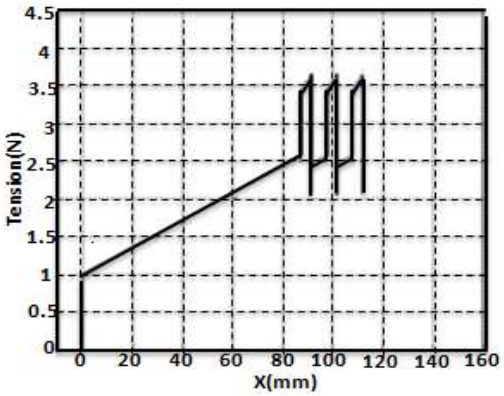

Figure 2.17 Simulated tension versus displacement (length of first spring=40mm)

The effect of spring length is now considered. In Figure 2.16, the maximum compressed length beyond preload of spring2 is changed from 4mm to 2 mm; this is intended to represent loss of tooth height h, which could be shortened by wear of the plastic spool tooth. Comparing to Figure 2.11, a worn tooth decreases tensions T_4 and T_{d1} in Table 2.3. Because the working length of spring is also shortened by 2 mm, T_4 decreases. T_{d1} will also decrease since spool rotation during release is still the same.

In Figure 2.17, the effect of a shorter pawl lift and relocated pulley1 is investigated by changing the length δ_1 from 47.5mm to 40 mm with the same preload. Additionally, δ_2 was also decreased from 51.5 to 44mm, which would be accomplished by relocating pulley1. Note that this exercise kept spring2 with the same free length and preload as previous. Comparing Figures 2.11 and 2.17, all tension in Figure 2.17 decrease except for T_1.

2.4 Experiment

An Instron tensile test machine measured the tension as it pulled yarn off the tensioning system (Figure 2.18).

Figure 2.18 Motion control components

The take up speed, $\dot{x}$, was set to 100 mm/min, pulling the aforementioned polyester monofilament. The tensioning system was refurbished and lubricated in accordance with specifications in order to achieve optimal performance. Experimental-derived operating regions with two release periods are shown in Figure 2.19. Separate release region and impact region are identified in 2.21, with the releasing period lasting 110ms and the impact 45ms.

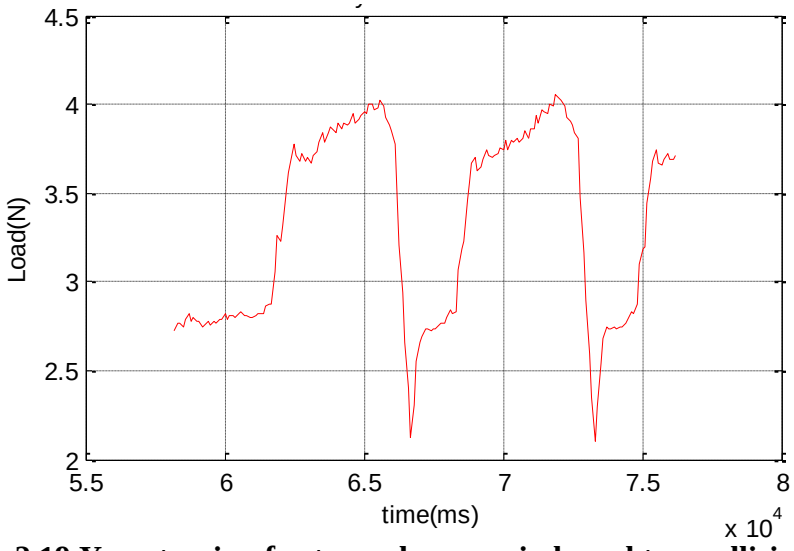

Figure 2.19 Yarn tension for two release periods and two collision periods

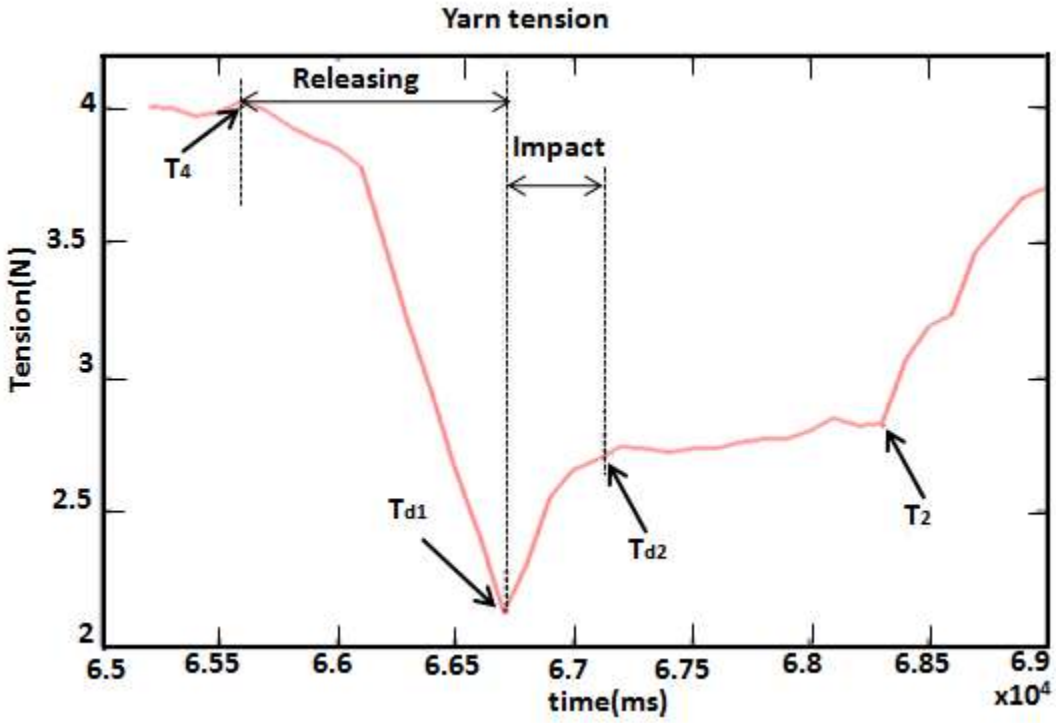

Figure 2.20 T_4: Start of spool release; T_{d1}: Spool stops, pulley2/plate starts to impact the yarn; T_{d2}: Spring1 is nowactive (the lowest point of pulley2/plate); T_2: Both spring1 and spring2 are now active.

Simulation and experiment results are plotted in Figure 2.21, validating that the mathematical modeled presented here is able to largely reproduce the experimentally-derived system response in all regions, although the model does not appear to be sophisticated enough to fully capture some dynamic effects, such as the tension low that occurs at release.

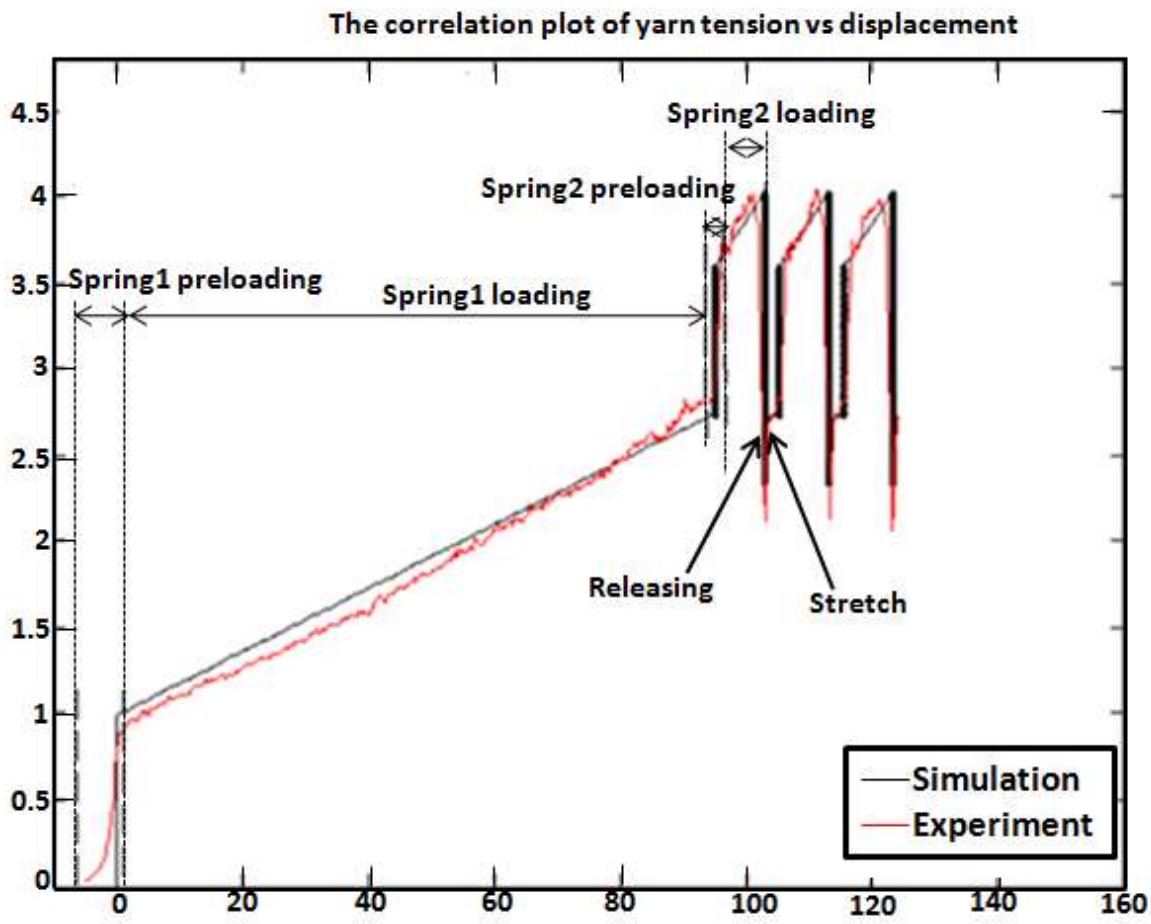

Figure 2.21 The tension versus displacement from experiment, yarn speed 100 mm/minute.

2.5 Conclusions

This article introduces and mathematically models the tension system typically used on a braiding machine carrier. The model reveals how spring stiffnesses, link mass properties, geometry and improper maintenance affect the response. The model is validated by correlating simulated response and experiment, and can incorporate elastic yarn effects. The model should be of value to the product designer seeking to select and size a tensioning system for a given braided structure and yarn or tow material. Future work could include design optimization of the tension system itself to, for example, minimize weight and tension variations.

2.6 List of References

[1] Lee, S. M., Braiding, *International Encyclopedia of Composites*. VCH Publishers, New York, 1990, 130-147.

[2] Zhang, Q, Beale, D., Broughton, R., "Analysis of Circular Braiding Process: Part I: Theoretical Investigation", *ASME Journal of Manufacturing Science and Engineering*, August 1999, 121: 345-350.

[3] Zhang, Q, Beale, D., Broughton, R., "Analysis of Circular Braiding Process: Part II: Mechanics and Analysis", *ASME Journal of Manufacturing Science and Engineering*, August 1999, 121:351-359.

[4] Bull et al, (1985). "Carrier for a strand supply bobbin," *Braiding Machine*, US Patent #4, 529, 147.

[5] Simon A, De Young, "Braiding Machine," US Patent, #4719838, 1988.

[6] Joseph E. Stahl, Easthampton, Mass, "Braiding Machine," US Patent, #3,774,497 1973.

2.7 Appendices

A.2.1 Calculating equivalent mass using Lagrange's Equation

Suppose the rotating angle of pawl is θ_{pawl} when spring move by δ. And the rotating angle of spool is θ_{spool}.

The kinetic energy of system is,

$$T = \frac{1}{2} I_{pawl} \dot{\theta}_{pawl}^2 + \frac{1}{2} m_{pawllift} \dot{\delta}^2 + \frac{1}{2} m_{plate} \dot{\delta}^2 + \frac{1}{2} m_{pulley2} \dot{\delta}^2 + \frac{1}{2} I_{pulley2} \left(\frac{2\dot{\delta}}{r_{pulley2}} \right)^2 + \frac{1}{2} I_{pulley1} \left(\frac{2\dot{\delta}}{r_{pulley1}} \right)^2 + \frac{1}{2} \frac{m_{spring1}}{3} \dot{\delta}^2 + \frac{1}{2} \frac{m_{spring2}}{3} \dot{\delta}^2 + \frac{1}{2} I_{spool} \dot{\theta}_{spool}^2$$

The potential energy is just potential energy of spring.

$$V = \frac{1}{2} K_1 (27 + \delta)^2 + \frac{1}{2} K_2 (12 + \delta_2 - \delta)^2$$

Using Lagrange's equation,

$$\frac{\partial T}{\partial \dot{\delta}} = I_{pawl} \frac{\dot{\delta}}{{l_1}^2} + m_{pawllift} \dot{\delta} + m_{plate} \dot{\delta} + m_{pulley2} \dot{\delta} + 4 I_{pulley2} \left(\frac{\dot{\delta}}{{r_{pulley2}}^2} \right) + 4 I_{pulley1} \left(\frac{\dot{\delta}}{{r_{pulley1}}^2} \right) + \frac{m_{spring1}}{3} \dot{\delta} + \frac{m_{spring2}}{3} \dot{\delta} + I_{spool} \frac{4\dot{\delta}}{D^2}$$

So,

$$\frac{d}{dt} \left(\frac{\partial T}{\partial \dot{\delta}} \right) = I_{pawl} \frac{\ddot{\delta}}{{l_1}^2} + m_{pawllift} \ddot{\delta} + m_{plate} \ddot{\delta} + m_{pulley2} \ddot{\delta} + 4 I_{pulley2} \left(\frac{\ddot{\delta}}{r_{pulley2}^2} \right) + 4 I_{pulley1} \left(\frac{\ddot{\delta}}{r_{pulley1}^2} \right) + \frac{m_{spring1}}{3} \ddot{\delta} + \frac{m_{spring2}}{3} \ddot{\delta} + I_{spool} \frac{4\ddot{\delta}}{D^2}$$

$$\frac{\partial T}{\partial \delta} = 0$$

$$\frac{\partial V}{\partial \delta} = K_1(27 + \delta) + K_2(12 + \delta_2 - \delta) = K_1\delta + P_1 + K_2(\delta_2 - \delta) + P_2.$$

So, $\frac{d}{dt}\left(\frac{\partial T}{\partial \dot{\delta}}\right) - \frac{\partial T}{\partial \delta} + \frac{\partial V}{\partial \delta} = 0,$

$$I_{pawl}\frac{\ddot{\delta}}{l_1^2} + m_{pawllift}\ddot{\delta} + m_{plate}\ddot{\delta} + m_{pulley2}\ddot{\delta} + 4I_{pulley2}\left(\frac{\ddot{\delta}}{r_{pulley2}^2}\right) + 4I_{pulley1}\left(\frac{\ddot{\delta}}{r_{pulley1}^2}\right) + \frac{m_{spring1}}{3}\ddot{\delta} + \frac{m_{spring2}}{3}\ddot{\delta} + I_{spool}\frac{4\ddot{\delta}}{D^2} + K_1\delta + P_1 + K_2(\delta_2 - \delta) + P_2 = 0$$

And, $\left[\frac{I_{pawl}}{l_1^2} + m_{pawllift} + m_{plate} + m_{pulley2} + \left(4\frac{I_{pulley2}}{r_{pulley2}^2}\right) + 4\frac{I_{pulley1}}{r_{pulley1}^2} + \left(\frac{4I_{spool}}{D^2}\right) + \frac{m_{spring1}}{3} + \frac{m_{spring2}}{3}\right]\ddot{\delta} + K_1\delta + P_1 + K_2(\delta_2 - \delta) + P_2 = 0$

So, $\left[\frac{I_{pawl}}{l_1^2} + m_{pawllift} + m_{plate} + m_{pulley2} + \left(4\frac{I_{pulley2}}{r_{pulley2}^2}\right) + 4\frac{I_{pulley1}}{r_{pulley1}^2} + \left(\frac{4I_{spool}}{D^2}\right) + \frac{m_{spring1}}{3} + \frac{m_{spring2}}{3}\right]\ddot{\delta} = -[K_1\delta + P_1 + K_2(\delta_2 - \delta) + P_2]$

So, the equivalent mass of system is

$$m_{e1} = \frac{I_{pawl}}{l_1^2} + m_{pawllift} + m_{plate} + m_{pulley2} + \left(4\frac{I_{pulley2}}{r_{pulley2}^2}\right) + 4\frac{I_{pulley1}}{r_{pulley1}^2} + \left(\frac{4I_{spool}}{D^2}\right) + \frac{m_{spring1}}{3} + \frac{m_{spring2}}{3},$$

Obviously,

$$m_{e2} = m_{plate} + m_{pulley2} + \left(4\frac{I_{pulley2}}{r_{pulley2}^2}\right) + \left(4\frac{I_{pulley1}}{r_{pulley1}^2}\right) + \frac{m_{spring1}}{3} + \frac{4I_{spool}}{D^2}.$$

Here, $I_{pawl} = \frac{\frac{1}{12}(4l_1^2+1)}{l_1^2}$, $I_{pulley2} = \frac{\frac{1}{2}m_{pulley2}r_{pulley2}^2}{r_{pulley2}^2} = \frac{1}{2}m_{pulley2}$, $I_{pulley1} = \frac{1}{2}m_{pulley1}$.

$I_{spool} = \frac{1}{2}m_{spool}$.

Actually, the equivalent mass except spool is considered for this paper. And the pulley2 is same as pulley1. Pulley2 is being represented pulley1.

So, $m_{e1} = \frac{I_{pawl}}{{l_1}^2} + m_{pawllift} + m_{plate} + m_{pulley2} + \left(4\frac{I_{pulley2}}{{r_{pulley2}}^2}\right) + \left(4\frac{I_{pulley2}}{{r_{pulley2}}^2}\right) + \frac{m_{spring1}}{3} + \frac{m_{spring2}}{3} \cong \frac{m_{pawl}}{3} + m_{pawllift} + m_{plate} + m_{pulley2} + 2m_{pulley2} + 2m_{pulley2} = \frac{m_{pawl}}{3} + m_{pawllift} + m_{plate} + 5m_{pulley2} + \frac{m_{spring1}}{3} + \frac{m_{spring2}}{3} = 30.4732\ g.$

$m_{e2} = m_{plate} + 4m_{pulley2} + \frac{m_{spring1}}{3} = 18.41g.$

A.2.2 MATLAB code for simulation plot in figure 2.21

```
% Hw3p5     guangli Ma
clear all
clc
load('instrondata.mat');
% plot(force)

G=0.00980665; %1gram=0.00980665N
K1=7.5*G*1000;
K2=14.5*G*1000;
delta1=47.5/1000;
delta2=4/1000;
d=26/1000; pi=3.14159026535897932;
delta3=pi*d/16;
% delta4=0.05;
Preload_length1=(154-127)/1000; %m
Preload_length2=(32-20)/1000; %m
P1=K1*Preload_length1; %N
P2=K2*Preload_length2; %N

%several period, force point
T1=P1/2;%+W_plate/2;
T2=P1/2+delta1*K1/2;
T3=(P1+P2)/2+delta1*K1/2;
T4=(P1+P2)/2+(delta1+delta2)*K1/2+de
lta2*K2/2;
% T5=2.318726688605510e+02;
T5=K1*(delta2-delta3)/2+T2;
Td1=2.3493;
% T7=T2;
% T8=T1; v=0.1/60; % m/s
x2=0:0.0001:delta1;
% t2=0:0.001/v:delta1/v;
% x3=delta1;
x4=delta1:0.0001:(delta1+delta2);
t4=delta1/v:0.001/v:
(delta1+delta2)/v;
x6=(delta1+delta3):.0001:
(delta1+2*delta3-delta2);
t6=(delta1+delta3):-.001:
(delta1+delta2);
x8=(delta1+delta3):.0001:
(delta1+delta2+delta3);
x10=(delta1+2*delta3):-.0001:
(delta1+delta2+delta3);
x12=(delta1+2*delta3):.0001:
(delta1+delta2+2*delta3);

y1=0:0.0001:T1;
x1=0*y1;
t1=0*y1;
y2=P1/2+K1*x2/2;
y3=T2:0.0001:T3;
x3=delta1;
t3=delta1/v;
% plot(x3,y3)
y4=(P1+P2)/2+(K1*x4+K2*
(x4-delta1))/2;
y5=T4:-0.0001:Td1;
x5=delta1+delta2;
x6=(delta1+delta3):-.0001:
```

```
(delta1+delta2);
y6=K1*(x6-delta1-delta3)/2+T2;
y7=T2:0.0001:T3;
x7=delta1+delta3;
y8=(P1+P2)/2+(K1*(x8-delta3)
+K2*(x8-delta1-delta3))/2;
y9=T4:-0.0001:Td1;
x9=delta1+delta2+delta3;

% x10=delta1+delta2+delta3;
y10=K1*(x10-delta1-2*delta3)/2
+T2;
y11=T2:0.0001:T3;
x11=delta1+2*delta3;
y12=(P1+P2)/2+(K1*(x12-2*delta3)
+K2*(x12-delta1-2*delta3))/2;
y13=T4:-0.0001:Td1;
x13=delta1+delta2+2*delta3;

% plot(2*x10+x0,y10)
figure(1)
plot(2*x1*1000,y1,'black',
text(120,4.2,'5','fontsize',14);
text(110,2.2,'6','fontsize',14);
% text(55,115,'7','fontsize',14);
text(58,130,'8','fontsize',14);
% text(55,102,'9','fontsize',14);
text(40,65,'10','fontsize',14);
% text(80,3,'2*\delta_1',
'fontsize',14 );
text(105,4.2,'2*\delta_2',
2*x2*1000,y2,'black',
2*x3*1000,y3,'black',2*x4*1000
,y4,'black',2*x5*1000,y5,
'black',2*x6*1000,y6,'black',
2*x7*1000,y7,'black',2*x8*1000,
y8,'black',2*x9*1000,y9,
'black',2*x10*1000,y10,'black',
2*x11*1000,y11,'black',2*x12*1000,y1
2,'black',2*x13*1000,y13,
'black')%,x10,y10)grid
% axis ([-5 60 0 300])
% title('The correlation of
simulation and experimental
%data of pulling the yarn of
single Spool,(speed=100mm/min)')%
xlabel('x(mm)')%,'fontsize','8')
ylabel('Tension(N)')%'fontsize','8')
% text(0,1.2,'1','fontsize',14);
text(45,2,'2','fontsize',14);
text(80,3.3,'3','fontsize',14);
% text(90,4.2,'4','fontsize',14);

'fontsize',16 )
% text(100,2,'2*\delta_3',
'fontsize',14 );
% % text(43,90,'2*\delta_4',
'fontsize',16 )
% text(70,2.42,'T_2','fontsize',
14 );
text(18,1.6,'T_1','fontsize',
14);
```

```
% text(80,3.8,'T_3','fontsize',
14);
text(96,4.2,'T_4','fontsize',
14 );
%text(80,1.8,'T_d1','fontsize',14 );
text(80,2,'T_d2','fontsize',14 );
%text(120,1.55,'T_5','fontsize',
14 );
%legend('Simulation','Experiment')
% hold on
plot(i2,handdata2(134:182,:),'r')
% in=0:0.158:129.402;
% % plot(instrondata)
plot(in,instrondata(1:820)*G*100,
'r')
legend('Simulation','Experiment')
% % hold on
% % plot(in,handdata2(134:182,:)
*G,'r')
% grid ,axis([-10 160 0 4.8])
%tension vs time
hold on
in=-5:0.158:124.402;
plot(in,instrondata(1:820)*G*100,'r')
```

A.2.3 MATLAB code for simulation plot in Figure 2.10

```
% PTS_dynamic_simulation.m    guangli
Ma
clear all
clc

global B K1 K2 P1 P2 delta1 delta2 I m1
m2 K delta0 T20 friction1 friction2
alpha

%Parameter
G=0.00980665;   %1gram=0.00980665N
K1=7.5*G*1000;    %Spring stiffnes of
first spring
K2=14.5*G*1000;     %Spring stiffnes
of 2nd spring
delta1=47.5/1000;
delta2=0.004;
B=0.026; pi=3.14159026535897932;
delta3=pi*B/(16);
% alpha=pi/4;
% B=d/2;K=628.4;
% % yarn stiffnes
% s=0.05; % yarn deflection

% delta4=0.05;
Preload_length1=(154-127)/1000; %m
Preload_length2= (32-20)/1000; %m
P1=K1*Preload_length1; %N
P2=K2*Preload_length2; %N
Fs10=K1*(delta1+delta2)+P1;
Fs20=K2*delta2+P2;
m1=(14.44*(20^2+5^2)/(3*20^2)+2.2/3
+15.754+2+6.98)/1000; %Kg
m2=(16.41+2)/1000;%Kg
friction1=m1*G*0.15*1000;
friction2=m2*G*0.15*1000;
I=0.05*((B/2)^2+0.007^2)/2;%Kg*m^2
% m_longplate=7; %gram
V=0.1/60;
one_8_perimeter=pi*B/16;
0.0515-one_8_perimeter

wn1=sqrt((K1+K2)*B^2/(16*I+B^2*m1
))
f1=wn1/(2*pi)
wn2=sqrt(K1*B^2/(16*I+B^2*m2))
f2=wn2/(2*pi)

[t1 x1]=ode45('greatthand1',[0,0.0127],
[0.0515 0]);
[t2 x2]=ode45('greatthand2',[0, 0.0018],
[x1(57,1), x1(57,2)]);
t1e=0.0127;
t=t1e+0.0018;
Fs1=(K1)*x1(:,1)+K2*(x1(:,1)-
delta1)+(P1+P2);
Fs2=K1*x2(:,1)+P1;

% -(B^2)*((K1+K2)*x(1)+(P1+P2)-
K2*delta1)/(8*I-m1*B^2)
```

```
 deltadoubledot1=-
(B^2)*((K1+K2)*x1(:,1)+(P1+P2)-
friction1-friction1-
K2*delta1)/(16*I+m1*B^2);
deltadoubledot2=-B^2*(K1*x2(:,1)+P1-
friction2)/(16*I+m2*B^2);
% deltadoubledot1=-
(B^2)*((K1+K2)*x1(:,1)-
0.1*x1(:,2)+(P1+P2)-
K2*delta1)/(16*I+m1*B^2);
% deltadoubledot2=-B^2*(K1*x2(:,1)-
0.1*x2(:,2)+P1)/(16*I+m2*B^2);
T1=-8*I*deltadoubledot1/B^2;
% T1=2*I*thetadoubledot1/B;
% T1=K*(-B*x1(:,3)/2+2*x1(:,1)-
2*(delta1+delta2));
T2=-8*I*deltadoubledot2/B^2;
% thetadot=-4*x2(:,2)/B
% thetadot(41)
deltat=0.0156
% F=I*thetadot(41)/(deltat*B)
%collation part
delta0=x2(41,1)
T20=T2(41);
[t3 y]=ode45('collation',[0,0.001923],
[x2(41,1), x2(41,2)]);
sdoubledot=-(4*K-K1)*(y(:,1)-
4*K*delta0-P1)/m2;%(-
(4*K+K1)*y(1)+4*K*delta0-P1)/m2
K1*y(:,1)/m2
% T3=(T2(41,1)+sdoubledot*m2)/2;
%+K*(delta0-y(:,1));
T3=T2(41)+K*(delta0-y(:,1))/2;
w_n=sqrt((4*K-K1)/m2)/(2*pi)
Time=w_n^(-1)
Tension_up=100*0.003187*K1/(2*60)
% F=m2*x2(:,2)/0.004701;

% thetadoubledot=4*deltadoubledot1/B;
subplot(3,1,1)
plot(t1,x1(:,1)*1000)
hold on
plot(t2+t1e,x2(:,1)*1000)
hold on
% plot(t+t3,y(:,1)*1000)
ylabel('\delta(mm)');
title('\delta vs time')
grid on,
subplot(3,1,2)
plot(t1,x1(:,2)*1000)
hold on
plot(t2+t1e,x2(:,2)*1000)
hold on
% plot(t+t3,y(:,2)*1000)
title('\delta.^dot vs time')
xlabel('time(s)');
ylabel('\deltadot(mm/s)');
grid on,
 %  figure(2)
subplot(3,1,3)
plot(t1,deltadoubledot1*1000)
```

```
hold on
 plot(t2+t1e,deltadoubledot2*1000)
hold on
% plot(t+t3,sdoubledot*1000)
xlabel('time(s)');ylabel('\deltadoubledot(
mm/s^2)');
 title('\deltadoubledot vs time')
grid on,
figure(3)
plot(t1,T1)
hold on
plot(t2+t1e,T2)
grid on
xlabel('time(s)');ylabel('Tension(N)');
title('Tension vs time')
hold on
plot(t+t3,T3,'b')
```

```
function xdot=greatthand1t(t,x)
global B K1 K2 P1 P2 delta1 I m1
friction1xdot=[x(2);(B^2)*((K1+K2)*x(
1) +(P1+P2)-friction1-K2*delta1)
/(16*I+m1*B^2)]; %*cos(alpha)
```

```
function xdot=greatthand1t(t,x)
global B K1 K2 P1 P2 I m1 K friction2
xdot=[x(2); -(B^2)*(K1*x(1)+P1-
friction2)/(16*I+m1*B^2)];
%*cos(alpha)
```

3 Modeling and Machine Vision Sensing of Braiding Point Motion

Braiding is a circular interlacing process where yarns converge and interlace at the braiding point. A 32-carrier Maypole braiding machine including a braiding motor, a take up motor and 32 carriers with corresponding yarn was used in this experimental study. The tension coming from single carrier remains nearly constant, varying within an acceptable range during braiding process, while releasing a certain amount of material from a spool when an upper limit of the tension is reached. A mathematical model of braiding process based on static, kinematic and dynamic levels is presented while considering the releasing tension and releasing material of a carrier. The tensioning system response after ratchet release is demonstrated as the reason for oscillation of the braiding point in steady state. The released amount of material determines the maximum range of the braiding point envelope. And the releasing frequency determines the frequency of braiding point oscillation. Correlated experiment and simulation response validate the mathematical model, for use as a designer's tool.

3.1 Introduction

Circular braiding is a long-established textile-manufacturing process, which is commonly used to braid textile, fabric, wire or composite preform tubes [1]. For the given yarn materials, the geometric structure of braided products also defines the properties and characteristics of the final braided products. The convergent zone

connected with the final braided products (Figure 3.1) is called “braiding point”, whose location and dynamic motion will determine the geometry of braided products. That means braiding point will determine all the properties of final braided products relative to geometrical structure. The geometrical parameters and the mechanical properties defined by these geometrical parameters are determined after braiding point making. A lot publications are focused on establishing the relationship between the main parameters governing the process and mechanical properties of layer-to-layer interlock 3D braided composites [2]. Its final objective considers the microstructure of braided composites. The authors consider what the structure of composite or braided products should be first, and then look for the right operation methods or braiding mechanisms to realize these structures. N. Tolosana et al, describe the 3D unit cell first, and then look for the right operation strategies or braiding mechanisms to realize these structures, the interlacing pattern of the braided products [3]. Many patents based on modified or invented machineries are presented for this reason. For example, Scherzinger invent a new circular braiding machine, which include an inner and outer group of spools assembled on a circular track coaxial with a rotation axis. The yarns coming from spool will wind around mandrel to make braids [4]. The mandrel is absolutely coaxial with the rotating axis.

Some researcher tried to control the braiding point to make the perfect structure of composite or braided products by tuning all the corresponding parameters. In order to control the location of braiding point, many people try to use different geometric mechanisms, for example, in Wardwell machine, there is big ring close to the side of braiding plane, which could prevent the braiding point from getting close to the braiding plane. And it also makes yarns during braiding process to have an effective diameter that

coincides with the rotating axis of carriers [5]. Some researcher put the take up ring on the take up side to keep braiding point in one location. These techniques are useful to control the braiding angle.

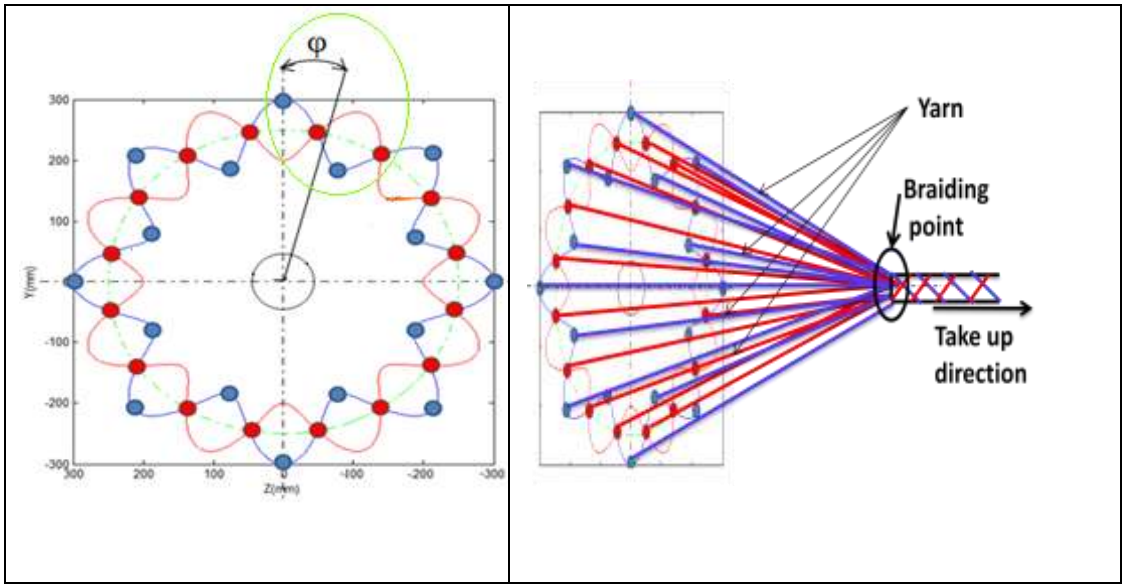

Figure3.1 Left: Braiding plane showing counterclockwise rotating carriers in blue and clockwise rotating in red. Right: Yarns and rope showing 3D braiding process

The braiding process based on a 32 carrier maypole braiding machine is a circular braiding process. The maypole path track is very useful for yarns to interlace. During braiding process, two sets of carriers rotate on a circular track with a nearly sinusoidal oscillation, one set moving clockwise and the other counterclockwise, and driven by a circular horn gear train. The clockwise moving sets interlace with the counterclockwise moving sets in the braiding point area. The formed tubular products are pulled and rolled onto a motor driven reel by certain take up speed. The braided products geometry is determined by the braiding angle, θ, which is half the angle of the interlacing between two responding yarns rotating in opposite direction with respect to the braiding direction. The properties, such as tightness, are reflected in the frequency of intertwining [6].

In this chapter, the braiding process, especially, the braiding process close to braiding point is modeled. Little research and few publications can be found regarding braiding process analysis and braiding process control with respect to a braiding machine and its key part, the carrier. Braiding process is the process of yarns interlacing in braiding point area. The modeling of braiding process is really difficult and complicated since the process based on many yarns, many carriers and take up devices. There are a few operating parameters changing and depending on each other. Amit Rawal and Prasad Polturi simulated the versatile braided structures based on various shape of mandrels. They mentioned the geometry of braided structure is determined by braiding machine parameters, which include rotating speed of carriers, take up speed, and radius of mandrel cross section [7].

The relationship between motion parameters and braiding geometry parameters were derived by Du and Popper [8]. They use this model built by the relationship to predict a braid angle. It turned out the braiding angle predicted is always bigger than that of measured. A. C. Long presents a model for the braiding process based on a general mandrel cross-section, which is composed of a number of flat facets [9]. A relatively simple geometric procedure is used, based on the paths of key braid tows that bound each flat facet. Locking or jamming of the braid is accounted for by concerning the effects of tow spacing and braid angle on the fiber architecture. The calculation of braiding angle is also based on the motion of mandrel. These studies neglect the tension interactions in the braiding point area and motion of braiding point.

These discussions, however, suppose that the braiding point is stable. And motion of the mandrel doesn't affect these parameters and final properties. Actually, this is not

possible especially without using a mandrel. Even though the new braiding mechanism is considered with the mandrel, the individual carrier will still affect the final structure of braided products. The carriers in this paper have discrete tension release and change little during braiding process, which is discussed in chapter 2. Bull et al invented a new carrier for a strand supply bobbin, which provide instantaneous braking action as well accurate tension setting and minimum variations in tension during strand release [10]. Unfortunately, this carrier does not appear to be commercially available.

The braided products necessarily need at least three strands [1]. In this chapter, three to 32 carriers are chosen to make rope. When the different number of strands are used in these experiments, their effects to performance of braiding point will be investigated.

The model of braiding point affecting performance of braided products will also benefit understanding of tension control. If the tension changes could be modeled during braiding process, the motion of braiding point could be controlled by control of carriers' motion using feedforward methods. And also if the model of how changing tension affect motion of braiding point is built, motion of braiding point can be also controlled using feedforward method combining with measurements, which are only used as feedback data in a few prior research efforts[11] and [12].

3.2. Mathematical Model of Braiding Process

During the braiding process, the braiding point is shown in red rectangle of Figure 3.2, always exhibits small x, y and z oscillations about its steady state x position, for a given constant take up speed and braider rotational speed. The carriers are rotating in

nearly sinusoidal path superimposed on a circle (Figure 3.1), which may be one reason for oscillation of braiding point. The changing tension and releasing of material of every carrier also contributes. The oscillation will be also affected by the stiffness of individual yarns and the final product. In this paper, however, the effect of yarn and rope stiffness characteristics is removed by experimenting only with an axially stiff but flexible yarn material (Kevlar 29). For clarification, the followings are assumed:

1) The yarns are massless.

2) The yarn and rope have infinite axial stiffness. That means they cannot be stretched by tensions.

3) The rope is short (1.6m) between the braiding point and the takeup motor reel. The yarns cannot have negative tensions.

4) Each yarn is straight in the braiding point area, and the interaction between yarns caused by interlacing effects (like friction) is neglected.

3.2.1 Static Model of the Braiding Machine

The model of braiding machine is 3-D model, which is shown in Figure 3.2. The plane from which yarns came out is called braiding plane. In Figure 3.2, x-y-z frame is put in braiding point and XYZ frame is put in center point of braiding plane, and x axis point to take up direction, y axis parallel to Y axis and z parallel to axis Z. There are 32 carriers uniformly distributed in braiding plane. One yarn is coming out from one carrier. There 16 carriers rotating in clockwise direction and the other 16 carriers rotating in counterclockwise direction. These yarns are centrosymmetric with respect to x direction.

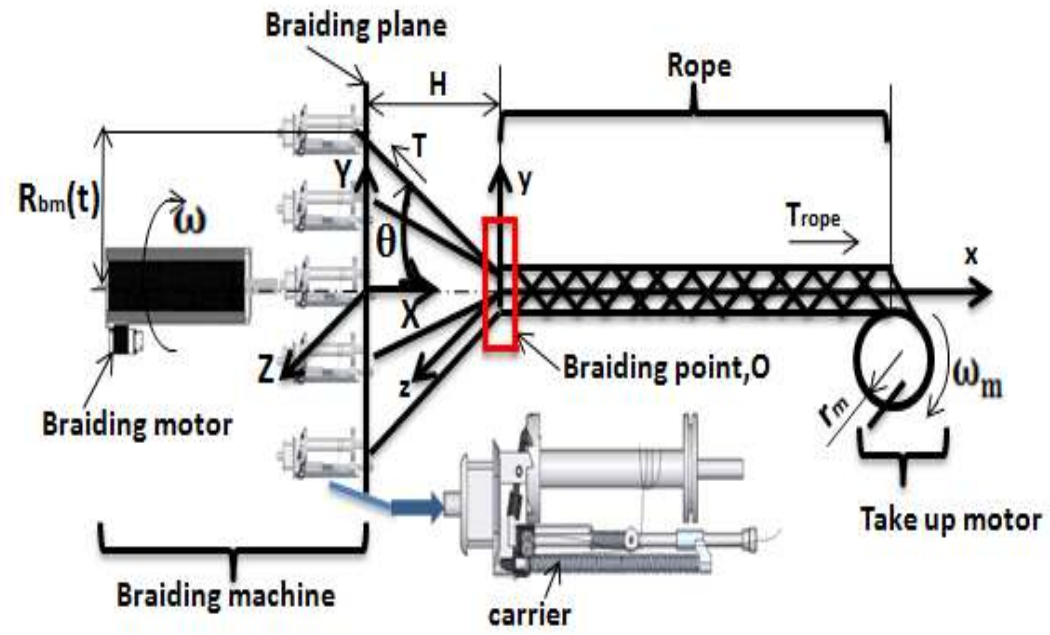

Figure 3.2 Freebody diagram of the braiding point with braiding machine and take up motor

During the braiding process, the tensions in every yarn of tow are T and tension in rope is T_{rope}. Braiding point is located at point, O. The braiding angle is θ. The tensions are satisfied the equation (1) in the steady state condition of the braiding point. The tensions of yarns in x direction are equal to the tension of rope provided by take up motor.

$$T_{rope} - \sum_{n=1}^{32} T_n \cos\theta_n = 0 \quad (1)$$

where, n=1,2,3, …32.

Because the carriers are rotating on a circular path track with a sinusoidal oscillation, the rotating radius of a chosen carrier on either track, $R_{1bm}(t)$ or $R_{2bm}(t)$, is changing (Figure 3.3). With the braiding machine, the carrier rotating at angular velocity, ω, the elapsed time, t, is shown in equation (2) for angle, φ, which is shown in left figure of Figure 3.1. The mathematical expressions of the path tracks are approximated in equation (3) and (4).

$$t = \frac{\varphi}{\omega} \quad (2)$$

For the blue curve (clockwise motion), $\begin{cases} Y = [R_c + A_p \cos 2\pi t]\sin\left(\frac{\pi}{4}t\right) \\ Z = [R_c + A_p \cos 2\pi t]\cos\left(\frac{\pi}{4}t\right) \end{cases}$ (3)

where A_p is the amplitude of the sinusoid.

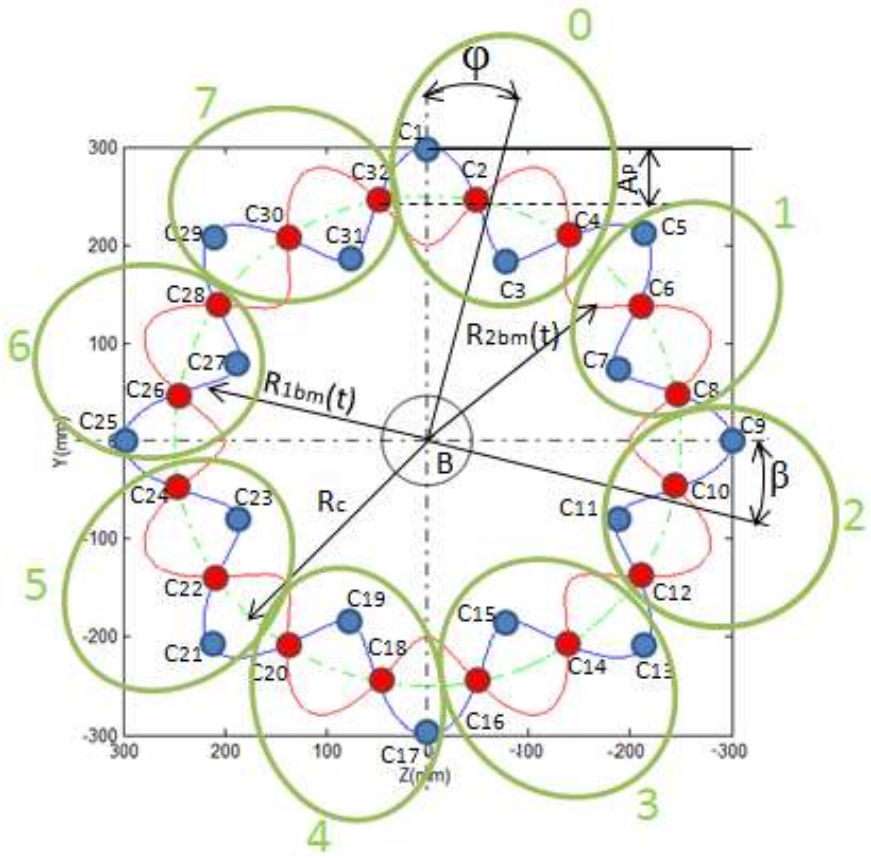

Figure 3.3 Path track of carriers, the red curve is for the counterclockwise direction and the blue curve is for the clockwise direction.

For the red curve (counterclockwise motion),

$$\begin{cases} Y = [R_c + A_p \cos(-\pi - 2\pi t)]\sin\left(-\frac{\pi}{4}t\right) \\ Z = [R_c + A_p \cos(-\pi - 2\pi t)]\cos\left(-\frac{\pi}{4}t\right) \end{cases} \quad (4)$$

The expressions inside the square brackets in Equations (3) and (4) are the rotating radius of the clockwise carriers, which is $R_{1bm}(t)$ for the red track, or $R_{2bm}(t)$ for the blue track in Figure 3. The radius of base circle in green circle of Figure 3.3 is R_c. There are four carriers in one "periodogram" (four neighboring carriers in a

green circle in Figure 3.3) of the path, and the rest of carriers in the other periodograms repeat the same activity. (A periodogram by definition is an artifice that can simplify the analysis of a complicated system by breaking it up into the sum of simple objects that can be studied separately and combined later). There are eight periodograms in Figure 3.3. The four carriers in one periodogram are only investigated here. The symbols, n, i and k in equation (5) are index of carriers C_n.(Figure 3.3), index of four carriers in one periodogram of pathtrack and index of periodogram, respectively. From equation (5), a particular carrier is located by knowing k and i. The phase shift between any two neighboring carriers is 90 degree. There is a 180 degree phase shift between any two neighboring carriers on the same track. So, the rotating radius of a particular carrier is shown in equation (6).

$$n = 4k + i + 1 \tag{5}$$

So, the rotating radius of every single carrier is shown in equation (6).

$$R_{1bm,k,i}(t) = R_c + A_p \cos\left(2k\pi + 2\pi t + \frac{i\pi}{2}\right) \tag{6}$$

where, k=0,1,2,3, …7, and i=0,1,2,3.

With the certain velocity ratio, the braiding point position is set as $H=H_0$ when braiding point locates in steady state point, O. At this moment, the cosine of braiding angle is able to be obtained in equation (7). Combining equation (7) with the equation (1), the equation (8) can be derived. The derivation of equation (8) is shown in appendix 3.1. After a series of calculations, the resultant tension of any 4 carriers in one periodogram of path track is proved to work equally in x direction as four carriers with equal radius, R_c at H_0=351.5mm. Even if braiding point isn't in this location, the difference between these two resultant tensions in x direction is still ignorable. So, R_c will used to replace

$R_{1bm,k,i}(t)$ in the rest calculation of this paper. These 4 carriers are any 4 neighboring carriers in one periodogram, which is an example as shown within green circle in left figure of Figure 3.1. The tension balance will be broken when one or more carriers release. The rotating radius, $R_{1bm,k,i}(t)$, will contribute to the tension unbalance. The difference will be talked about in section 3.2.2.1.

$$\cos\theta_n = \frac{H_0}{\sqrt{H^2+R_{bm}^2(t)}} = \frac{H_0}{\sqrt{H^2+R_{1bm,k,i}(t))^2}} \quad (7)$$

where, k=0,1,2,3, …7, and i=0,1,2,3.

$$T_{rope} - \sum_{n=1}^{32} 8T \frac{H_0}{\sqrt{H_0^2+R_c^2}} = 0 \quad (8)$$

where, k=0,1,2,3, …7, and i=0,1,2,3.

3.2.2 Dynamic Model of the Braiding Process in Steady State

Since the rotating radius, $R_{1bm,k,i}(t)$ is not the reason for the oscillation of braiding point, the releasing tension and releasing material of yarn should be the reason. In this section, it is discussed how the releasing tension and material affects motion of braiding point and how the braiding point moves in area close to its steady state.

3.2.2.1 Dynamic Model of Braiding Point at Steady State

As discussed in last chapter, the carrier is a complex tensioning system with spring, ratchet, mass and damping [13]. Tension of single yarn vs. time is shown in Figure 3.4. The tension inside single carrier always changes from T_2 to T_4 and release to T_{d1} during braiding process, which is highlighted by blue rectangle in Figure 4.

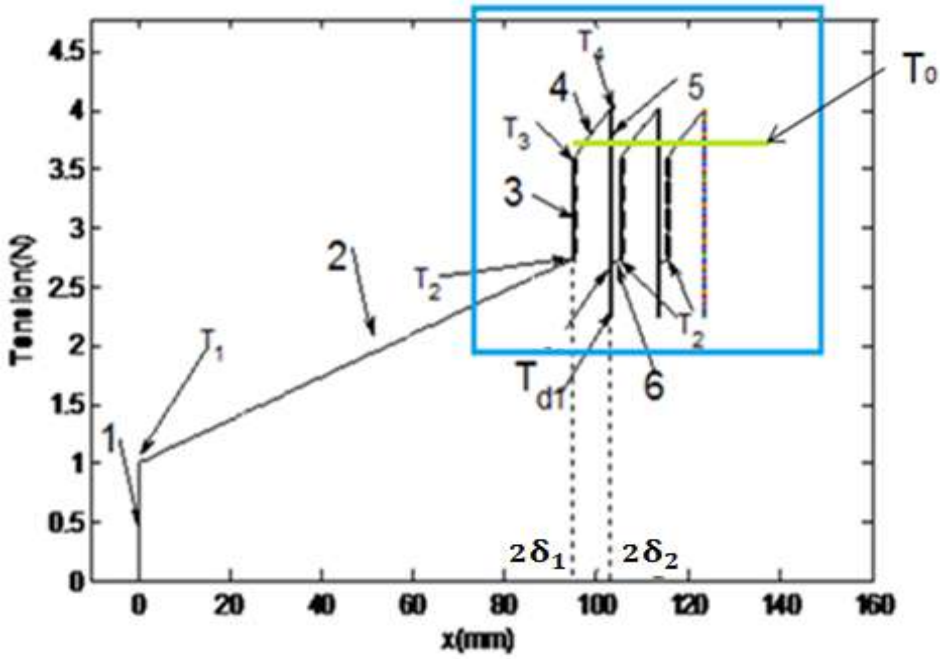

Figure 3.4 Simulation plot and average tension T_0

During braiding process, single carrier mainly goes through two periods, which are two springs compressed period and releasing period. The tension during two spring compressed is shown in equation (9). And the expression of T_4 is shown in equation (10).

$$\text{For } 2\delta_1 < \Delta < 2\delta_2 \quad T = \frac{1}{2}(P_1 + P_2) + \frac{1}{2}k_1\delta_1 + \frac{1}{4}(k_1 + k_2)(\Delta - 2\delta_1) \tag{9}$$

$$\text{For } \Delta = 2\delta_2 \quad T_4 = \frac{1}{2}(P_1 + P_2) + \frac{1}{2}k_1\delta_2 + \frac{1}{2}k_2(\delta_2 - \delta_1) \tag{10}$$

As the tension increases beyond T_3, the pawl starts to slide down the ratchet tooth face of height h in Figure 2.2. Both springs exert a downward force on pulley2/plate. In this region the increase in displacement, Δ, is constrained by the relationship (since l_1=l_2 here for the geometry of this particular tensioning system). In this period, force and moment of braiding point are not absolute balance because all carriers are asynchronous. Even if the releasing period is skipped, the braiding point will still quiver in a very small value because of small difference of symmetric tension in equation (9). Even though the releasing period T_4 to T_{d1} is so short, their effects on the balance of force acting through

the yarns on the braiding point are not ignorable because of the material releasing. Since there are 8 teeth on the gear of the ratchet (Figure 2.1), the nearly instantaneous yarn unwind from the spool rotation is $\pi d/8$, where d is the diameter of plastic spool. The diameter including the thickness added by the yarn previously wrapped on the spool. Hence $\Delta\delta$, the total amount δ drops during release, is: $\Delta\delta = \pi d/16$**.** Actually, the release length of single yarn is set as L_{rl}, which is shown in equation (11). Substituting the values of parameters, the releasing length is about, 10.2mm every time. This releasing period will affect the balance of braiding point a lot. In order to simply the calculation, the tension in single carrier is averaged to T_0=3.6N [13], which is green line in Figure 3.4.

$$L_{rl} = 2\Delta\delta = \frac{\pi d}{8} \tag{11}$$

The left figure of Figure 3.5 is right side view of Figure 3.2. In order to simplify the sketch, the two yarns, the top yarn and the bottom one, are only drawn here. If the bottom yarn is supposed as the releasing yarn in this moment, the equation (7) cannot be satisfied any more. The red cross in Figure 3.5 represents the yarn releases. The braiding point will be moved by the tension, (T_4-T_{d1}) =1.6751N, which is shown in the right figure of Figure 3.5. The tension is called as releasing tension. Here, the braiding point can be treated as a particle. The resultant tension and moment will actuate the braiding point, and then move the rope. Meanwhile, the other end of rope will be an involute around the capstan.

The resultant tension and moment will drive the braiding point, and then move the rope. The moved braiding point causes the changing of braiding angle in every yarn.

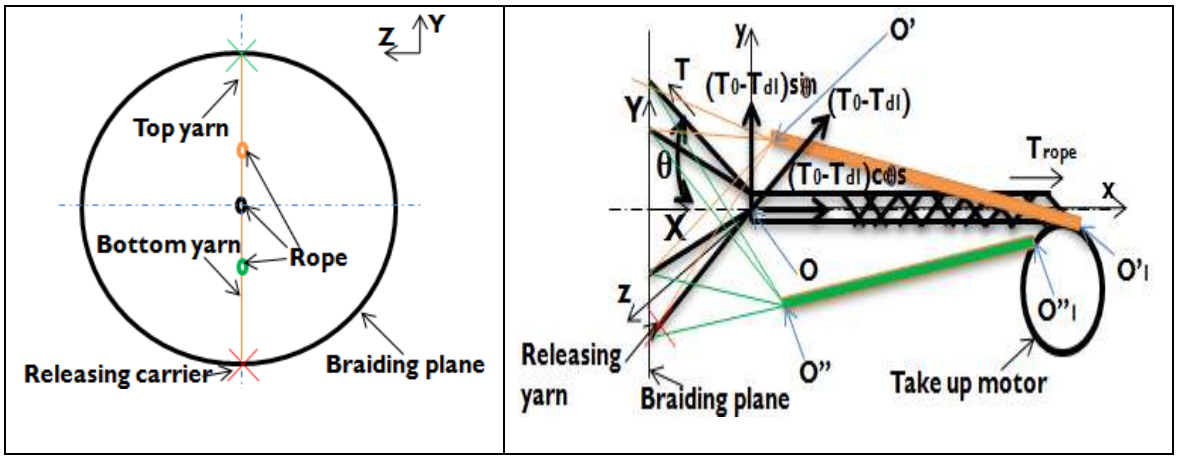

Figure 3.5 Left: Braiding machine showing top yarn, bottom yarn and rope. Right: Freebody diagram of braiding point. When the most bottom yarn releases, the rope will move to the yellow dash line. If the top yarn release, the green dash line is the most bottom location of rope.

Meanwhile, the other end of rope will be involute around the capstan. The resultant tension and moment always change because these angles and tensions in equation (12) are changing with the moved braiding point. Equation (12) represents the moment from releasing tension, and tensions difference of rest of the yarns actuates the rope in the reverse extending direction of the releasing yarn. The braiding angles of the carriers, θ_{bj}, are located at the same half circle of braiding plane with the release yarn. And the angles, θ_{ti}, are located at the other half. The equation represents releasing tension actuates braiding point rotating in XY plane is shown in equation (12).

$$\sum_{ti=1}^{16} T_0 \sin\theta_{ti} = \sum_{bj=1}^{15} T_0 \sin\theta_{bj} + (T_4 - T_{d1})\sin\theta_{16} + T_{rope}\sin\alpha \qquad (12)$$

where $\theta_{ti}, i = 1,2, \ldots 16$ represent the angles of top yarns

$\theta_{bj}, j = 1,2 \ldots 15$ represent the angles of bottom yarns except the most bottom one

During the braiding process, $\theta_{ti}, t\, i = 1,2, \ldots 16$ and $\theta_{bj}, bj = 1,2 \ldots 15$ are also related to the speed at which material is taken off the carrier, which depends on the braiding

machine speed and take up speed. If this speed is slow, the braiding point has enough time to move a full distance. Otherwise, the releasing period will end soon and the tension can rebuild and quickly pull the braiding point back toward the steady state position. The trajectory of braiding point will also change if any other of the 31 other yarns releases. Also, the instant of release of every individual carrier is different and random. It's not possible to exactly calculate the time history of locations of the braiding point. The outermost contour of the braiding point, however, can be determined and located. Note the yellow line, $o'o_1'$ and green line, $o''o_1''$ shown in Figure 3.7. The YZ view of braiding point motion is envisioned in Figure 3.6, based on experimental observation. The blue curve in left figure of Figure 3.6 tracks braiding point motion if only one yarn releases, and demonstrates that it is possible for the maximum calculated displacement to be achievable. However, if more than one yarns release, the trajectory should look like the blue curve in the right figure of Figure 3.6, where maximum calculated displacement is not achieved by this analysis. Hence this analysis reveals an upper expected upper limit of braid point motion. It should be noted that the time for the blues curve in Figure 3.6 to complete their cycle is not the same as the amount of time for a carrier to circle the braiding machine. This calculation will be shown later in this chapter.

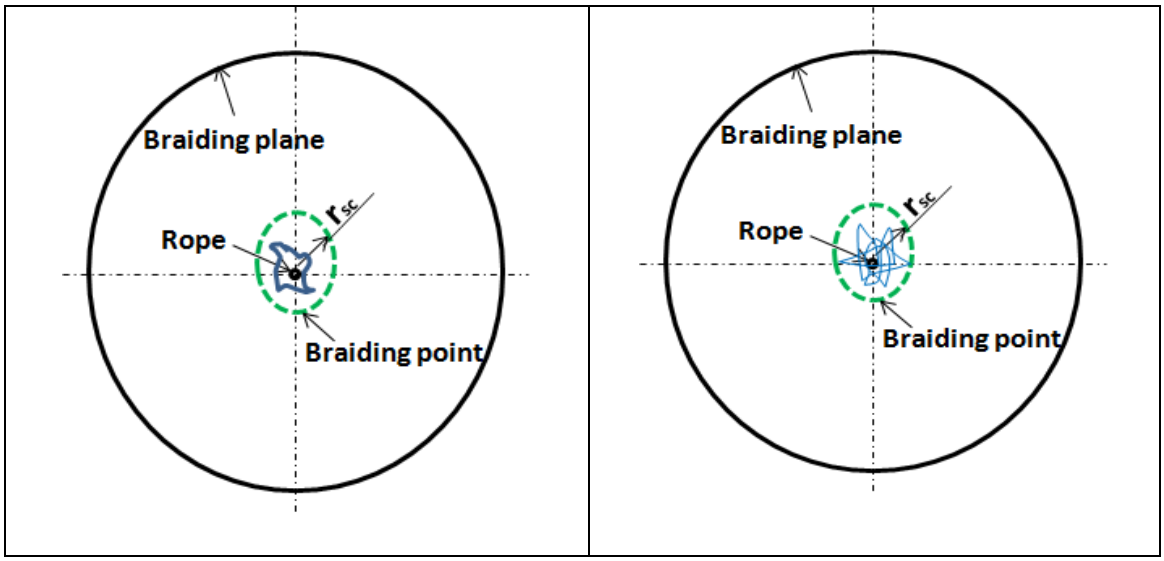

Figure 3.6 The left: the trajectory of braiding point when one yarn releases; The right: the trajectory of braiding point when all yarns releases

Whatever the permutation and combination of releasing yarns are, the trajectory of braiding point will locate on an ellipsoidal cap, which is shown in the shaded areas of Figure 3.7. The base radius and height of the ellipsoidal cap will be getting smaller when the takeup speed of yarns increase. If considering the XY plane, the rope moves like an involute curve around the take up motor's capstan. Setting the base radius and height of the ellipsoidal cap are r_{sc} and h_{sc}, which are shown in Figure 3.7 and Figure 3.8. When $r_{sc}>0$, it is the release of the most bottom yarn, the expressions for r_{sc} \and h_{sc} are shown in equation (13), and the corresponding tensions equations are shown in equation (14). When $r_{sc}<0$, which is the release of the most top yarn, Based on release of the top most yarn, the expressions for r_{sc} and h_{sc} are shown in equation (15), and the corresponding tensions equations are shown in equation (16). Substituting equation (13) to equation (14) and equation (15) to equation (16), respectively, the base radii of ellipsoidal cap are able to be calculated using a nonlinear Newton solver, obtaining, 9.5 mm and 7.2mm

with the parameters in Table 3.1. If considering the XZ plane, the rope moves like a pendulum with constant length. In this case, the equation (13) leads to equation (17).

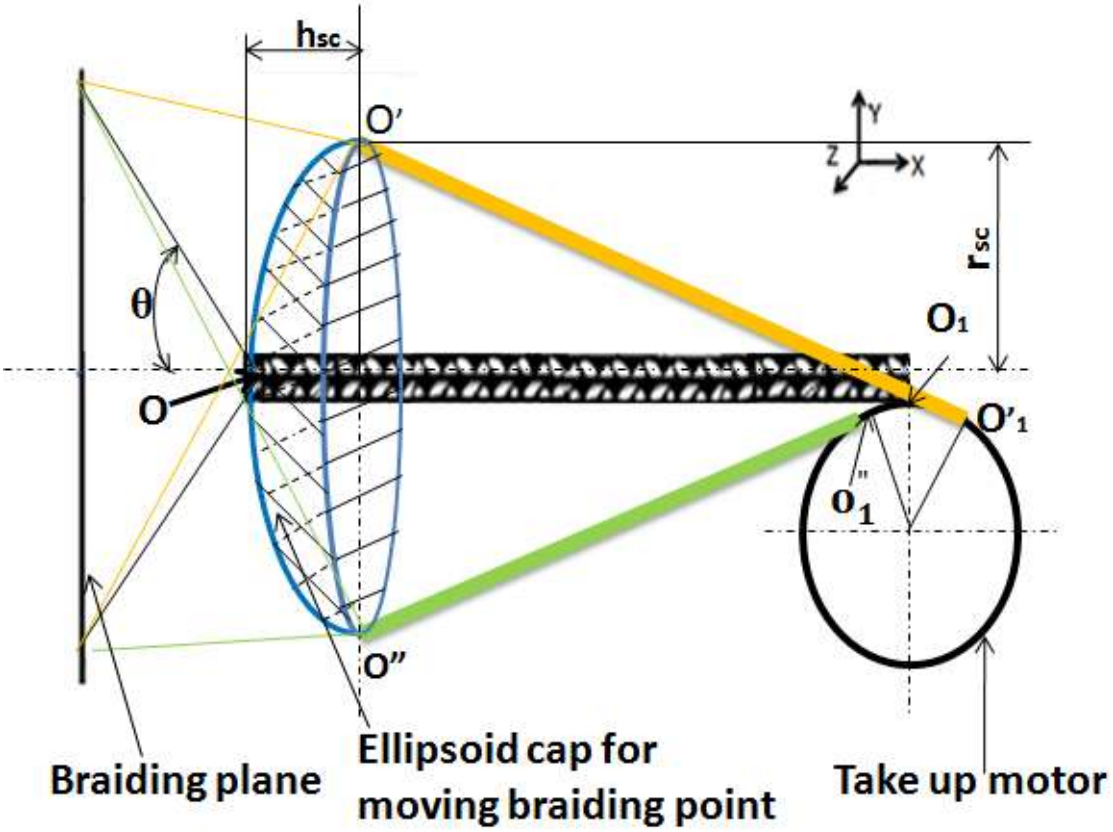

Figure 3.7 The 3D trajectory of braiding point

Parameter	Value	Parameter	Value
Rc	250mm	r_m	150mm
Ap	50mm	L_{rl}	10.2mm
ω	5rpm	r_{rope}	2.5mm
L	3m	H_0	351.5mm
T_0	3.6N	d	26mm

Table 3.1 The value of all parameters used in this paper

Substitute the equation (17) to (14), the base radius in x direction is 4.6mm. So, the ellipsoidal cap has a short horizontal axis of 4.6mm and a long vertical axis of 9.5mm up and 7.2mm down. The height h_{sc} was calculated to be 0.4mm using equations (13) and (15). Using these values, the green dash ellipse is able to be drawn in Figure 3.6. The derivation of (13), (14), (15), (16) and (17) are shown in Appendix A.3.2. These calculations were also based on the dimensions of the take up capstan. If a take up ring is right put at point, O_1, the cap will be ellipsoidal cap with base radius as 4.6 mm.

$r_{sc}>0$ $$\begin{cases} r_{sc} = L\sin\alpha + r_{lc}\alpha\sin\alpha - r_{lc} + r_{lc}\cos\alpha \\ h_{sc} = L - L\cos\alpha - r_{lc}\alpha\cos\alpha + r_{lc}\sin\alpha \end{cases} \quad (13)$$

$$\frac{T_0((R_c+A_p)\sin\frac{\pi}{2}-r_{sc})}{\sqrt{\left((R_c+A_p)\cos\frac{\pi}{2}\right)^2+(H_0+h_{sc})^2+\left((R_c+A_p)\sin\frac{\pi}{2}-r_{sc}\right)^2}} + \sum_{ti=2,6}\frac{2T_0((R_c-A_p)\sin\frac{ti\pi}{16}-r_{sc})}{\sqrt{\left((R_c-A_p)\cos\frac{ti\pi}{16}\right)^2+(H_0+h_{sc})^2+\left((R_c-A_p)\sin\frac{ti\pi}{16}-r_{sc}\right)^2}} +$$

$$\frac{2T_0((R_c+A_p)\sin\frac{\pi}{4}-r_{sc})}{\sqrt{\left((R_c+A_p)\cos\frac{\pi}{4}\right)^2+(H_0+h_{sc})^2+\left((R_c+A_p)\sin\frac{\pi}{4}-r_{sc}\right)^2}} + \sum_{ti=1,3,5,7}\frac{2T_0(R_c\sin\frac{ti\pi}{16}-r_{sc})}{\sqrt{\left(R_c\cos t\frac{i\pi}{16}\right)^2+(H_0+h_{sc})^2+\left(R_c\sin\frac{ti\pi}{16}-r_{sc}\right)^2}}$$

$$= \frac{(T_4-T_{d1})[r_{sc}+(R_c+A_p)\sin\frac{\pi}{2}]}{\sqrt{\left((R_c+A_p)\cos\frac{\pi}{2}\right)^2+(H_0+h_{sc})^2+\left(r_{sc}+(R_c+A_p)\sin\frac{\pi}{2}\right)^2}} + \sum_{bj=2,6}\frac{2T_0(r_{sc}+(R_c-A_p)\sin\frac{bj\pi}{16})}{\sqrt{\left((R_c-A_p)\cos\frac{bj\pi}{16}\right)^2+(H_0+h_{sc})^2+\left(r_{sc}+(R_c-A_p)\sin\frac{bj\pi}{16}\right)^2}} +$$

$$\sum_{bj=0,4}\frac{2T_0(r_{sc}+(R_c+A_p)\sin\frac{bj\pi}{16})}{\sqrt{\left((R_c+A_p)\cos\frac{bj\pi}{16}\right)^2+(H_0+h_{sc})^2+\left(r_{sc}+(R_c+A_p)\sin\frac{bj\pi}{16}\right)^2}} + \sum_{bj=1,3,5,7}\frac{2T_0(R_c\sin\frac{bj\pi}{16}+r_{sc})}{\sqrt{\left(R_c\cos\frac{bj\pi}{16}\right)^2+(H_0+h_{sc})^2+\left(R_c\sin\frac{bj\pi}{16}+r_{sc}\right)^2}} +$$

$$T_{rope}\sin\alpha \quad (14)$$

$r_{sc}<0$ $$\begin{cases} r_{sc} = L\sin\alpha + r_{lc}\alpha\sin\alpha + r_{lc} - r_{lc}\cos\alpha \\ h_{sc} = L - L\cos\alpha + r_{lc}\alpha\cos\alpha - r_{lc}\sin\alpha] \end{cases} \quad (15)$$

$$\frac{T_0((R_c+A_p)\sin\frac{\pi}{2}+r_{sc})}{\sqrt{\left((R_c+A_p)\cos\frac{\pi}{2}\right)^2+(H_0+h_{sc})^2+\left(r_{sc}+(R_c+A_p)\sin\frac{\pi}{2}\right)^2}} + \sum_{ti=2,6}\frac{2T_0[(R_c-A_p)\sin\frac{ti\pi}{16}+r_{sc}]}{\sqrt{\left((R_c-A_p)\cos\frac{ti\pi}{16}\right)^2+(H_0+h_{sc})^2+\left((R_c-A_p)\sin\frac{ti\pi}{16}+r_{sc}\right)^2}} +$$

$$\frac{2T_0((R_c+A_p)\sin\frac{\pi}{4}+r_{sc})}{\sqrt{\left((R_c+A_p)\cos\frac{\pi}{4}\right)^2+(H_0+h_{sc})^2+\left((R_c+A_p)\sin\frac{\pi}{4}+r_{sc}\right)^2}} + \sum_{ti=1,3,5,7}\frac{2T_0(R_c\sin\frac{ti\pi}{16}+r_{sc})}{\sqrt{\left(R_c\cos\frac{ti\pi}{16}\right)^2+(H_0+h_{sc})^2+\left(R_c\sin\frac{ti\pi}{16}+r_{sc}\right)^2}})$$

$$= \frac{(T_4 - T_{d1})(-r_{sc} + (R_c + A_p)\sin\frac{\pi}{2})}{\sqrt{\left((R_c + A_p)\cos\frac{\pi}{2}\right)^2 + (H_0 + h_{sc})^2 + \left((R_c + A_p)\sin\frac{\pi}{2} - r_{sc}\right)^2}} + \sum_{bj=2,6} \frac{2T_0(-r_{sc} + (R_c - A_p)\sin\frac{bj\pi}{16})}{\sqrt{\left((R_c - A_p)\cos\frac{bj\pi}{16}\right)^2 + (H_0 + h_{sc})^2 + \left((R_c - A_p)\sin\frac{bj\pi}{16} - r_{sc}\right)^2}} +$$

$$\sum_{bj=0,4} \frac{2T_0(-r_{sc} + (R_c + A_p)\sin\frac{bj\pi}{16})}{\sqrt{\left((R_c + A_p)\cos\frac{bj\pi}{16}\right)^2 + (H_0 + h_{sc})^2 + \left((R_c + A_p)\sin\frac{bj\pi}{16} - r_{sc}\right)^2}} + \sum_{bj=1,3,5,7} \frac{2T_0(R_c\sin\frac{bj\pi}{16} - r_{sc})}{\sqrt{\left(R_c\cos\frac{bj\pi}{16}\right)^2 + (H_0 + h_{sc})^2 + \left(R_c\sin\frac{bj\pi}{16} - r_{sc}\right)^2}} +$$

$$T_{rope}\sin\alpha \tag{16}$$

$$r_{sc} > 0 \qquad \begin{cases} r_{sc} = L\sin\alpha \\ h_{sc} = L - L\cos\alpha \end{cases} \tag{17}$$

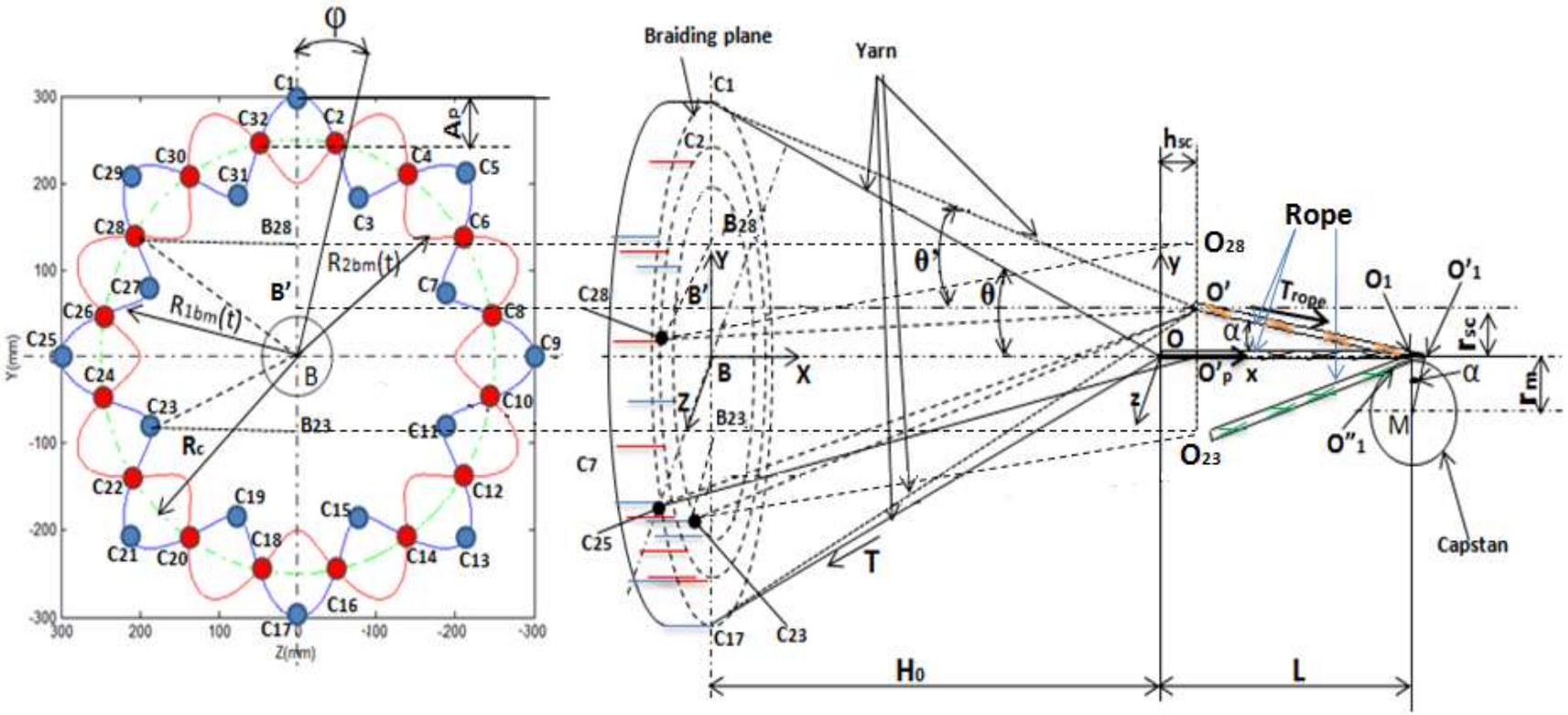

Figure 3.8 3D model of braiding process. Left: Front view of braiding process model. All the carriers marking as C_1…C_{32}; Right: Right side ISO view of braiding process model. All parameters and geometry for calculations are shown.

3.2.2.2 The Change of Braiding Angle

From the Figure 3.8, the geometric expression of braiding angle can be obtained in equation (18). In this section, the change of braiding angle will be discussed during the braiding process. The rotating radius of carriers, r_c, is always supposed to be constant, so the change of braiding angle only depend on H_0. From the above discussion, the two parameters are proved as changing with time. So, the braiding angle is not constant based on the current carriers during braiding process. The Figure 3.9 is shown the plot of braiding angle vs H_0. Since the change of R_c is because of oscillation of braiding point, this change is small and can be ignorable. Even if braided products made from current carriers with mandrel, the braiding angle will also change with time because of the motion of braiding point.

$$\tan\theta = \frac{r_c}{H} \tag{18}$$

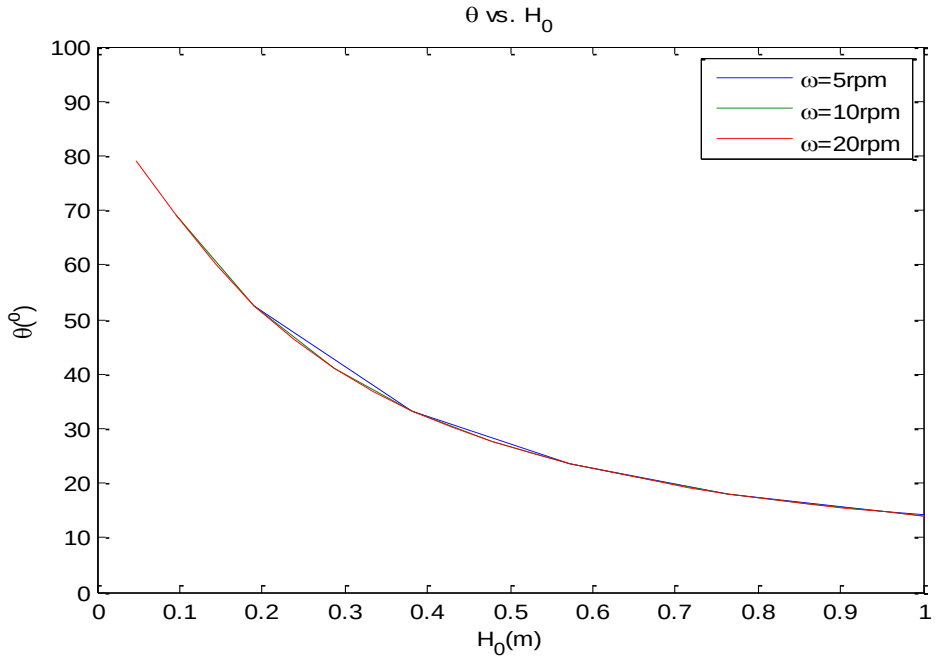

Figure 3.9 The relationship of θ vs H0 for different angular velocities of the braiding machine.

3.2.2.3 Frequency Calculation about Periodic Motion of Braiding Point

If the system is stable, the motion of braiding point will be a periodic process, which is related with the braiding speed, braiding angle and releasing length of a single yarn. If any one of 32 carriers is set as the first carrier that is starting to release, the time period of tension release and rebuild is the time for one period, T_{time}, which is shown in equation (19).

$$T_{time} = L_{rl}/c \tag{19}$$

In the previous work about braiding machine [14], the take up speed of single yarn, c is relative with angular velocity of braiding machine. If the radius of rope is r_{rope}, the equation about c and angular velocity is shown in equation (20).

$$c = (\omega r_{rope}/\sin\theta) \tag{20}$$

Combining with equation (19) and (20), and substitute the values of corresponding parameters in Table 3.1, the period time is calculated as 4.5159s. And therefore the frequency of this periodic motion of braiding point, f (1/T), will be 0.2214Hz.

3.2.3 Dynamic Model of the Braiding Process Close to Steady State

Since the effect of releasing tension to the braiding point cannot be skipped, the equation of motion for braiding point close to its steady state should be investigated in equation (21).

$$T_{rope} - \sum_{i=0}^{3} 8T \frac{H_0}{\sqrt{H_0^2+(R_c+A_p\cos\left(2k\pi+2\pi t+\frac{i\pi}{2}\right))^2}} - b\dot{x} = 32m_{yarn}\overline{\alpha}\overline{e}_r \tag{21}$$

where, m_{yarn} is mass of yarn between braiding plane and braiding point.

b is interaction damping of yarns

3.2.3.1 Calculate the Acceleration of Yarns

Since the yarn also rotates at ω with braiding motor, the yarn should have acceleration. The origin of spherical coordinates is put in braiding point, O. Using spherical coordinates, the acceleration in yarn extension direction, $\bar{e}_r$, will be obtained in equation (22).

$$\overline{\alpha e}_r = \left[\ddot{L}_{yarn} - l\dot{\theta}^2 - L_{yarn}\omega^2 \sin^2(\theta)\right] \tag{22}$$

Obviously, the length of yarn is easy to calculate in equation (23) with $H=H_0+x$, where x is small change of braiding point position. The velocity and acceleration of pulling yarn are obtained by differentiating the equation (23).

$$L_{yarn} = \sqrt{H^2 + R_c^2} = \sqrt{(H_0 + x)^2 + R_c^2} \tag{23}$$

$$\dot{L}_{yarn} = \frac{(H_0+x)\dot{x}}{\sqrt{(H_0+x)^2+R_c^2}} \tag{24}$$

$$\ddot{L}_{yarn} = \frac{l^2(\dot{x}^2+H\ddot{x})-H^2\dot{x}^2}{l^3} = \frac{[(H_0+x)^2+R_c^2](H_0+x)\ddot{x}+R_c^2\dot{x}^2}{[(H_0+x)^2+R_c^2]\sqrt{(H_0+x)^2+R_c^2}} \tag{25}$$

Differentiate the equation (18), $\dot{\theta}$ is able to obtain in equation (26).

$$\dot{\theta} = \frac{-R_c\dot{x}^2}{[(H_0+x)^2+R_c^2]} \tag{26}$$

The acceleration in $\bar{e}_r$ direction is shown in equation (27). Since the yarn cannot have the negative tension, the acceleration only drives on certain length of yarn, L_{yarn}. So, the yarn can be supposed massless since its mass is so small. And the interaction damping of yarns is supposed be zero, too. So, the equation (21) is changing back to equation (8), which braiding point locates at its steady state. And, the neighboring area of steady state of braiding point is considered as steady state.

$$\overline{\alpha e}_r = \left\{\frac{[(H_0+x)^2+R_c^2]H\ddot{x}-R_c^2\dot{x}^2}{[(H_0+x)^2+R_c^2]\sqrt{(H_0+x)^2+R_c^2}} - \sqrt{(H_0+x)^2+R_c^2}\left(\frac{1}{[1+\left(\frac{R_c}{H}\right)^2]^2}\right) - \sqrt{(H_0+x)^2+R_c^2}\omega^2\frac{R_c^2}{(H_0+x)^2+R_c^2}\right\} \tag{27}$$

$$\text{So,}\quad \sum F_r \approx 0\left\{\frac{[(H_0+x)^2+R_c^2](H_0+x)\ddot{x}-R_c^2\dot{x}^2-(H_0+x)^4-R_c^2\omega^2((H_0+x)^2+R_c^2)}{(\sqrt{(H_0+x)^2+R_c^2})^3}\right\}=0$$

3.2.3.2 Determine the Tension inside Carriers

The steady state of braiding point is part of the dynamic braiding process. The yarns always unwind from the carriers and braided rope will be wound onto the take up motor's capstan. As discussed in section 2.2.1, the tension inside a single carrier always changes from T_2 to T_4 and release to T_{d1} during the braiding process. Actually, the system works in period between T_3 and T_4 in most of time of braiding process. The release and rebuild period works only in 0.163% of whole braiding process (0.0163s, which is shown in Figure 2.20 when take up speed=10mm/min). The releasing tension is 1.3N, which is only 1.13% of T_{rope}. The tension doesn't change so much, however, the release length of yarn is about 10.2mm. Since the mass of yarns and rope are ignorable, the braiding point could be move very quickly even if very small releasing tension. It will let braiding point move about full distance of releasing material if the time is enough. Even though their effects to the balance of force and moment are ignorable and the elapsed time of these effects is very short, the braiding point will still quiver during moving period because of difference of symmetric forces and moments of 32 carriers. In addition, all the carriers are asynchronous. It's not possible to know what time one carrier will release when 32 carriers are considered together. Since the releasing tension doesn't affect braiding point too much in x direction, the calculation are able to be simplified by the tensions of all carriers averaged as T_0, which is shown is Figure 3.5. And the equation of motion of braiding point can be expressed in equation (28). During the braiding process, the tension in single carrier will be $T_0 + w_i$, where w_i is process disturbance and intertwining friction

of single yarn. T_0 is actually expectation of tension in single carrier. And the standard variance are able to be calculated using the data of precious work as σ=0.3N.

$$T_{rope} = \sum_{n=1}^{32} T_n \cos\theta = 32T_0\cos\theta + w_n\cos\theta \quad (28)$$

Where, n represent the index of carriers.

From equation (28), the initial force produced by load torque of take up motor is $T_{rope,0}=32T_0\cos\theta$. Basing on those parameters, the equation (28) is also used to analysis dynamic model of braiding machine.

3.3 Experiment Setting Up and Position Acquiring Program

Based on the simulation in the above section, position of braiding point will be measured by machine vision sensing program based on Labview software in PC. Using USB camera acquire the position data of braiding point, the program will find the braiding point pattern, transfer to position data and write this data to a file automatically.

3. 3.1 Experiment Setting Up

In this chapter, the position of braiding point is only tracked to check the simulation. USB camera could be simply put close to braiding point pattern without touching the object. The take up motor can be any motor, which could produce certain constant speed as needed. Controlling program is based on position of braiding point machine vision sensed. The present camera is philips spc 900nc/00, which acquire the images by 320x240[pixel] and 30 fps.

Figure 3.10 is a visual representation of the machine vision sensing hardware including some actual components and their connectivity. The USB camera is the main

part for image acquiring, which acquires the template of braiding point pattern. Machine vision program will process these images acquired in Labview software.

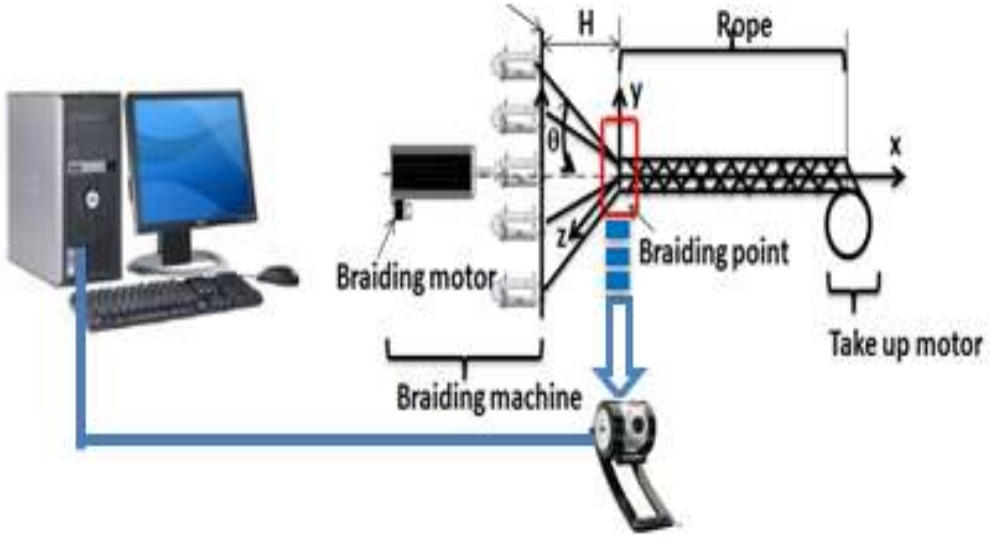

Figure 3.10 Sketch of braiding machine with controller and fabric product

3.3.2 Control Program

Labview is very powerful in image processing. Labview software has a series of powerful tools or commands to acquire images, process them, learn them and recognize them. Using machine vision, USB camera could be used for image acquirement and PC is used to process image. In this chapter, how to acquire the position data of braiding point is only discussed. The controlling program will go through a few steps to get the position data, which is shown in flow chart of Figure 3.11. How these commands acquire position data and how they work will be talked about in next chapter in details. And the front panel of Labview program is shown in Figure 3.12. Actually, this front panel is more like the control board of real machine.

The window in the middle of front panel is monitor window for acquiring images. After you start to run the program, the monitor start to acquire an image per 50ms

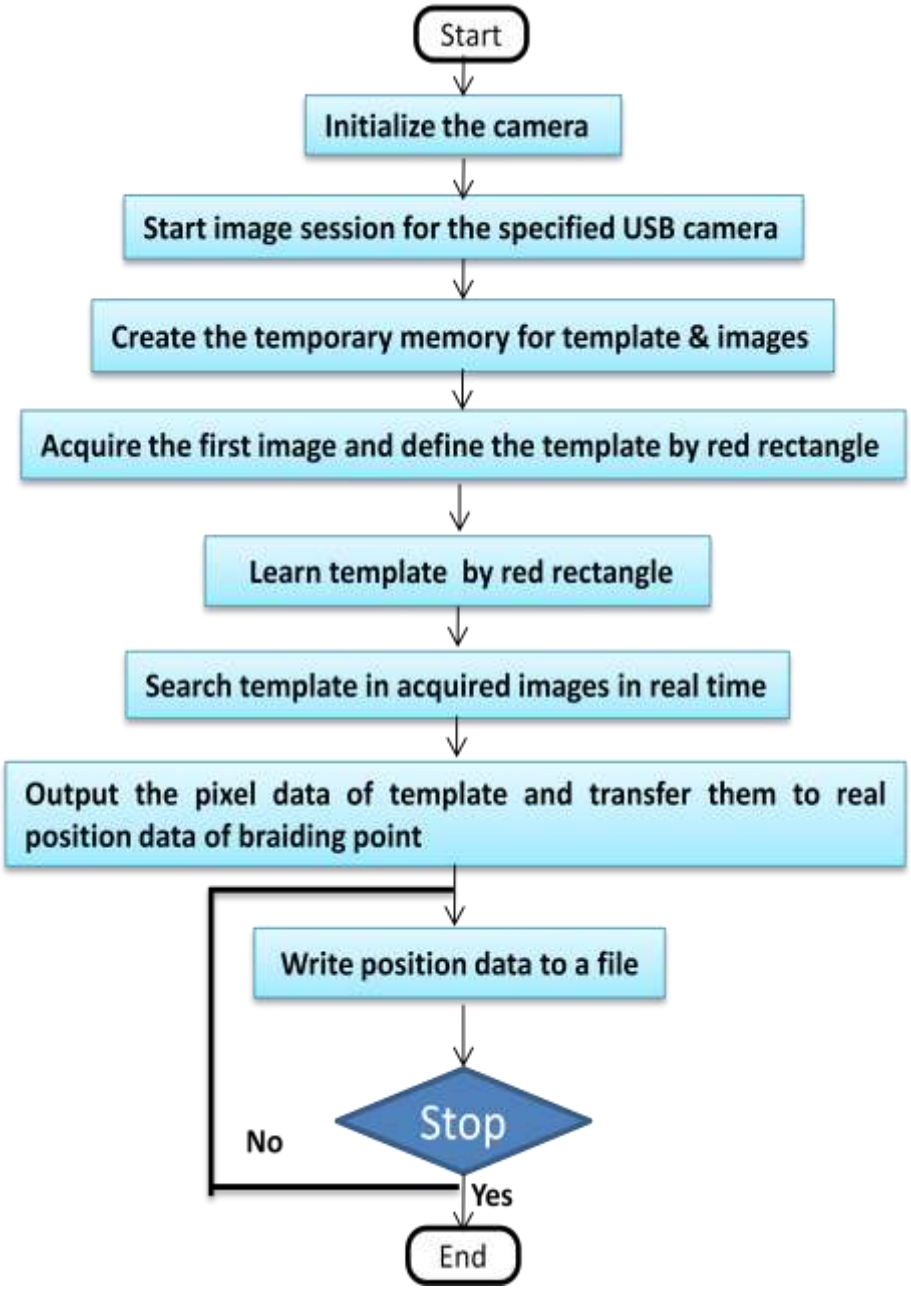

Figure 3.11 Flow chart of control program

automatically. Under the current camera, philips spc 900nc/00, the images grabbed by camera are RGB images, which will be needed to convert to grayscale, 8 bit images. Then, the template will be defined in image acquiring window by red rectangle. The red rectangle is drawing on our Region of Interest (ROI), braiding point. The centroid of

rectangle will be located right on the braiding point. After defining the template, the program will learn the template if the “learn” button is pressed. Then you should push the search button in order that the program can recognize the template in the new image acquired automatically. When the program recognizes the position of braiding point, the program will write these data to a file automatically.

Because the yarns and rope are continuously interlaced with each other and always move, the program may miss some frames of acquired image. This means that the braiding point pattern in new images cannot match the template. If this is because the poor light conditions in background of images, the corresponding threshold needs to be set. This is shown in “Mini Score” indicator of Figure 3.12. If there is an accidently big move of braiding point, the posture of yarns may need to be adjusted or the carriers need to be fixed.

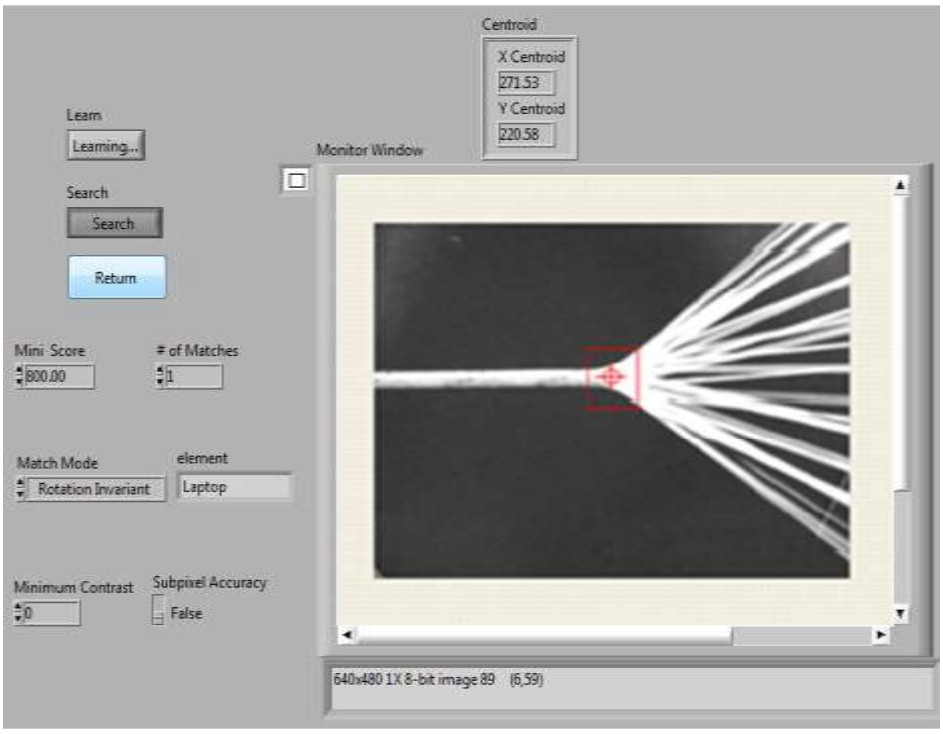

Figure 3.12 Front panel of control program

3.4 Correlation between Simulation and Experimental Data

In order to confirm our simulations, a lot position data of braiding point is acquired automatically using our controlling program. And using MATLAB code, the experimental data validate simulations. It turns out the controlling program works well. And experimental data also confirm our simulation well.

3.4. 1 Ellipsoidal Cap

Since two cameras cannot be used at the same time (Labview cannot support), 3D position data of braiding point cannot be able to be obtained at the same time. However, planar data are able to be obtained in Figure 3.13, 3.14 and 3.15, respectively. Figure 3.13 is showing YZ view of braiding point with unit, mm. A green dash circle is also drawn to

compare with right figure of Figure 3.6. The measured points outside green circle may be caused by many neighboring carriers releasing or one carrier being stuck. The diameter of this green dash circle in Figure 3.13 is maximum displacement between two different locations of braiding point. The base radiuses in Figure 3.13 are long axis about 8.5mm and 6mm and short axis close to 5mm, which are close to the values calculated. And Figure 3.14 and Figure 3.15 are showing the base radius and height of ellipsoidal cap in XY view and XZ view, respectively. The height is about 1 to 1.5mm, which is really small comparing with the base radius. In Figure 3.16, the braiding points mostly locate in the range from -10mm to 15 mm of Y axis (r_{sc}), which confirm the long axis of ellipsoidal cap. In Figure 3.15, the braiding points mostly locate in the range from -10mm to 10 mm of Z axis (r_{sc}), which confirm the short axis of ellipsoidal cap.

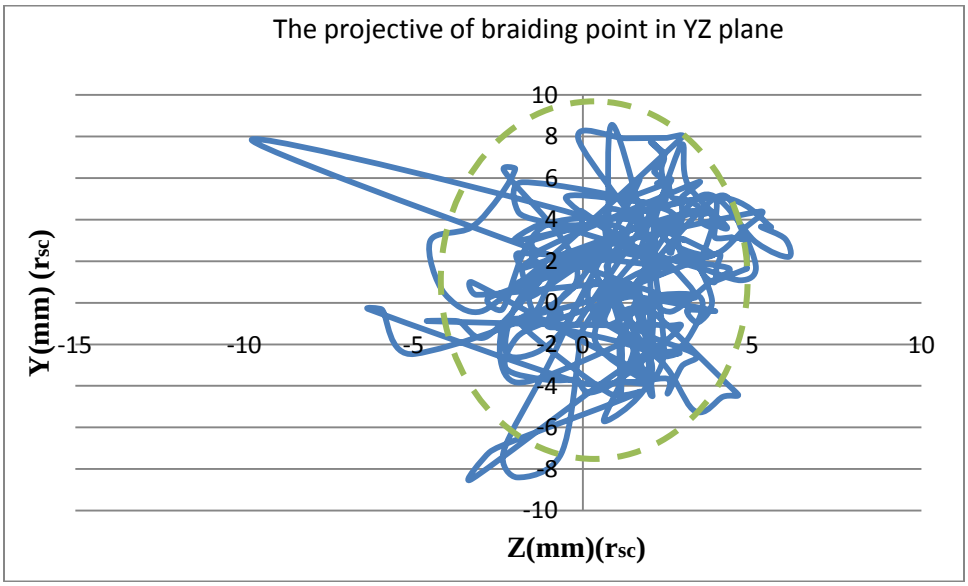

Figure 3.13 Calculated braiding point envelope in YZ view (green dash circle). Experimental braiding point envelope (blue lines) in YZ view.

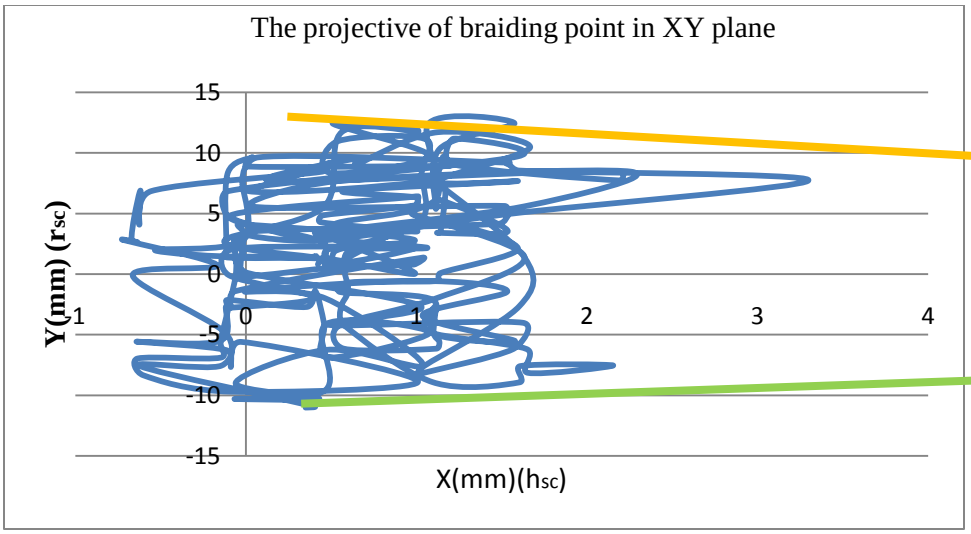

Figure 3.14 Calculated braiding point envelope in XY view (green dash circle). Experimental braiding point envelope (blue lines) in XY view.

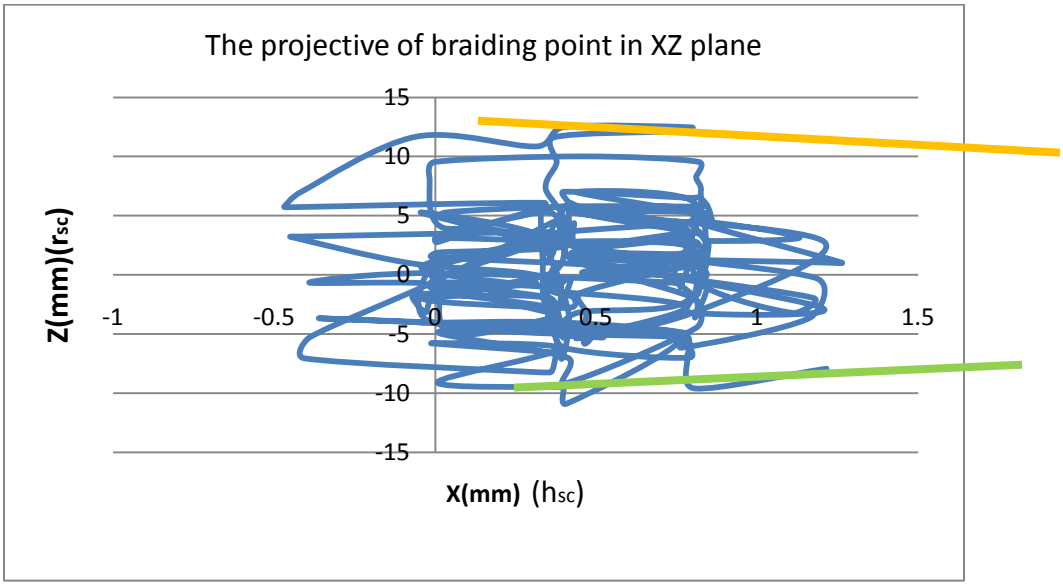

Figure 3.15 Calculated braiding point envelope in XZ view (green dash circle). Experimental braiding point envelope (blue lines) in XZ view

3.4.2 Frequency for Periodic Motion of Braiding Point

The measured position data is shown in Figure 3.16, which acquired from braiding point near its steady state. The little sawtooth is caused by the smallest unit of

camera at 0.40625mm/pixel. Actually, the experimental plot has some little oscillations, which confirms the mathematical model of braiding point in section 3.2.2. From Figure 3.16, green lines are used to mark every trough of one period. One period time is the time between two green lines. It is about 5s, which is close the period time, T=4.5159s, which is calculated in equation (19). The period time of carrier, T_c, experimental period time of oscillation and corresponding frequencies, f_c, f_{oc}, f_{oe} are summarized in Table 3.2.

Period time	T_c	T_{time}	T_{oe}
Value	1.5s	4.5159s	5s
Frequency	f_c	f_{oc}	f_{oe}
Value	0.667Hz	0.2214Hz	0.2Hz

Table 3.2 The value of all periods and frequencies used in this paper

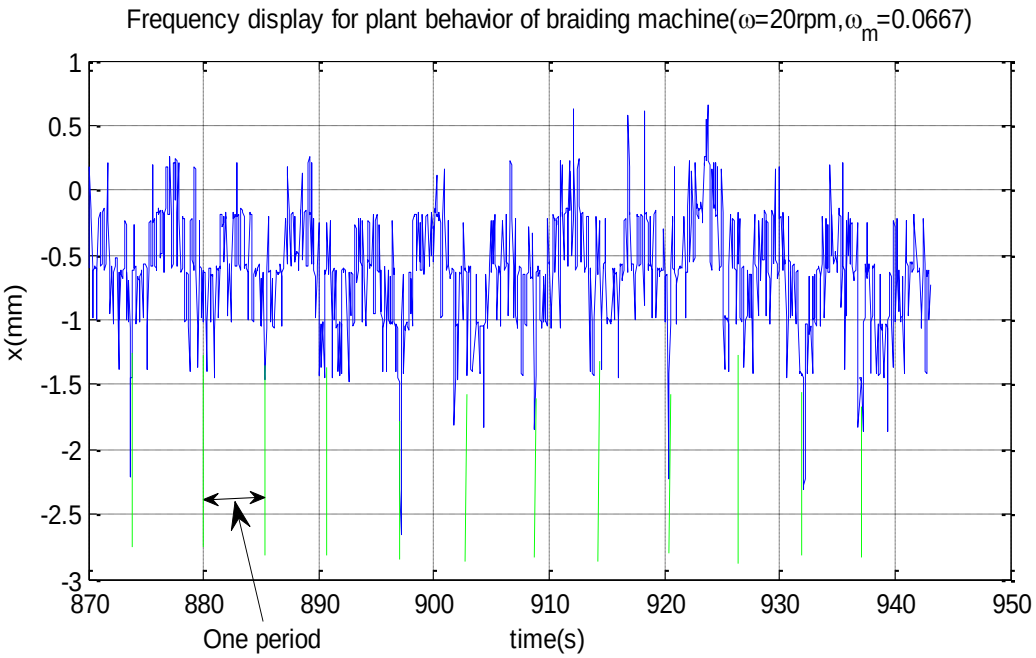

Figure 3.16 Displaying frequency of oscillation of braiding point, the period between two green lines marking troughs is one period

3.5 Conclusion

This chapter presented approaches to model the braiding process. To achieve these goals, the static and dynamic model of braiding process is analyzed at first. The braiding process based on motion of braiding point is defined. Then, MATLAB code is used to calculate the base radius and height of ellipsoidal cap. And how rotating radius of carrier affects the motion of braiding point is discussed, too.

Then, experiment and use Labview program is set to track braiding point. Using machine vision sensing methods in Labview software, the position of braiding point is acquired automatically. And the experimental data with simulation is correlated using MATLAB code. As you see, the experimental data validates simulation pretty well.

3.6 List of References

[1] Burkhard Wulfhors, Thomas Gries, Dieter Veit, *Textile Technology*, pp. 188.

[2] D. Bigaud, L. Dréano, P. Hamelin, "Models of interactions between process, microstructure and mechanical properties of composite materials—a study of the interlock layer-to-layer braiding technique," *Composite Structure* v67, pp 99-114, 2005.

[3] N. Tolosana, S. V. Lomov, A. Miravete, "Development of a geometrical model for a 3d braiding unit cell based on braiding machine emulation," *Finite element modeling of textiles and textile composites*, St-Peterburg, Sep, 26-28, 2007. http://www.mtm.kuleuven.be/Research/C2/poly/NewWWW/research/downloads/sl_modelling_3D_braids_paper.pdf.

[4]Werner Scherzinger, "Braiding Machine", US Patent #5,787,784, 1949.

[5] Bull et al., "Apparatus for control of moving strands fro rotating strand supply bobbins, "Braiding Machine," US Patent #4,535,674, 1985.

[6] Frank K. Ko, "Braiding," in *Engineered Materials Handbook,* ASM International, Metals Park, OH, 1987, pp. 519-528.

[7] Amit Rawal, Prasad Potluri, "Geometrical modeling of the yarn paths in three-dimensional braided structures," *Journal of industrial textiles*, v35, I 2, p 115, 2005.

[8]Du, G.W. , Popper, P., "Analysis of a circular braiding process for complex shapes," *Journal of the Textile Institute*, v 85, n 3, p 316-337, 1994.

[9] A. C. Long, "Process modelling for liquid moulding of braided performs,"

International Conference on Automated Composites, Bristol, ROYAUME-UNI (22/09/1999) 2001, vol. 32, n° 7 (81 p.) (24 ref.), pp. 941-953.

[10] Bull et al, "Carrier for a strand supply bobbin," *Braiding Machine*, US Patent #4, 529, 147, 1985.

[11] C. Pastore and F. Ko, "CIM of Braided Preforms for Composties", *Computer Aided Design in Composite Material Technology, Proceedings of the International Conference*, Southampton, 1988, pp.135-155.

[12]Similarly, Ebler, N. A., Arnason, R., and Michaelis, G., "Tension Control: Dancer Rolls or Load Cells," *IEEE Trans. Ind. Appl*., 29, No. 4, 1993,pp. 727–739.

[13] Guangli Ma, David Brancomb, David G. Beale, "Modeling of the Tensioning System on a Braiding Machine," *Elsevier Editorial System(tm) for Mechanism and Machine Theory (in review).*

[14] Zhang, Q, Beale, D., Broughton, R., "Analysis of Circular Braiding Process: Part I: Theoretical Investigation, " *ASME Journal of Manufacturing Science and Engineering*, August 1999, 121: 345-350.

3.7 Appendices

A.3. 1The Derivation of Equilibrium Equation of Braiding Point

The path track of carriers is shown in Figure 3.3. There are actually two similar paths. One path is for carriers rotating in clockwise direction. And the other is for carriers rotating counter clockwise direction. The radius of base circle is R_c, which is always constant. The mathematical expression of base circle in Cartesian coordinates is shown in equation (A.1.1).

$$\begin{cases} Y = R_c \sin(\varphi) \\ Z = R_c \cos(\varphi) \end{cases} \tag{A.1.1}$$

Where, φ is rotating angle of carriers in the pathtracks, which is shown in Figure 3.3. Since carriers are also following the cosine curve, R_c will change with rotating angle. The periodogram of cosine curve is smallest periodogram in this pathtrack and supposed to be 2π. Within one periodogram of base circle, there are eight periodograms of cosine curve, which are marked as green circle in Figure 3.3. When cosine curve completes one periodogram, the rotating angle of base circle will complete $\frac{2\pi}{8}$. That means value of φ is $\frac{\pi}{4}$ when cosine curve complete its one periodogram. The blue curve in Figure 3.3 is supposed as the path track of carriers rotating in clockwise direction. And the red one is for carriers rotating in counterclockwise direction. The amplitude of cosine curve is A_p. The radius of the blue curve is set as $R_{1bm}(t)$, which is shown in equation (A.1.2) and Figure 3.3. And the rotating radius of the red curve is set as$R_{2bm}(t)$, which is shown in equation (A.1.3) and Figure 3.3. The index of every periodogram of path track is set as k, which is shown as green circle 0,1,2,3…,7, in Figure 3.3. The time, t, inside these

equations is elapsed time when rotated angle of a carrier is about φ. Their relationship is shown in equation (A.1.4).

$$R_{1bm,k}(t) = R_c + A_p \cos(2k\pi + 2\pi t) \tag{A.1.2}$$

where, k=0,1,2 ….7

$$R_{2bm,k}(t) = R_c + A_p \cos(-(2k+1)\pi - 2\pi t) \tag{A.1.3}$$

where, k=0,1,2 ….7, and negative sing inside cosine function means carriers rotating in this path are in counterclockwise direction.

$$\varphi = k\frac{\pi}{4} + \frac{\pi}{4}t \tag{A.1.4}$$

Replacing the R_c in equation (A.1.1) by equation (A.1.2) and (A.1.3) and combining with equation (A.1.4), the mathematical expression of blue cure can be obtained in equation (A.1.5) and expression of red cure in equation (A.1.6), respectively.

$$\begin{cases} Y = (R_c + A_p \cos(2\pi t))\sin(\frac{\pi}{4}t) \\ Z = (R_c + A_p \cos(2\pi t))\cos(\frac{\pi}{4}t) \end{cases} \tag{A.1.5}$$

$$\begin{cases} Y = (R_c + A_p \cos(-\pi - 2\pi t))\sin(-\frac{\pi}{4}t) \\ Z = (R_c + A_p \cos(-\pi - 2\pi t))\cos(-\frac{\pi}{4}t) \end{cases} \tag{A.1.6}$$

Using the equation (A.1.5) and (A.1.6), the path tracks are able to be plotted in Figure 3.3. In this section, however, the rotating radius of carriers is only considered using the equations (A.1.2) and (A.1.3), whose plots are shown in Figure A.3.1. Figure A.3.1 is only showing the rotating radiuses of blue curve and red curve. Center point, B, in Figure 3.3 is actually zero of R_{1bm} or R_{2bm} axis in Figure A.3.1.

These rotating radii are used to calculate resultant tensions of all carriers. Now, the expressions of rotating radius need to be written about every carrier. There are 32 carriers in this system. The index of them is mark as C_n in Figure 3.3. From the highest

carrier, it is marked as C_1. Then, C_2, C_3… C_{32} are marked in clockwise direction. Also, these symbols are representing the locations of 32 carriers in this moment. Comparing Figure 3.3, there are same marks in Figure A.3.1. In this moment, carrier C_1 is highest and its location is supposed as starting point, which is in first periodogram, k=0 and i=0 from equation (5). The mathematical expression of its rotating radius just likes $R_{1bm,1}(t)$ in equation (A.1.2) and φ =0. Carriers C_5, C_9, C_{13}, C_{17}, C_{21}, C_{25}, C_{29} are including in equation (A.1.2) and k=1, 2, 3, 4,5,6,7, respectively.

For the carrier C_2, it locates in red cosine curve. And the mathematical expression of its radius is shown in equation (A.1.7) and k=0.

$$R_{2bm,k}(t) = R_c + A_p \cos\left(-(2k+1)\pi - 2\pi t + \frac{\pi}{2}\right) \quad \text{(A.1.7)}$$

where, k=0,1,2,3, …7.

Transforming equation (A.1.7) to equation (A.1.8)

$$R_{2bm,k}(t) = R_c + A_p \cos\left(2k\pi + 2\pi t + \frac{\pi}{2}\right) \quad \text{(A.1.8)}$$

where, k=0,1,2,3, …7.

Comparing equation (A.1.8) with equation (A.1.2), carrier C_2 has phase shift about $\frac{\pi}{2}$ relative to carrier C_1. It seems carrier 2 locate in blue path. Actually, the value for rotating radius of carriers in red curve just likes that in blue curve. Comparing Figure 3.3, the carriers in blue curve of Figure A.3.1 are moving to right direction and carriers in red curve are moving to left direction. After this moment, whichever direction carriers in red curve are moving to, their rotating radius is keeping same value. So, all carriers are in blue curve are only considered with phase shift. Similarly, the phase shift of carrier C_3 is π comparing to carrier C_1. The expression of its rotating radius is shown in equation

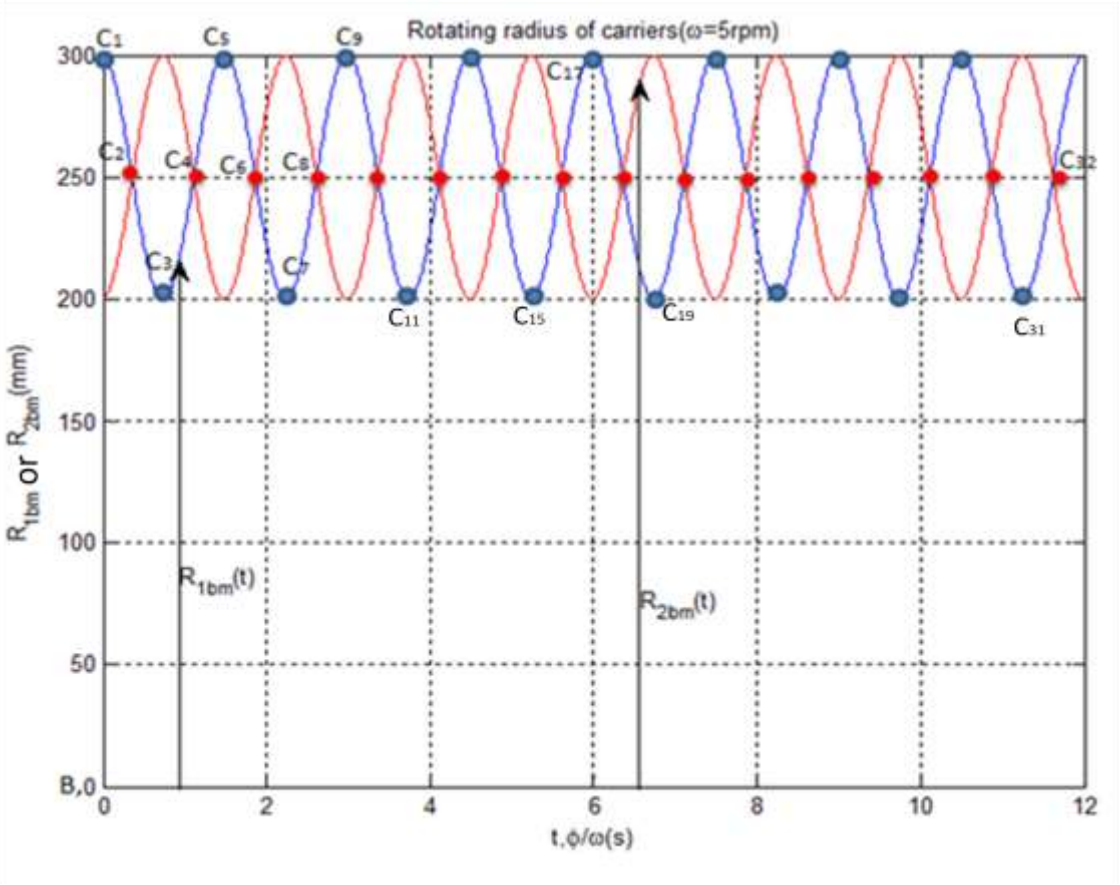

Figure A.3.1 Transforming the rotating radius of carriers from Figure 3.8

(A.1.9) and k=0. And carrier C_4 has its similar expression in equation (A.1.10) with phase shift, $\frac{3\pi}{2}$ and k=0.

$$R_{1bm,k}(t) = R_c + A_p\cos(2k\pi + 2\pi t + \pi) \quad \text{(A.1.9)}$$

where, k=0,1,2,3, …7.

$$R_{1bm,k}(t) = R_c + A_p\cos(2k\pi + 2\pi t + \frac{3\pi}{2}) \quad \text{(A.1.10)}$$

where, k=0,1,2,3, …7.

As all know, the phase shift between any two neighboring carriers is $\frac{\pi}{2}$ and π between any two neighboring carriers in same curve. So, carriers C_6, C_{10}, C_{14}, C_{18}, C_{22}, C_{26}, C_{30} are including in equation (A.1.8) and k=1, 2, 3, 4,5,6,7, respectively. Carriers C_7, C_{11}, C_{15}, C_{19}, C_{23}, C_{27}, C_{31} are including in equation (A.1.9) and k=1, 2, 3, 4,5,6,7,

respectively. And carriers C_8, C_{12}, C_{16}, C_{20}, C_{24}, C_{28}, C_{32} are including in equation (A.1.10) and k=1, 2, 3, 4,5,6,7, respectively. Now, the expressions of rotating radius are obtained for all the carriers. They are separated by four groups, which are expressed by four equations. Since rotating radius of carriers are considered in same path, blue cosine curve or red cosine curve, the one equation of the rotating radius of carriers is written as equation (A.1.11). The sub index, i, is for the four carriers in one periodogram.

$$R_{1bm,k,i}(t) = R_c + A_p \cos\left(2k\pi + 2\pi t + \frac{i\pi}{2}\right) \quad \text{(A.1.11)}$$

where, k=0,1,2,3, …7, and i=0,1,2,3.

In Figure 3.8, the original location of braiding point locates point, O. The origin of universal coordinate is put in point, B. The length of line OB, H_0, is distance between braiding point and braiding plane. In order to investigate the X component of resultant tension, the cosθ, which is shown in equation (A.1.12), should be calculated. Simplifying the equation (A.1.12), the tension of these 32 carriers in X direction is able to be described as equation (A.1.13). In this derivation section, resultant tension is meant to be X component of resultant tension except special notice.

$$\cos\theta = \frac{H_0}{\sqrt{H_0^2 + R_{bm}^2(t)}} = \frac{H_0}{\sqrt{H_0^2 + (R_{1bm,k,i}(t))^2}} \quad \text{(A.1.12)}$$

where, k=0,1,2,3, …7, and i=0,1,2,3.

$$T_{rope} - \sum_{i=0}^{3} 8T\cos\theta = T_{rope} - \sum_{i=0}^{3} 8T \frac{H_0}{\sqrt{H_0^2 + (R_c + A_p \cos\left(2k\pi + 2\pi t + \frac{i\pi}{2}\right))^2}} = 0 \quad \text{(A.1.13)}$$

Using equation (A.1.13), a lot plots are got with different H_0. In Figure A.3.2, the resultant tensions of 32 carriers are so close between value getting form constant radius of base circle and that getting from changing rotating radius. Their difference is only 0.08N comparing resultant tension, 88.5N. The real resultant tension should like the blue curve in Figure A.3.3. Its value has a little oscillation with amplitude, 0.001N. This

oscillation could be actually ignored comparing the total resultant tension. Two curves of resultant tension are coming to together, which showed in Figure A.3.4 with tension axis from 0 to 89N. When H_0 decreases, this means braiding point moves closely to braiding plane. The difference of resultant tension between the value getting from R_c and that from $R_{1bm,k,i}(t)$ increases. But, the difference is still really small. This plot is shown in Figure A.3.5 with H_0=200mm. And the resultant tension from R_c is also smaller than that from $R_{1bm,k,i}(t)$. The resultant has a little oscillation with amplitude, 0.002N, which is shown in Figure A.3.6. If H_0 is changed to 600mm, the results are shown in Figure A.3.7. In this time, the resultant tension getting from R_c is bigger than that getting from $R_{1bm,k,i}(t)$. Even if the oscillation is pretty small and two calculated resultant tension are close, the best H_0 is still needed to find. Error and trial, H_0=351.5mm, in which the resultant tensions are shown in Figure A.3.8. The resultant tension from R_c is right in the middle of oscillated resultant tension from $R_{1bm,k,i}(t)$. the resultant tension getting from R_c is supposed equal to that from $R_{1bm,k,i}(t)$.

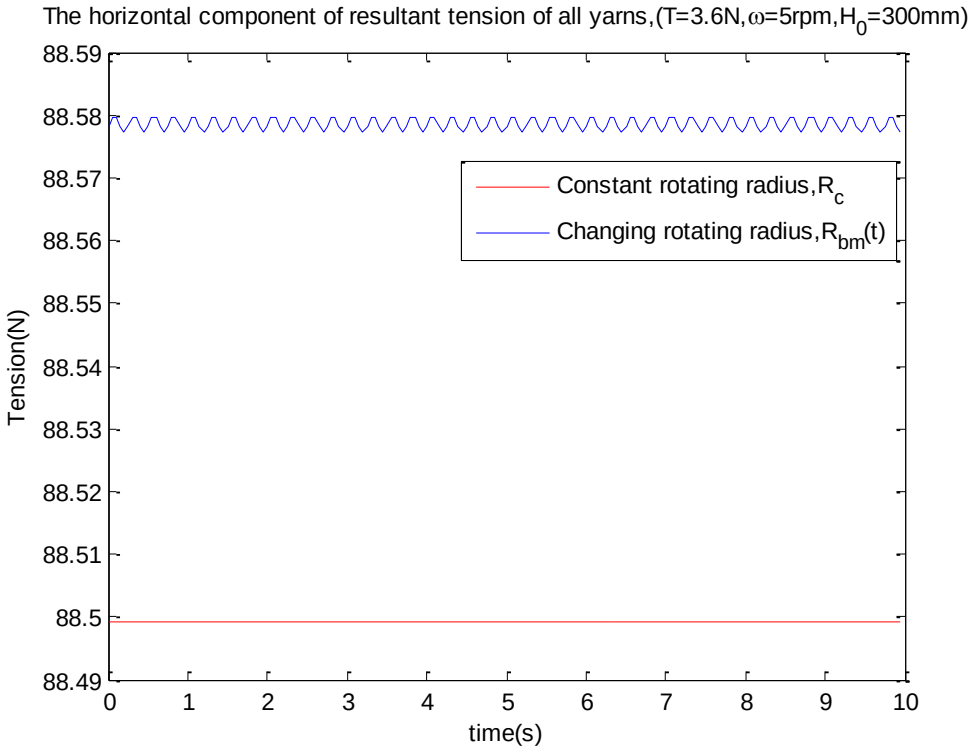

Figure A.3.2 Resultant tension plots of all yarns from constant rotating radius and $R_{1bm,k,i}(t)$

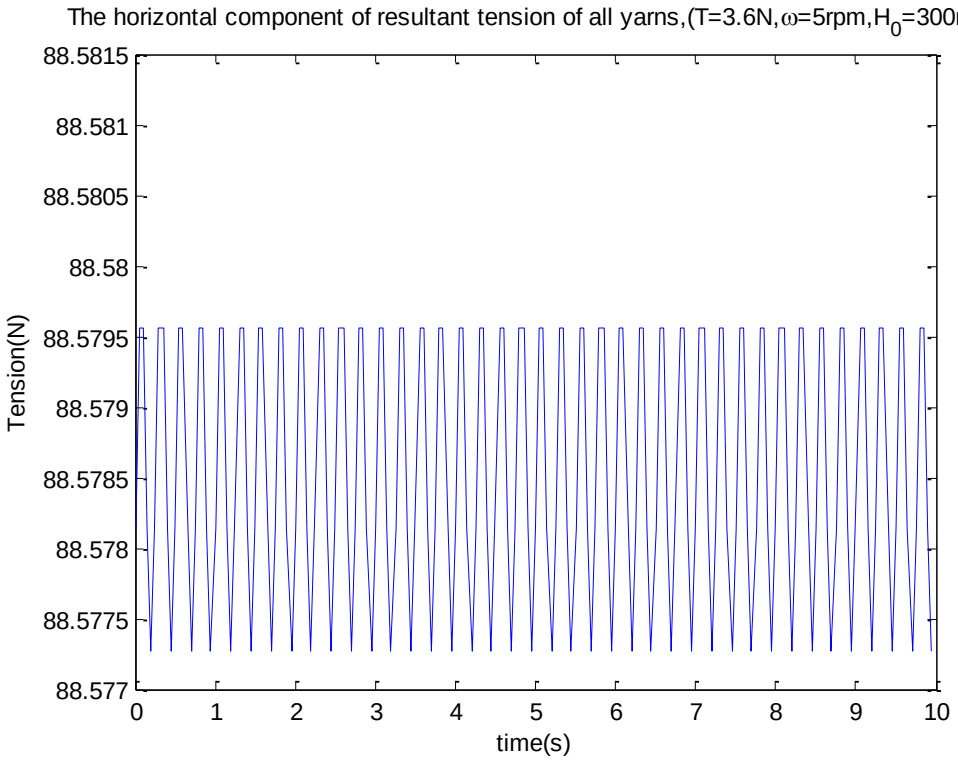

Figure A.3.3 Resultant tension of all yarns plot from $\mathbf{R_{1bm,k,i}(t)}$

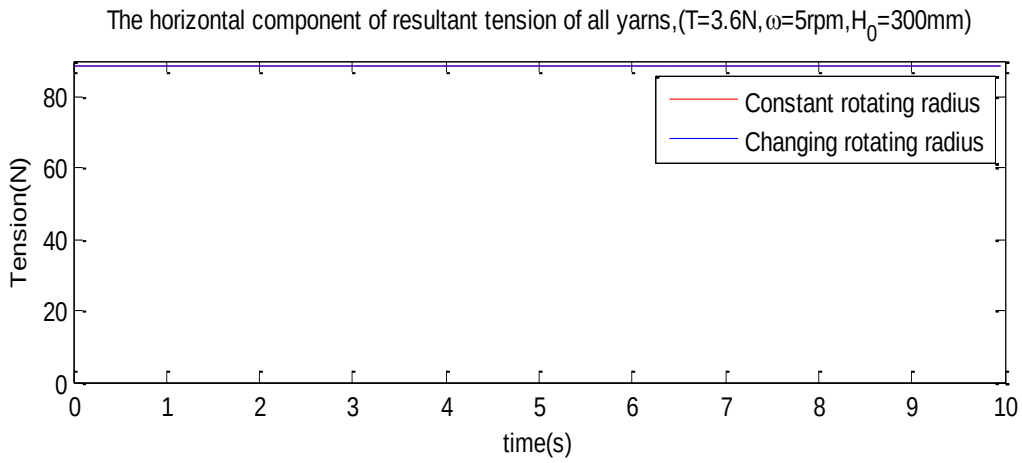

Figure A.3.4 Resultant tension plots of all yarns from constant rotating radius and $\mathbf{R_{1bm,k,i}(t)}$ in full Y scale.

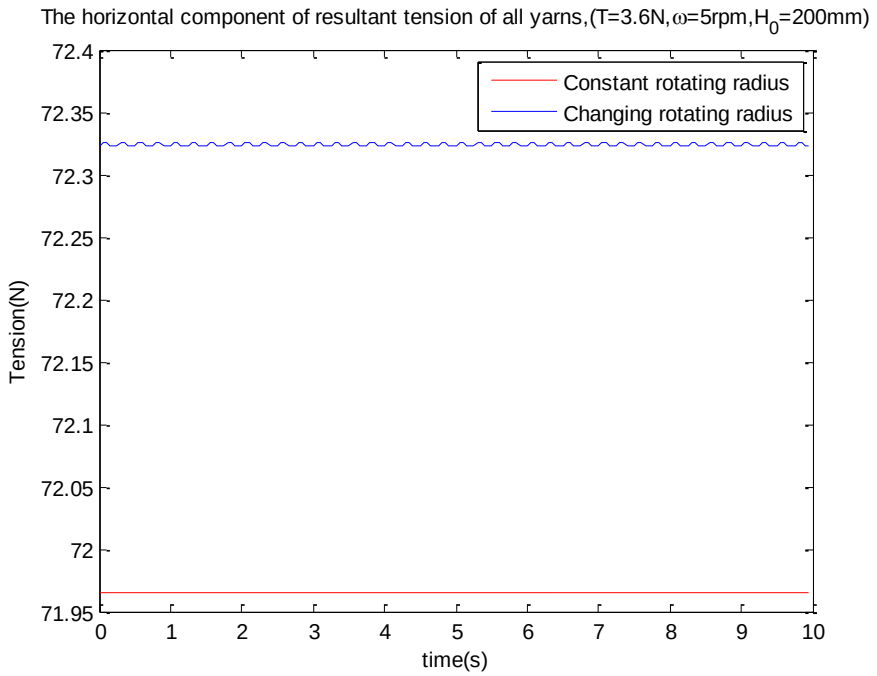

Figure A.3.5 Resultant tension plots of all yarns from constant rotating radius and $R_{1bm,k,i}(t)$ in H_0=200mm

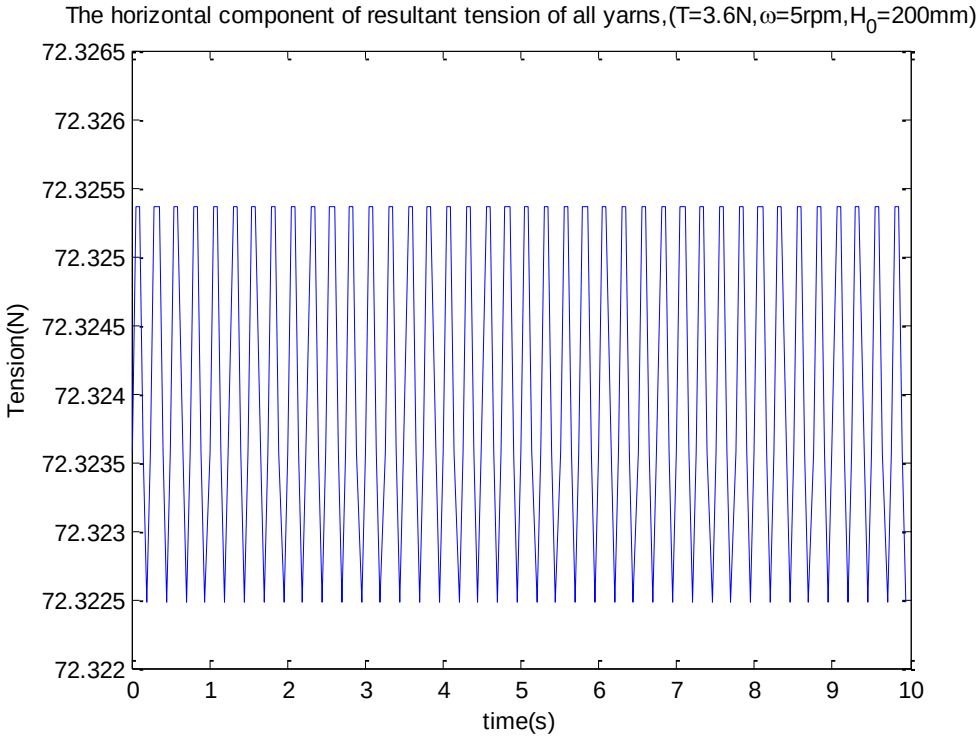

FigureA.3.6 Resultant tension plot of all yarns from $R_{1bm,k,i}(t)$in H_0=200mm

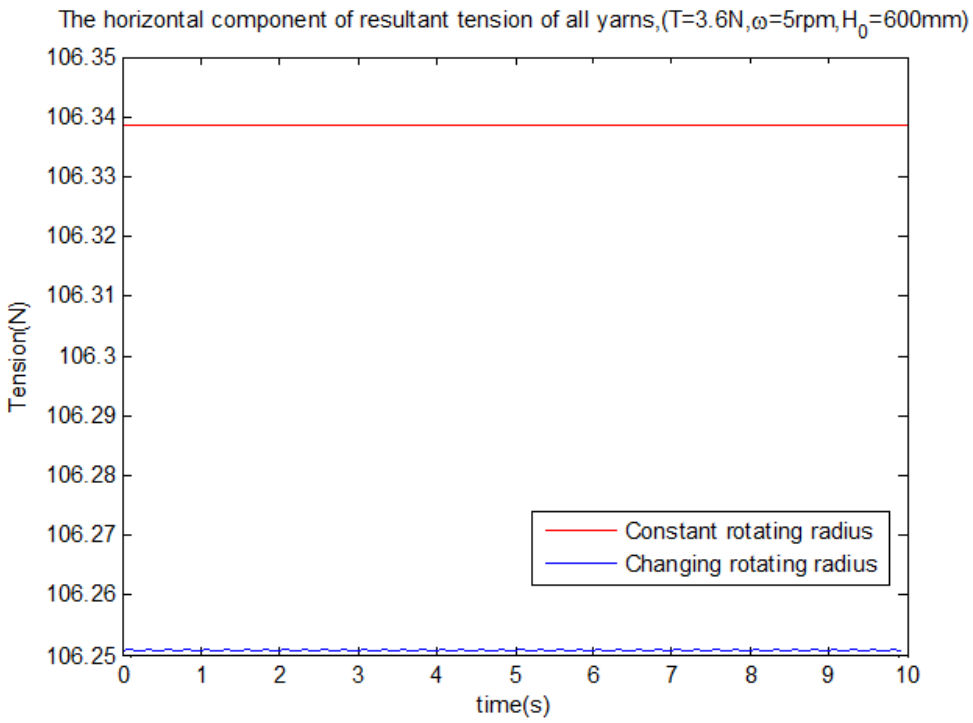

Figure A.3.7 Resultant tension plots of all yarns from constant rotating radius and $R_{1bm,k,i}(t)$ in H_0=600mm

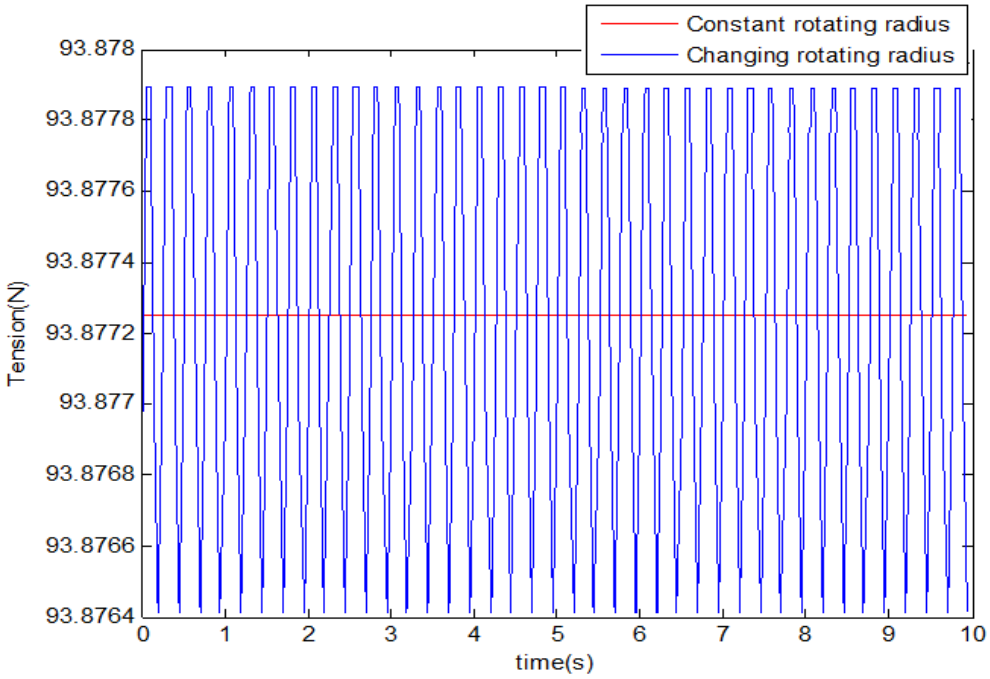

Figure A.3.8 Resultant tension plots of all yarns from constant rotating radius and $R_{1bm,k,i}(t)$ in H_0=351.5mm

The different quantities of carriers and different combinations of carriers are also tried to use. Some really interesting results are found. In Figure A.3.9, 16 carriers is studied and picked up from every first two carriers in any periodogram of their path track. The plot is noticed with relative big oscillation. And the resultant tension cannot be accepted as constant and this combination cannot be used in experiment or real products producing. It is the same as in Figure A.3.10, which is getting from the resultant tension of picking up the every second and third carriers in any periodogram of pathtrack. And it's not doubt for picking up the last two carriers in any periodogram of pathtrack. When the first two carriers in first periodogram and the second two carriers in second periodogram of pathtrack are picked up, that means 4 different carriers with different phase shift in those four different groups of carriers are picked up and the total amount of carriers are still 16. The resultant plot is shown in Figure A.3.11, in which the oscillation decreases. That means the better resultant tension could be also obtained if the same amount of carriers are picked up in each group of four groups of carriers. The much better resultant tension of 16 carriers is shown in Figure A.3.12, in which the oscillation is ignorable. These above combinations are considering keeping the circular balance of braiding point. For the Figure A.3.13 and A.1.14, the first 16 carriers and second 16 carriers are picked up, respectively. Even if the good X component of resultant could be obtained, the circular resultant tension is not balanced.

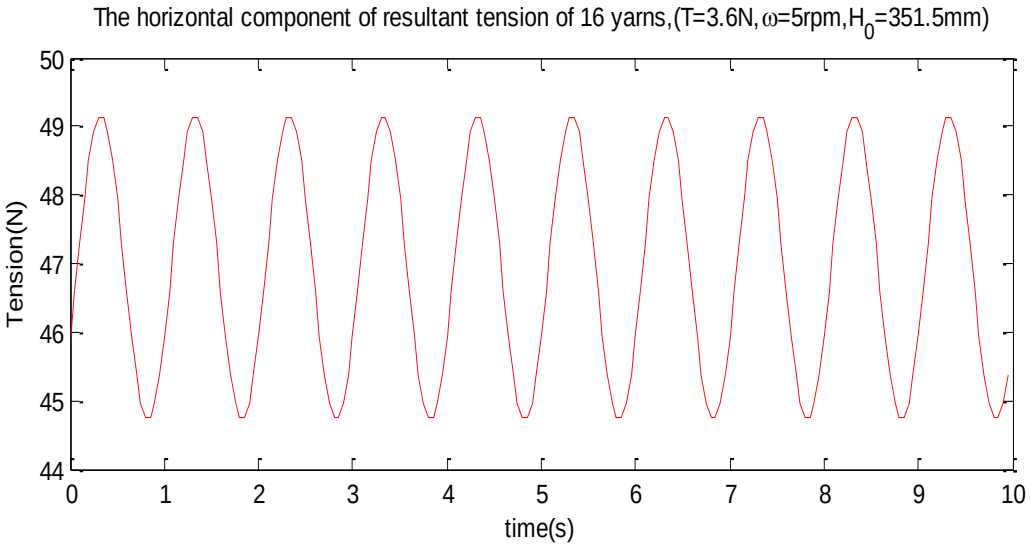

Figure A.3.9 Pick up the first two carriers in every periodogram at 16 yarns

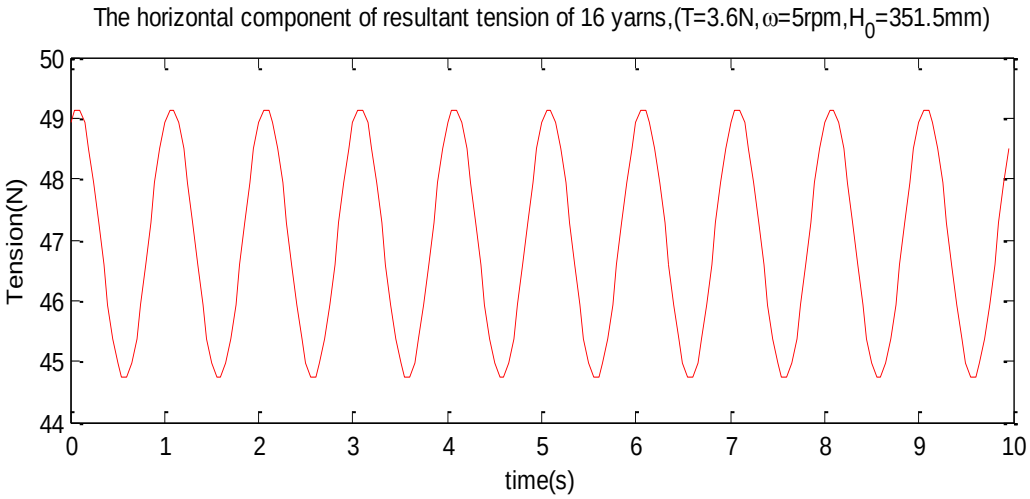

Figure A.3.10 Pick up the second and third carrier in every periodogram at 16 carriers

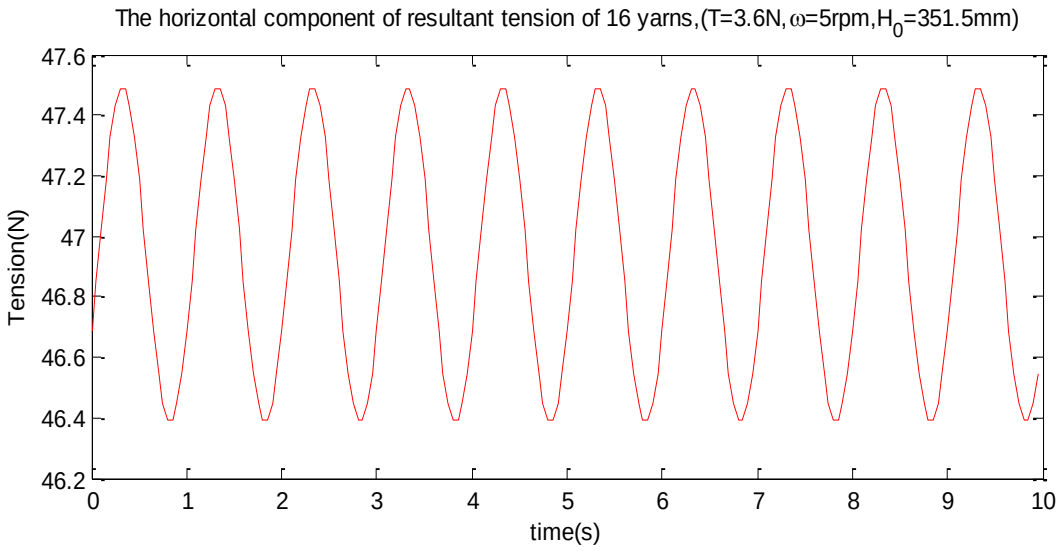

Figure A.3.11 Pick up the first two in one periodogram and the second two in the other periodogram at 16 yarns

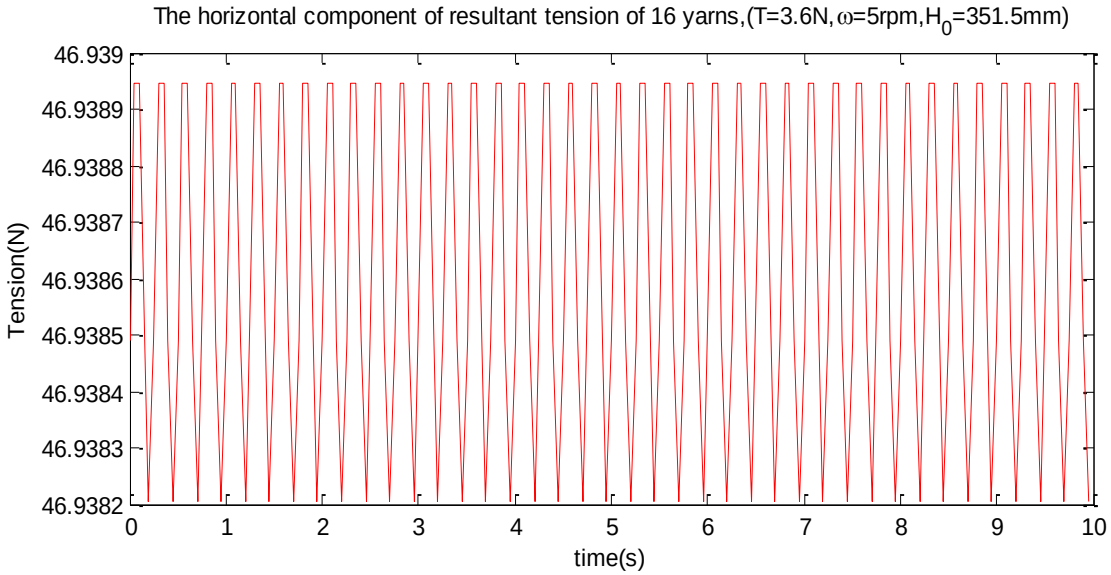

Figure A.3.12 Pick up the second and third in one periodogram and the first and fourth in the other periodogram at 16 yarns

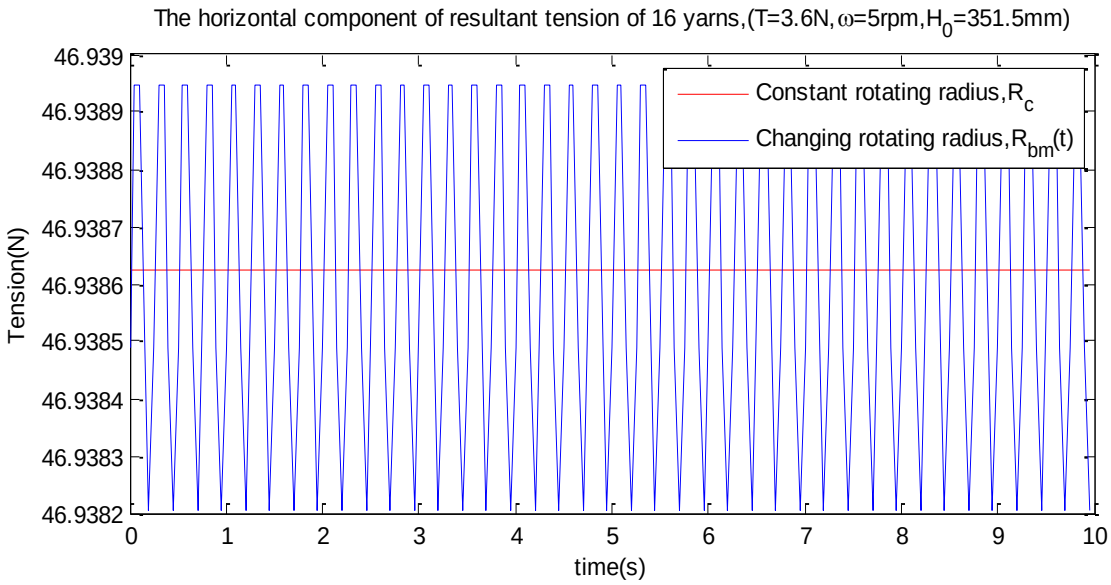

Figure A.3.13 Pick up the first 16 yarns

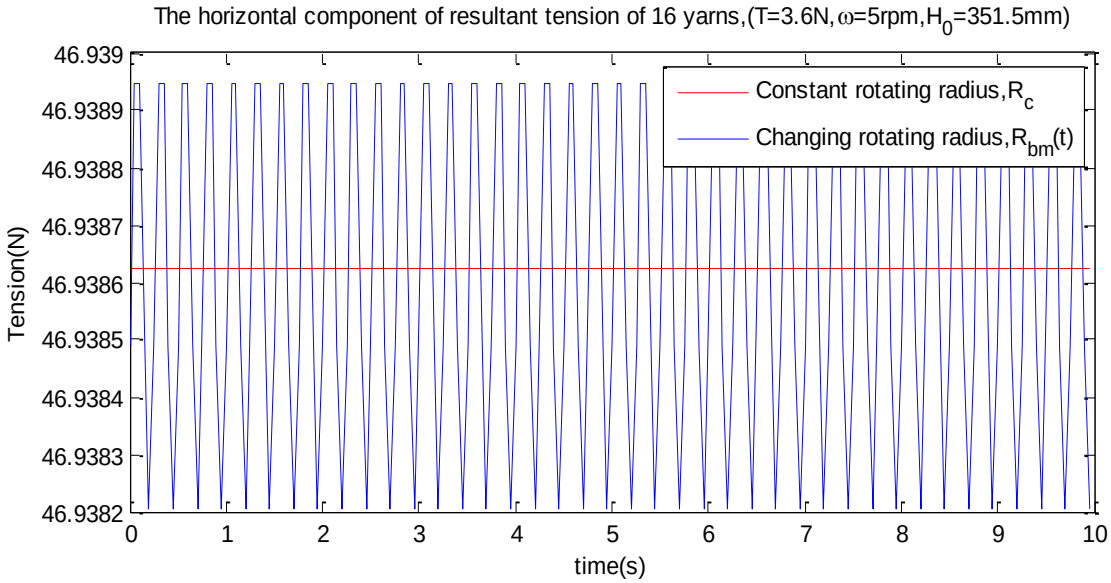

Figure A.3.14 Pick up the second 16 yarns

A.3.2 The Derivation of Base Radius and Height of Elliptic Cap

The Figure A.3.15 is zoomed in from Figure 3.8, which is shown the 3 D model of braiding process during releasing period. The braiding point locates point, O. the tangent point of rope with capstan locates in point, O_1. The line OO_1 is original location of rope. The length of line OO_1 is L. The rotating angle is α. When the most bottom yarn release, the braiding point moves to point O' in xy plane. In this section, braiding point moving in xy plane and yz plane is only discussed. And tangent point of rope with capstan involutes to O_1'. The line $O'O_1'$ is supposed the most top border of moved rope. Except the original length of rope, L, the length of rope has certain increment, $r_1\alpha$, which is involute curve from O_1 to O_1' in the perimeter of capstan. The angle, α, is rotating angle of rope

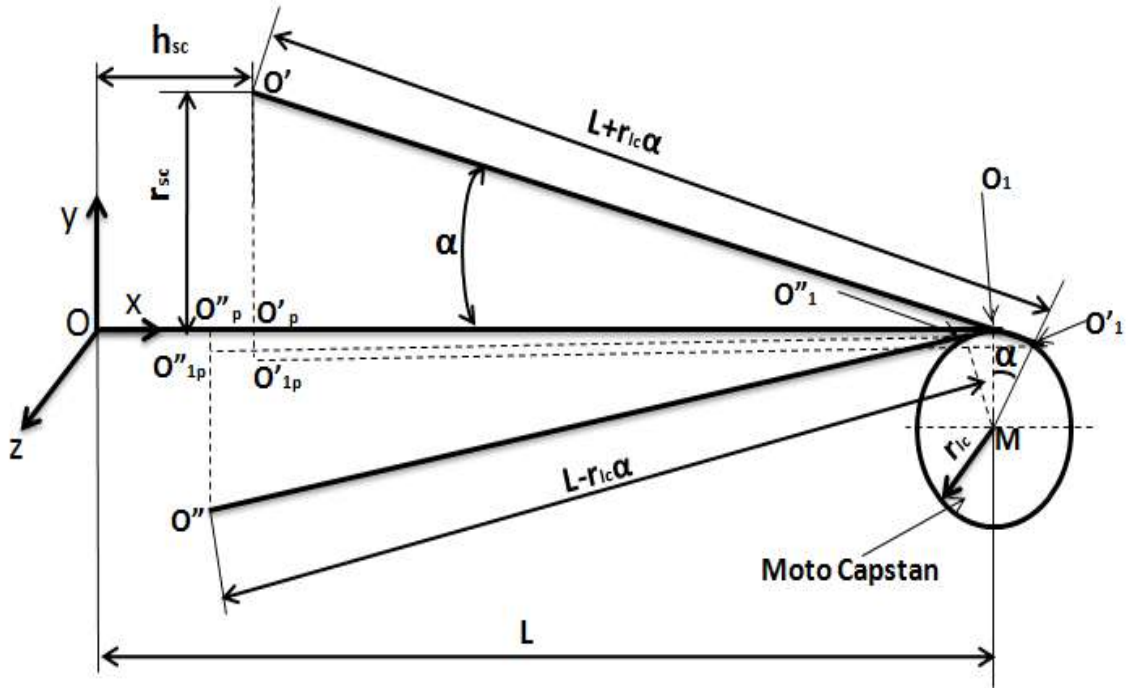

Figure A.3.15 The zoom in geometric model of moving rope

from original location. And the line $O''O_1''$ is supposed the most bottom border of moved rope. The braiding point moves to point O". And tangent point with capstan locates in O_1''. Except the original length of rope, L, the length of rope has certain decrement, $r_1\alpha$.

For the line $O'O_1'$, its length includes arc length $\widehat{O_1O_1'}$ and L. In Figure A.3.15, the perpendicular point of O' on x axis is set at O_p'. The y component of O' in equation (A.2.3) can be calculated by the expressions in equation (A.2.1). Also, x coordinate of O' can be obtained using expressions in equation (A.2.2). Combining with equation (A.2.1), the coordinates of braiding point, O' are able to derived in equation (A.2.3).

$$\begin{cases} \widehat{O_1O_1'} = r_{lc}\alpha \\ O'O_1' = L + r_{lc}\alpha \\ O_p'O_{1p}' = r_{lc} - r_{lc}\cos\alpha \\ y_{O'} = O'O_{1p}' - O_p'O_{1p}' \\ O'O_{1p}' = O'O_1'\sin\alpha \\ y_{O'} = O'O_1'\sin\alpha - O_p'O_{1p}' = (L + r_{lc}\alpha)\sin\alpha - (r_{lc} - r_{lc}\cos\alpha) \end{cases} \quad \text{(A.2.1)}$$

$$\begin{cases} O_{1p}'O_1' = O'O_1'\cos\alpha \\ x_{O'} = x_{O_1'} - O_{1p}'O_1' \\ x_{O_1'} = OO_1 + r_{lc}\sin\alpha \\ x_{O'} = OO_1 + r_{lc}\sin\alpha - O'O_1'\cos\alpha = L + r_{lc}\sin\alpha - (L + r_{lc}\alpha)\cos\alpha \end{cases} \quad \text{(A.2.2)}$$

$$\begin{cases} x_{O'} = L + r_{lc}\sin\alpha - L\cos\alpha - r_{lc}\alpha\cos\alpha \\ y_{O'} = L\sin\alpha + r_{lc}\alpha\sin\alpha - r_{lc} + r_{lc}\cos\alpha \end{cases} \quad \text{(A.2.3)}$$

Actually, the coordinates, $x_{O'}$ and $y_{O'}$, are the height and base radius of ellipsoid cap, respectively. If the base radius and height are set r_{sc} and h_{sc}, their expressions in equation (A.2.4) could be obtained, this equation is called equation (14) in paper. The sign of r_{sc} really means it is on the top of x axis when the sign is positive and on the bottom of x axis if the sign is negative. Using the similar principle, the coordinates of O" are obtained as equations (A.2.5) and (A.2.6). Similarly, the base radius and height of ellipsoid cap are expressed in equation (A.2.7), which is equation (16) in the paper.

$$r_{sc}>0 \qquad \begin{cases} r_{sc} = L\sin\alpha + r_{lc}\alpha\sin\alpha - r_{lc} + r_{lc}\cos\alpha \\ h_{sc} = L - [L\cos\alpha + r_{lc}\alpha\cos\alpha - r_{lc}\sin\alpha] \end{cases} \quad \text{(A.2.4)}$$

$$y_{O''} = (L - r_{lc}\alpha)\sin\alpha + y_{O_1''} = (L - r_{lc}\alpha)\sin\alpha + (r_{lc} - r_{lc}\cos\alpha) = L\sin\alpha - r_{lc}\alpha\sin\alpha + r_{lc} - r_{lc}\cos\alpha \quad (A.2.5)$$

$$x_{O''} = x_{O_1''} - (L - r_{lc}\alpha)\cos\alpha = (L - r_{lc}\sin\alpha) - (L\cos\alpha - r_{lc}\alpha\cos\alpha) = L - r_{lc}\sin\alpha - L\cos\alpha + r_{lc}\alpha\cos\alpha \quad (A.2.6)$$

$r_{sc}<0$ $$\begin{cases} r_{sc} = L\sin\alpha - r_{lc}\alpha\sin\alpha + r_{lc} - r_{lc}\cos\alpha \\ h_{sc} = L - [L\cos\alpha - r_{lc}\alpha\cos\alpha + r_{lc}\sin\alpha] \end{cases} \quad (A.2.7)$$

If the bottom yarn release, the braiding point directly moving to O' in XY plane. So, the resultant tension in X direction still balances and tension from yarn doesn't change. The angles of all the carriers relative to X axis will change. Since every carrier has different phase, their tensions have different component in Y direction. To describe the component, β is set as the angle of different carrier relative to Z axis, which is shown in Figure 3.8. Actually, the relationship of angle β and φ is shown in equation (A.2.8). Points, B_{23} and B_{28} in Y axis represent the projective points of carrier C_{23} and carrier C_{28}. And O'_p is projective point of O' on X axis (x axis). B' is projective point of O' on Y axis. And now, Y component of resultant tension of carrier C_{25} is studied. For carrier C_{25}, β is equal to π. The length of yarn from carrier C_{25} is $O'C_{25}$. Using right triangle method, all the responding equations are shown in equation (A.2.9). From the equation (A.2.9), Y component of tension from carrier C_{25}, T_{25}, is shown in equation (A.2.10).

$$\beta = \varphi + \frac{\pi}{2}, \quad -\pi \le \beta \le \pi, -\frac{\pi}{2} \le \varphi \le \frac{3\pi}{2}, \quad (A.2.8)$$

$$\begin{cases} O'C_{25} = \sqrt{(C_{25}O'_p)^2 + (O'O'_p)^2}, \text{ in right triangle } \Delta C_{25}O'O'_p \\ C_{25}B = R_c + A_p \\ BO'_p = H_0 + h_{sc} \\ (C_{25}O'_p)^2 = (C_{25}B)^2 + \left(BO'_p\right)^2 \\ O'O_p = r_{sc} \\ \beta = \pi \end{cases} \quad (A.2.9)$$

$$T_{25,Y} = T\frac{O'O'_p}{O'C_{25}} = T\frac{r_{sc}}{\sqrt{(C_{25}O'_p)^2+(O'O'_p)^2}} = T\frac{r_{sc}}{\sqrt{(C_{25}B)^2+(BO'_p)^2+(r_{sc})^2}} = T\frac{r_{sc}}{\sqrt{(R_c+A_p)^2+(H_0+h_{sc})^2+(r_{sc})^2}}$$

So,
$$T_{25,Y} = T_0\frac{r_{sc}}{\sqrt{(R_c+A_p)^2+(H_0+h_{sc})^2+(r_{sc})^2}} \quad (A.2.10)$$

The carrier C_9 has the same situation as $C_{25.}$ And it also has the same expression for Y component of its tension. Because there are 32 carriers in one circle of path track, the value of β between any two neighboring carriers is stepped by $\frac{\pi}{16}$. For 32 carriers, their angle, β are shown in equation (A.2.11). For their Y component, the distance between any carrier and moved braiding point is simply r_{sc} plus R_{bm} multiplied by sinβ. Since the carriers are symmetric, i could defined as -8,-7,..,0,1,2,...,8. There are two carriers for one index except that there is only one when i=-8 and 8. For carriers C_{25} and C_9, their tensions should be as equation (A.2.10). For carrier C_{23}, the similar expressions in equation (A.2.9) are shown in equation (A.2.12). Y component of the tension form carrier C_{23} is calculated in equation (A.2.13). The carrier C_{11} has the same mathematical expression as $C_{23.}$

$$\beta = \frac{i\pi}{16}\text{, i=-15, -14,-13…, 0, 1, 2….16.} \quad (A.2.11)$$

$$\begin{cases} O'C_{23} = \sqrt{(C_{23}O_{23})^2 + (O'O_{23})^2} \\ (C_{23}O_{23})^2 = (C_{23}B_{23})^2 + (B_{23}O_{23})^2 \\ C_{23}B_{23} = C_{23}B\cos\beta \\ C_{23}B = R_c - A_p \\ B_{23}O_{23} = H_0 + h_{sc} \\ O'O_{23} = r_{sc} + O'_pO_{23} \\ O'_pO_{23} = BB_{23} \\ BB_{23} = C_{23}B\sin\beta \\ \beta = \frac{14}{16}\pi \end{cases} \quad (A.2.12)$$

$$T_{23,Y} = T\frac{O'O_{23}}{O'C_{23}} = T\frac{r_{sc}+O'_pO_{23}}{\sqrt{(C_{23}O_{23})^2+(O'O_{23})^2}} = T\frac{r_{sc}+C_{23}B\sin\beta}{\sqrt{(C_{23}B_{23})^2+(B_{23}O_{23})^2+(r_{sc}+O'_pO_{23})^2}}$$

$$= T\frac{r_{sc} + (r_{bm} - A_p)\sin\beta}{\sqrt{\left((R_c - A_p)\cos\beta\right)^2 + (H_0 + h_{sc})^2 + \left(r_{sc} + (R_c - A_p)\sin\beta\right)^2}}$$

So, $$T_{25} = T_0\frac{r_{sc}+(R_c-A_p)\sin\beta}{\sqrt{\left((R_c-A_p)\cos\beta\right)^2+(H_0+h_{sc})^2+\left(r_{sc}+(R_c-A_p)\sin\beta\right)^2}} \quad (A.2.13)$$

For carriers C_{28}, it locates on the base circle and its radius is R_c . For carrier C_{28}, the similar expressions as equation (A.2.9) are shown in (A.2.14). Y component of the tension form carrier C_{23} is shown in equation (A.2.15). The carrier C_6 has the same mathematical expression as C_{28}.

$$\begin{cases} O'C_{28} = \sqrt{(C_{28}O_{28})^2 + (O'O_{28})^2} \\ (C_{28}O_{28})^2 = (C_{28}B_{28})^2 + (B_{28}O_{28})^2 \\ C_{28}B_{28} = C_{28}B\cos\beta \\ C_{28}B = R_c \\ B_{28}O_{28} = H_0 + h_{sc} \\ O'O_{28} = r_{sc} + O'_pO_{28} \\ O'_pO_{28} = BB_{28} \\ BB_{28} = C_{28}B\sin\beta \\ \beta = -\frac{13}{16}\pi \end{cases} \quad (A.2.14)$$

$$T_{28,Y} = T\frac{O'O_{28}}{O'C_{28}} = T\frac{r_{sc}+O'_pO_{28}}{\sqrt{(C_{28}O_{28})^2+(O'O_{28})^2}} = T\frac{r_{sc}+C_{28}B\sin\beta}{\sqrt{(C_{28}B_{28})^2+(B_{28}O_{28})^2+\left(r_{sc}+O'_pO_{28}\right)^2}}$$

$$= T\frac{r_{sc} + R_c\sin\beta}{\sqrt{(R_c\cos\beta)^2 + (H_0 + h_{sc})^2 + (r_{sc} + R_c\sin\beta)^2}}$$

So, $$T_{25} = T_0\frac{R_c\sin\beta+r_{sc}}{\sqrt{(R_c\cos\beta)^2+(H_0+h_{sc})^2+(R_c\sin\beta+r_{sc})^2}} \quad (A.2.15)$$

Similar with carriers C_{25} and C_9, the situations of carriers C_1, C_5, C_{29}, C_{13}, C_{21} and C_{17} have the same expressions as equation (A.2.13) if the sign of A_p is changed to positive. Since their symetricity of carriers C_5 and C_{29}, C_{13} and C_{21}, and C_{23} and C_9, the angle β doesn't affect the final result of theirs. The tension of carrier 17 will change to $(T_4 - T_{d1})$ because of the bottom yarn releasing. For the carriers C_3, C_{31}, C_7, C_{27}, C_{11}, C_{23}, C_{15} and C_{19}, the expressions of their tension as equation (A.2.13) and i=-6,-10, -2, -

14, 2, 14, 6, and 10, respectively. For the rest carriers, their rotating radius is just R_c expressed by equation (A.2.15). To sum the above discussion, Y components of all the tensions from carriers are added together in equation (A.2.16) referring to equation (7). After a series algebraic, the equation (2.2.17) is obtained. The tensions pulling braiding point up to original location are shown in left hand side of equation (A.2.17). Repeating the same steps, the tensions pull the braiding point close to original location, O, are shown in right hand side of equation (A.2.17). The sign of r_{sc} is changed to negative in left hand side. Using same routine, the equation (A.2.18) will be obtained for the most top yarn releasing. Actually, equation (A.2.18) is totally same as equation (A.2.17) if combining with their equation (A.2.4) and (A.2.7), respectively. In the following Figure A.3.16, the left figure is showing the tensions of all carriers right before the carrier C_{17} release. The tension of carrier is T_4 at this moment. The others are all T_0. The right figure is showing the tensions of 32 carriers right after the carrier C_{17} release. At this moment, the tension of carrier C_{17} is T_{d1}. The tensions of the other carriers are still same.

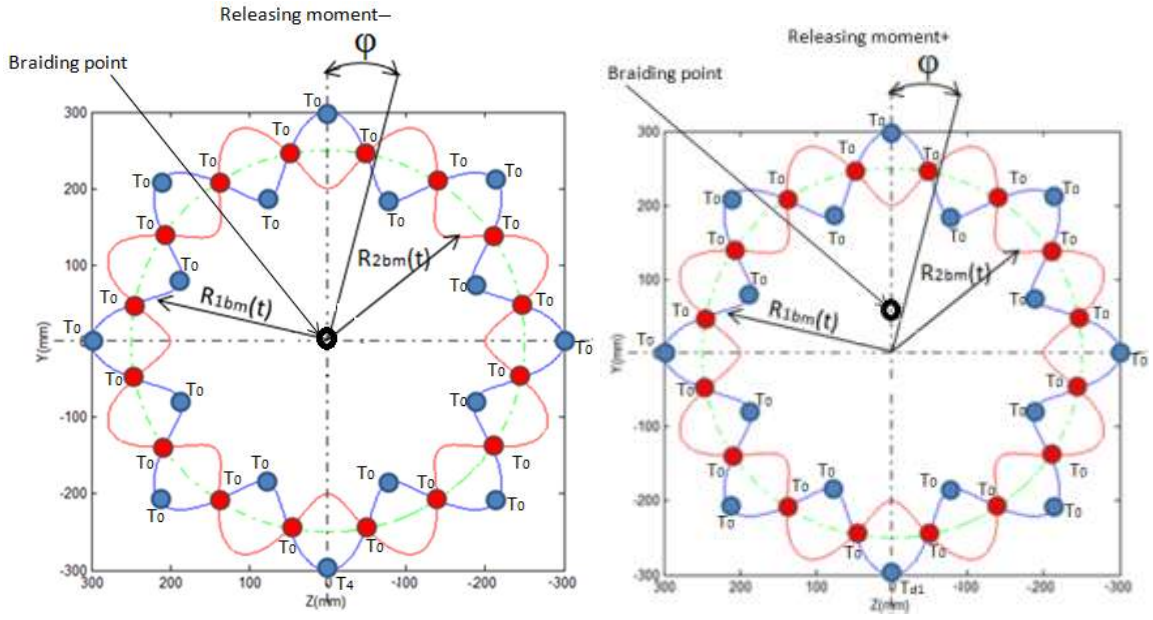

Figure A.3.16 Carriers on braiding plane

$$T_0\left(\sum_{i=-14,-10,-6}^{-2,2,6,10,14}\frac{r_{sc}+(R_c-A_p)\sin\frac{i\pi}{16}}{\sqrt{\left((R_c-A_p)\cos\frac{i\pi}{16}\right)^2+(H_0+h_{sc})^2+\left(r_{sc}+(R_c-A_p)\sin\frac{i\pi}{16}\right)^2}}+\right.$$

$$\sum_{i=-12,-8,-4}^{0,4,,12,16}\frac{r_{sc}+(R_c+A_p)\sin\frac{i\pi}{16}}{\sqrt{\left((R_c+A_p)\cos\frac{i\pi}{16}\right)^2+(H_0+h_{sc})^2+\left(r_{sc}+(R_c+A_p)\sin\frac{i\pi}{16}\right)^2}}$$

$$\left.+\sum_{i=-15,-13,-11,-9,-7,-5}^{-3,-1,1,3,5,7,9,11,13,15}\frac{R_c\sin\frac{i\pi}{16}+r_{sc}}{\sqrt{\left(R_c\cos\frac{i\pi}{16}\right)^2+(H_0+h_{sc})^2+\left(R_c\sin\frac{i\pi}{16}+r_{sc}\right)^2}}\right)+(T_4-$$

$$T_{d1})\frac{r_{sc}+(R_c+A_p)\sin\frac{8\pi}{16}}{\sqrt{\left((R_c+A_p)\cos\frac{8\pi}{16}\right)^2+(H_0+h_{sc})^2+\left(r_{sc}+(R_c+A_p)\sin\frac{8\pi}{16}\right)^2}}+T_{rope}\sin\alpha=0 \qquad \text{(A.2.16)}$$

Transforming 1 (separating by the similar carriers)

$$T_0\left(\sum_{i=-14,-10,-6}^{-2,2,6,10,14}\frac{r_{sc}+(R_c-A_p)\sin\frac{i\pi}{16}}{\sqrt{\left((R_c-A_p)\cos\frac{i\pi}{16}\right)^2+(H_0+h_{sc})^2+\left(r_{sc}+(R_c-A_p)\sin\frac{i\pi}{16}\right)^2}}+\right.$$

$$\sum_{i=-12,-8,-4}^{0,4,,12,16}\frac{r_{sc}+(R_c+A_p)\sin\frac{i\pi}{16}}{\sqrt{\left((R_c+A_p)\cos\frac{i\pi}{16}\right)^2+(H_0+h_{sc})^2+\left(r_{sc}+(R_c+A_p)\sin\frac{i\pi}{16}\right)^2}}$$

$$\left.+\sum_{i=-15,-13,-11,-9,-7,-5}^{-3,-1,1,3,5,7,9,11,13,15}\frac{R_c\sin\frac{i\pi}{16}+r_{sc}}{\sqrt{\left(R_c\cos\frac{i\pi}{16}\right)^2+(H_0+h_{sc})^2+\left(R_c\sin\frac{i\pi}{16}+r_{sc}\right)^2}}\right)+(T_4-$$

$$T_{d1})\frac{r_{sc}+(R_c+A_p)\sin\frac{8\pi}{16}}{\sqrt{\left((R_c+A_p)\cos\frac{8\pi}{16}\right)^2+(H_0+h_{sc})^2+\left(r_{sc}+(R_c+A_p)\sin\frac{8\pi}{16}\right)^2}}+T_{rope}\sin\alpha=0$$

Transforming 2,

$$2T_0\left(\sum_{i=-6,-2}\frac{r_{sc}+(R_c-A_p)\sin\frac{i\pi}{16}}{\sqrt{\left((R_c-A_p)\cos\frac{i\pi}{16}\right)^2+(H_0+h_{sc})^2+\left(r_{sc}+(R_c-A_p)\sin\frac{i\pi}{16}\right)^2}}+\right.$$

$$\frac{r_{sc}+(R_c+A_p)\sin\frac{-4\pi}{16}}{\sqrt{\left((R_c+A_p)\cos\frac{-4\pi}{16}\right)^2+(H_0+h_{sc})^2+\left(r_{sc}+(R_c+A_p)\sin\frac{-4\pi}{16}\right)^2}}$$

$$\left.+\sum_{i=-7,-5}^{-3,-1}\frac{R_c\sin\frac{i\pi}{16}+r_{sc}}{\sqrt{\left(R_c\cos\frac{i\pi}{16}\right)^2+(H_0+h_{sc})^2+\left(R_c\sin\frac{i\pi}{16}+r_{sc}\right)^2}}\right)+\frac{T_0(r_{sc}+(R_c+A_p)\sin\frac{-8\pi}{16})}{\sqrt{\left((R_c+A_p)\cos\frac{-8\pi}{16}\right)^2+(H_0+h_{sc})^2+\left(r_{sc}+(R_c+A_p)\sin\frac{-8\pi}{16}\right)^2}}$$

$$+(T_4 - T_{d1})\frac{r_{sc}+(R_c+A_p)\sin\frac{8\pi}{16}}{\sqrt{\left((R_c+A_p)\cos\frac{8\pi}{16}\right)^2+(H_0+h_{sc})^2+\left(r_{sc}+(R_c+A_p)\sin\frac{8\pi}{16}\right)^2}}+$$

$$2T_0\left(\sum_{i=2,6}\frac{r_{sc}+(R_c-A_p)\sin\frac{i\pi}{16}}{\sqrt{\left((R_c-A_p)\cos\frac{i\pi}{16}\right)^2+(H_0+h_{sc})^2+\left(r_{sc}+(R_c-A_p)\sin\frac{i\pi}{16}\right)^2}}+\right.$$

$$\left.\sum_{i=0,4}\frac{r_{sc}+(R_c+A_p)\sin\frac{i\pi}{16}}{\sqrt{\left((R_c+A_p)\cos\frac{i\pi}{16}\right)^2+(H_0+h_{sc})^2+\left(r_{sc}+(R_c+A_p)\sin\frac{i\pi}{16}\right)^2}}+\sum_{i=1,3,5,7}\frac{R_c\sin\frac{i\pi}{16}+r_{sc}}{\sqrt{\left(R_c\cos\frac{i\pi}{16}\right)^2+(H_0+h_{sc})^2+\left(R_c\sin\frac{i\pi}{16}+r_{sc}\right)^2}}\right)+$$

$$T_{rope}\sin\alpha = 0$$

Separating,

$$\frac{T_0((R_c+A_p)\sin\frac{\pi}{2}-r_{sc})}{\sqrt{\left((R_c+A_p)\cos\frac{\pi}{2}\right)^2+(H_0+h_{sc})^2+\left(-r_{sc}+(R_c+A_p)\sin\frac{\pi}{2}\right)^2}}+\sum_{ti=2,6}\frac{2T_0((R_c-A_p)\sin\frac{ti\pi}{16}-r_{sc})}{\sqrt{\left((R_c-A_p)\cos\frac{ti\pi}{16}\right)^2+(H_0+h_{sc})^2+\left((R_c-A_p)\sin\frac{ti\pi}{16}-r_{sc}\right)^2}}+$$

$$\frac{2T_0((R_c+A_p)\sin\frac{\pi}{4}-r_{sc})}{\sqrt{\left((R_c+A_p)\cos\frac{\pi}{4}\right)^2+(H_0+h_{sc})^2+\left((R_c+A_p)\sin\frac{\pi}{4}-r_{sc}\right)^2}}+\sum_{ti=1,3,5,7}\frac{2T_0(R_c\sin\frac{ti\pi}{16}-r_{sc})}{\sqrt{\left(R_c\cos\frac{ti\pi}{16}\right)^2+(H_0+h_{sc})^2+\left(R_c\sin\frac{ti\pi}{16}-r_{sc}\right)^2}})$$

=

$$(T_4 - T_{d1})\frac{r_{sc}+(R_c+A_p)\sin\frac{\pi}{2}}{\sqrt{\left((R_c+A_p)\cos\frac{\pi}{2}\right)^2+(H_0+h_{sc})^2+\left(r_{sc}+(R_c+A_p)\sin\frac{\pi}{2}\right)^2}}+$$

$$\sum_{bj=2,6}\frac{2T_0(r_{sc}+(R_c-A_p)\sin\frac{bj\pi}{16})}{\sqrt{\left((R_c-A_p)\cos\frac{bj\pi}{16}\right)^2+(H_0+h_{sc})^2+\left(r_{sc}+(R_c-A_p)\sin\frac{bj\pi}{16}\right)^2}}+$$

$$\sum_{bj=0,4}\frac{2T_0(r_{sc}+(R_c+A_p)\sin\frac{bj\pi}{16})}{\sqrt{\left((R_c+A_p)\cos\frac{bj\pi}{16}\right)^2+(H_0+h_{sc})^2+\left(r_{sc}+(R_c+A_p)\sin\frac{bj\pi}{16}\right)^2}}+\sum_{bj=1,3,5,7}\frac{2T_0(R_c\sin\frac{bj\pi}{16}+r_{sc})}{\sqrt{\left(R_c\cos\frac{bj\pi}{16}\right)^2+(H_0+h_{sc})^2+\left(R_c\sin\frac{bj\pi}{16}+r_{sc}\right)^2}}+$$

$$T_{rope}\sin\alpha \qquad \text{(A.2.17)}$$

$$\frac{T_0((R_c+A_p)\sin\frac{\pi}{2}+r_{sc})}{\sqrt{\left((R_c+A_p)\cos\frac{\pi}{2}\right)^2+(H_0+h_{sc})^2+\left(r_{sc}+(R_c+A_p)\sin\frac{\pi}{2}\right)^2}}+\sum_{ti=2,6}\frac{2T_0[(R_c-A_p)\sin\frac{ti\pi}{16}+r_{sc}]}{\sqrt{\left((R_c-A_p)\cos\frac{ti\pi}{16}\right)^2+(H_0+h_{sc})^2+\left((R_c-A_p)\sin\frac{ti\pi}{16}+r_{sc}\right)^2}}+$$

$$\frac{2T_0((R_c+A_p)\sin\frac{\pi}{4}+r_{sc})}{\sqrt{\left((R_c+A_p)\cos\frac{\pi}{4}\right)^2+(H_0+h_{sc})^2+\left((R_c+A_p)\sin\frac{\pi}{4}+r_{sc}\right)^2}}+\sum_{ti=1,3,5,7}\frac{2T_0(R_c\sin\frac{ti\pi}{16}+r_{sc})}{\sqrt{\left(R_c\cos\frac{ti\pi}{16}\right)^2+(H_0+h_{sc})^2+\left(R_c\sin\frac{ti\pi}{16}+r_{sc}\right)^2}})$$

=

$$\frac{(T_4-T_{d1})(-r_{sc}+(R_c+A_p)\sin\frac{\pi}{2})}{\sqrt{\left((R_c+A_p)\cos\frac{\pi}{2}\right)^2+(H_0+h_{sc})^2+\left(-r_{sc}+(R_c+A_p)\sin\frac{\pi}{2}\right)^2}}+\sum_{bj=2,6}\frac{2T_0(-r_{sc}+(R_c-A_p)\sin\frac{bj\pi}{16})}{\sqrt{\left((R_c-A_p)\cos\frac{bj\pi}{16}\right)^2+(H_0+h_{sc})^2+\left(-r_{sc}+(R_c-A_p)\sin\frac{bj\pi}{16}\right)^2}}+$$

$$\sum_{bj=0,4}\frac{2T_0(-r_{sc}+(R_c+A_p)\sin\frac{bj\pi}{16})}{\sqrt{\left((R_c+A_p)\cos\frac{bj\pi}{16}\right)^2+(H_0+h_{sc})^2+\left(-r_{sc}+(R_c+A_p)\sin\frac{bj\pi}{16}\right)^2}}+$$

$$\sum_{bj=1,3,5,7}\frac{2T_0(R_c\sin\frac{bj\pi}{16}-r_{sc})}{\sqrt{\left(R_c\cos\frac{bj\pi}{16}\right)^2+(H_0+h_{sc})^2+\left(R_c\sin\frac{bj\pi}{16}-r_{sc}\right)^2}}+T_{rope}\sin\alpha \qquad \text{(A.2.18)}$$

For rope moving in the horizontal plane, the expressions of base radius and height of ellipsoidal cap are a little different with before because tangent point located on capstan doesn't move. So, braiding point only like pendulum. Their expressions of base radius and height are shown in equation (A.2.11). The expression of tensions is same as (A.2.19).

$$r_{sc}>0 \qquad \begin{cases} r_{sc}=L\sin\alpha \\ h_{sc}=L-L\cos\alpha \end{cases} \qquad \text{(A.2.19)}$$

A.3.3 MATLAB Code for Drawing Path track of Carriers

```
%braidingpathtrack.m
clear all
clc
pi=3.1415926535897932;
for t1=1:1:8000;
X1(t1)=(50*cos(2*pi*0.05*t1)+250)
*cos(pi/4+pi*0.05*t1/4);
Y1(t1)=(50*cos(2*pi*0.05*t1)+250)
*sin(pi/4+pi*0.05*t1/4);
% circle(t1)=(15/8+16.5/2)
*cos((-pi*0.01*t1/4));
Xc(t1)=250*cos(-pi*0.01*t1/4);
Yc(t1)=250*sin(-pi*0.01*t1/4);
% circle(t1)=(15/8+16.5/2)
*cos((-pi*0.01*t1/4));
%
X1(t1)=((15*cos(2*pi*0.01*t1)/8+16.5/
2)+(15*cos(2*pi*0.01*t1+pi/2)/8+16.5/
2)+(15*cos(2*pi*0.01*t1+pi)/8+16.5/2)
+(15*cos(2*pi*0.01*t1+3*pi/2)/8+16.5/
2))*cos(-pi*0.01*t1/4);
%
Y1(t1)=((15*cos(2*pi*0.01*t1)/8+16.5/
2)+(15*cos(2*pi*0.01*t1+pi/2)/8+16.5/
2)+(15*cos(2*pi*0.01*t1+pi)/8+16.5/2)
+(15*cos(2*pi*0.01*t1+3*pi/2)/8+16.5/
2))*sin(-pi*0.01*t1/4);
% circle(t1)=(15/8+16.5/2)
*cos((-pi*0.01*t1/4));

for t2=1:1:800;
X2(t2)=(50*cos(2*pi+2*pi*0.05*t2+pi)
+250)*cos(pi/4-pi*0.05*t2/4);
Y2(t2)=(50*cos(2*pi+2*pi*0.05*t2+pi)
+250)*sin(pi/4-pi*0.05*t2/4);
end
t=0:0.015:11.985;
plot(X1,Y1)
% plot(X1)
% plot(Y1)
hold on
plot(X2,Y2,'r')
hold on
plot(Xc,Yc,'g')
 title('Pathtrack of carriers');
xlabel('Z(mm)');ylabel('Y(mm)');
% title('Rotating radius of carriers');
xlabel('t,\phi/\omega(s)');
ylabel('R_1_b_m and R_2_b_m(mm)');
% axis([0 12 0 300])
grid;
legend('R_1_b_m','R_2_b_m','Base
circle')
```

A.3.4 MATLAB Code for Calculating Ellipsoid Cap

```
%% Caculation.m
%Guangli Ma

clear all
clc
%Parameters defination
pi=3.1415926535897932;
load('experiment_10error95400');
r_tf=0.0025; r_bm=0.25; rl=0.15;
%radius of rope, brading mchine and
load shaft
omega=5*2*pi/60; %braiding speed
V=0.0018405;  wl0=V/rl;
 %take up speed; initial angular speed of
load shaft
theta=atan(r_tf*omega/V);  % braiding
angle/radian
H0=r_bm/tan(theta); %the position of
braiding point;
T0= 3.50865;
T_rope=32*T0*H0/sqrt(H0^2+r_bm^2);
%tension of single braid and rope/N

% Parameters of Servo motor
J_m=0.000113;
J_l=0.022362059116777;
%Motor inertia/Kg/m^2 %load shaft
inertia/Kg/m^2
Kt=0.191;   Ke=0.191;  Kb=0.191;
%Torque constant/ Nm/A; %voltage
constant/ V/rad/sec; %back-emf constant
Rm=1800;  bm=0;      bl=0;
%Resistance of motor circuit/ ohms
%damping of motor  %damping of load
shaft
n=15;                %ratio of gear train
J_meq=J_m+n^2*J_l;
b_meq=bm+n^2*bl;  J_leq=J_l+J_m/n^2
;      b_leq=bl+bm/n^2;
me=18.41/1000;   K=215.75;  b=0;
%gram,me2=19.91gram; spring constant
N/m; damping;
%%
L=1.6;alpha=0.00697;alpha2=0.00481;al
pha3=0.003388;
r_sc1=L*sin(alpha)+rl*alpha*sin(alpha)
-rl+rl*cos(alpha);
h_sc1=L-(L*cos(alpha)+rl*alpha
*cos(alpha)-rl*sin(alpha));
r_sc2=L*sin(alpha2)-
rl*alpha2*sin(alpha2)+rl-rl*cos(alpha2);
h_sc2=L-(L*cos(alpha2)-
rl*alpha2*cos(alpha2)+rl*sin(alpha2));
r_sc3=L*sin(alpha3);
h_sc3=L-L*cos(alpha3);
r_pt=0.05;
% for i11=1:2:7
```

```
temp11(i11)=2*T0*(r_bm*sin(i11*pi/16
)-r_sc1)/sqrt((r_bm*cos(i11*pi/16))^2+
(r_bm*sin(i11*pi/16)-
r_sc1)^2+(H0+h_sc1)^2 );
% end
% for i12=2:4:6
%     temp12(i12)=2*T0*((r_bm-
r_pt)*sin(i12*pi/16)-r_sc1)/sqrt(((r_bm-
r_pt)*cos(i12*pi/16))^2+((r_bm-
r_pt)*sin(i12*pi/16)-
r_sc1)^2+(H0+h_sc1)^2 );
% end
%
temp13=2*T0*((r_bm+r_pt)*sin(4*pi/1
6)-r_sc1)/sqrt(((r_bm-
r_pt)*cos(4*pi/16))^2+((r_bm+r_pt)*sin
(4*pi/16)-r_sc1)^2+(H0+h_sc1)^2 );
% toptension1=T0*(r_bm+r_pt-
r_sc1)/sqrt((r_bm+r_pt-
r_sc1)^2+(H0+h_sc1)^2)+sum(temp11)
+sum(temp12)+temp13;
% for j11=1:2:7
%
temp21(j11)=2*T0*(r_bm*sin(j11*pi/16
+r_sc1))/sqrt((r_bm*cos(j11*pi/16))^2+(
r_bm*sin(j11*pi/16)+r_sc1)^2+(H0+h_s
c1)^2);
% end
% for j12=1:4:5
%
temp22(j12)=2*T0*((r_bm+r_pt)*sin((j
12-1)*pi/16+r_sc1))/sqrt(((r_bm+r_pt)
*cos((j12-1)*pi/16))^2+((r_bm+r_pt)
*sin((j12-1)*pi/16)+r_sc1)^2
+(H0+h_sc1)^2);
% end
% for j13=2:4:6
% temp23(j13)=2*T0*((r_bm-
r_pt)*sin(j13*pi/16+r_sc1))/sqrt(((r_bm-
r_pt)*cos(j13*pi/16))^2+((r_bm-
r_pt)*sin(j13*pi/16)+r_sc1)^2+(H0+h_s
c1)^2);
% end
% %
temp24=2*T0*((r_bm+r_pt)*sin(4*pi/1
6-r_sc1))/sqrt((r_bm+r_pt)^2+
((r_bm+r_pt)*sin(i2*pi/16)-r_sc1)^2
+(H0+h_sc1)^2 );
%
bottomtension1=sum(temp21)+sum(tem
p22)+sum(temp23)+1.4*(r_bm+r_pt+r_s
c1)/sqrt((r_bm+r_pt+r_sc1)^2+(H0+h_s
c1)^2
)+32*T0*sin(alpha)%32*sin(alpha);
% figure(1);plot(toptension1); hold on;
plot(bottomtension1)
for in21=1:2:7
tempn21(in21)=2*T0*(r_bm*sin(in21*p
i/16)-r_sc2)/sqrt((r_bm
```

```
*cos(in21*pi/16))^2+(r_bm*sin(in21*pi/
16)-r_sc2)^2+(H0+h_sc2)^2 );
end
for in22=2:4:6
   tempn22(in22)=2*T0*((r_bm-
r_pt)*sin(in22*pi/16)-
r_sc2)/sqrt(((r_bm-
r_pt)*cos(in22*pi/16))^2+((r_bm-
r_pt)*sin(in22*pi/16)-
r_sc2)^2+(H0+h_sc2)^2 );
end

tempn23=2*T0*((r_bm+r_pt)*sin(4*pi/
16)-
r_sc2)/sqrt(((r_bm+r_pt)*cos(4*pi/16))^
2+((r_bm+r_pt)*sin(4*pi/16)-
r_sc2)^2+(H0+h_sc2)^2 );

bottomtension2=T0*(r_bm+r_pt-
r_sc2)/sqrt((r_bm+r_pt-
r_sc2)^2+(H0+h_sc2)^2)+sum(tempn21
)+sum(tempn22)+tempn23;%+32*T0*si
n(alpha2)32*sin(alpha);

for jn21=1:2:7
tempn31(jn21)=2*T0*(r_bm*sin(jn21*p
i/16+r_sc2))/sqrt((r_bm*cos(jn21*pi/16)
)^2+(r_bm*sin(jn21*pi/16)+r_sc2)^2+(
H0+h_sc2)^2);
end

for jn22=1:4:5
tempn32(jn22)=2*T0*((r_bm+r_pt)*sin(
(jn22-
1)*pi/16+r_sc2))/sqrt(((r_bm+r_pt)*cos(
(jn22-
1)*pi/16))^2+((r_bm+r_pt)*sin((jn22-
1)*pi/16)+r_sc2)^2+(H0+h_sc2)^2);
end

for jn23=2:4:6
tempn33(jn23)=2*T0*((r_bm-
r_pt)*sin(jn23*pi/16+r_sc2))/sqrt(((r_b
m-r_pt)*cos(jn23*pi/16))^2+((r_bm-
r_pt)*sin(jn23*pi/16)+r_sc2)^2+(H0+h_
sc2)^2);
end
%
temp24=2*T0*((r_bm+r_pt)*sin(4*pi/1
6-
r_sc1))/sqrt((r_bm+r_pt)^2+((r_bm+r_pt
)*sin(i2*pi/16)-r_sc1)^2+(H0+h_sc1)^2
);
toptension2=sum(tempn31)+sum(tempn
32)+sum(tempn33)+1.4*(r_bm+r_pt+r_s
c2)/sqrt((r_bm+r_pt+r_sc2)^2+(H0+h_s
c2)^2
)+32*T0*sin(alpha2)%32*sin(alpha);
% figure(2);plot(toptension2); hold
on;plot(bottomtension2)
% for i41=1:2:7
```

```
%
temp41(i41)=2*T0*(r_bm*sin(i41*pi/16
)-r_sc3)/sqrt((r_bm*
cos(i41*pi/16))^2+(r_bm*sin(i41*pi/16)
-r_sc3)^2+(H0+h_sc3)^2 );
% end
% for i42=2:4:6
%     temp42(i42)=2*T0*((r_bm-
r_pt)*sin(i42*pi/16)-r_sc3)/sqrt(((r_bm-
r_pt)*cos(i42*pi/16))^2+((r_bm-
r_pt)*sin(i42*pi/16)-
r_sc3)^2+(H0+h_sc3)^2 );
% end
%
temp43=2*T0*((r_bm+r_pt)*sin(4*pi/1
6)-r_sc3)/sqrt(((r_bm+r_pt)
*cos(4*pi/16))^2+((r_bm+r_pt)*sin(4*pi
/16)-r_sc3)^2+(H0+h_sc3)^2 );
% righttension4=T0*(r_bm+r_pt-
r_sc3)/sqrt((r_bm+r_pt-
r_sc3)^2+(H0+h_sc3)^2)+sum(temp41)
+sum(temp42)+temp43;
% for j41=1:2:7
%
temp51(j41)=2*T0*(r_bm*sin(j41*pi/16
)+r_sc3)/sqrt((r_bm*cos(j41*pi/16))^2+(
r_bm*sin(j41*pi/16)+r_sc3)^2+(H0+h_s
c3)^2);
% end
% for j42=1:4:5
%
temp52(j42)=2*T0*((r_bm+r_pt)*sin((j
42-
1)*pi/16)+r_sc3)/sqrt(((r_bm+r_pt)*cos(
(j42-
1)*pi/16))^2+((r_bm+r_pt)*sin((j42-
1)*pi/16)+r_sc3)^2+(H0+h_sc3)^2);
% end
% for j43=2:4:6
% temp53(j43)=2*T0*((r_bm-
r_pt)*sin(j43*pi/16)+r_sc3)/sqrt(((r_bm-
r_pt)*cos(j43*pi/16))^2+((r_bm-
r_pt)*sin(j43*pi/16)+r_sc3)^2+(H0+h_s
c3)^2);
% end
% %
temp24=2*T0*((r_bm+r_pt)*sin(4*pi/1
6-r_sc1))/sqrt((r_bm+r_pt)^2
+((r_bm+r_pt)*sin(i2*pi/16)-
r_sc1)^2+(H0+h_sc1)^2 );
%
lefttension4=sum(temp51)+sum(temp52
)
+sum(temp53)+1.4*(r_bm+r_pt+r_sc3)/
sqrt((r_bm+r_pt+r_sc3)^2+(H0+h_sc3)^
2 )+32*T0*sin(alpha3)%32*sin(alpha);
```

A.3.5 MATLAB Code for Frequency Calculation.

```
%% statespacemodel.m
%Guangli Ma

clear all
clc
%Parameters defination
pi=3.1415926535897932;
%Ki10Kp7p5(Ki=20,Kp=12);
Ki50Kp10;Ki200Kp70=Ki1Kp50;
r_tf=0.0025;r_bm=0.25; rl=0.15;
%radius of tubular fabric, brading mchine and load shaft
omega=5*2*pi/60; V=0.0018407;
wl0=V/rl; wl0degree=V*180/(rl*pi);
rpm=wl0*60/(2*pi);
%braiding speed %take up speed, initial angular speed of load shaft
theta=atan(r_tf*omega/V);
thetadegree=atan(r_tf*omega/V)*180/pi;
% braiding angle/radian
H0=r_bm/tan(theta);
T0= 3.50865;  T_rope=32*T0*H0
/sqrt(H0^2+r_bm^2);  %the position of braiding point; %tension of single braid and rope/N
% Parameters of Servo motor
J_m=0.000113;
J_l=0.022362059116777;
%Motor inertia/Kg/m^2 %load shaft inertia/Kg/m^2
Kt=0.191;Ke=0.191;Kb=0.191;
%Torque constant/ Nm/A; %voltage constant/ V/rad/sec; %back-emf constant
Rm=1800;bm=0;bl=0;
%Resistance of motor circuit/ ohms
%damping of motor
 %damping of load shaft
n=15;                %ratio of gear train
J_meq=J_m+n^2*J_l;
b_meq=bm+n^2*bl;
J_leq=J_l+J_m/n^2;
b_leq=bl+bm/n^2;
me=18.41/1000;
K=215.75;b=0;
%gram,me2=19.91gram;
spring constant N/m; damping;
%observer and feedback parameter
speed=omega*r_tf/sin(theta);
time=0.0102/speed;
frequency=1/time
```

4 Material Flow System Definition and Position Control of Braiding Point Motion

Braiding is a manufacturing process for making tubular braided products. Analogous to the common process of controlling a liquid level in a tank, a 32-carrier braiding machine includes the braiding motor (yarn) speed as inflow, take up motor (rope) speed as outflow and 32 yarns as the flowing material. The braiding process close to braiding point is defined as Material Flow System (MFS) and compared to a Liquid Level System (LLS). In order to control the braid angle, the position of braiding point is controlled. Machine vision senses the braiding point using the Geometric Pattern Matching method. A simple piecewise PI controller on the take up motor reduces the settling time of braiding process using feedback signals from a machine vision sensor. This settling time is commonly called setup time for braided products, which is one of further development trend in textile technology [1]. The definition of MFS is defining an algorithm between machine controls and the position of yarns, which is another trends of this book. Correlated experiment and simulation response validate the mathematical model, for use as a designer's tool.

4.1 Introduction

Braiding is a historically important but still relevant textile-manufacturing process to interlace yarns. Circular braiding based on a geared maypole braider is perhaps the oldest and still most common method, and is commonly used to braid textile, fabric, wire

and composite preform tubes [1]. The mathematic mode of braiding process is quite complicated since the process based on the sliding motion of interacting, elastic, and flexible material during interlaces. The quality of braided product is depending on the geometric structure parameters, especially, the braiding angle [2]. Du, G.W. and P. Popper mathematically model circular braiding process by kinematic analysis for braiding process on mandrel [3]. The relationship between motion parameters and braiding geometry parameters were derived. They created a mathematical model for predicting the braiding angle, and named the fell points as the braiding point. They discussed how the yarns move in braiding point area by successfully predicting the change in braiding angle. They did not discuss the motion of the braiding point and variation of braiding angle during braiding.

In order to achieve good braiding angle, the motion of braiding point needs to be controlled. Q. Zhang et al analyzed yarns' motion and how the sliding motions affect the final structure [4]. They were focus on the interaction in convergent zone. David Branscomb ran a take up motor to achieve a constant take up velocity using a separate take-up motor [5]. P. Potluri talked about how to move mandrel to get the different layer and structure by changing take-up speed [6]. They were mainly focus on the operation of braiding machine. Fischer use two set of ultrasonic sensors to detect the amount of strand material on the supply carrier. Based on the detected decrease in the amount of strand material inside the carriers, computers are provided for progressively increasing the travel speed of the strand supply carrier shuttles [7]. They use sensor feedback of the material left on the carrier to control the travel speed of mandrel. In [7], the precision could not be guaranteed and the ultrasonic sensors were as large as the size of braiding machine. No

effort was made to control the take up motor or mandrel automatically, in real time, in order to establish the motion of braiding point.

Actually, the braiding process is also transporting material or mass if yarns and rope are considered as tubes and material or mass of material inside this tube. Traditionally, the MFS is used to manage the manufacturing process, which deals with many individual system components and their interactions [8]. And one of the popular approaches to transport material in industries is the use of automated guided vehicle (AGV) systems [9]. The operating speed of this system depends on the working speed of AGV. A conveyor fed system is another example, for sorting and packing various kinds of bundle of cigarettes. It uses different machines to produce several bundle-types of cigarettes, and then releases them onto a common belt conveyor [10]. This MFS is pretty similar with braiding process. Many conveyors with various bundles are merged into a conveyor for packing. In this case, the braiding process is a simple material system, which includes 32 same inflows, yarns and one outflow, the rope.

Also, the braiding process is much like Liquid Level System (LLS) such as sewerage, which includes many inflows and main output sewer drain [11]. Of course, the big ERP management system is managing much bigger MFS, which not only include tons of materials, parts, equipments and machines, but the thousands of people and maybe business in many countries. And its speed depends on the speed of machines and the activities of people involved. If braiding process is defined as MFS, it is easy to control motion of braiding point. No previous publications have discussed the braiding process as a MFS before. In this work the braiding process is found to be really similar with the MFS.

With the development of machine vision, it is useful and possible to use this technology in the braiding field. The application of computer vision to industry and manufacturing is machine vision, which has numerous applications with computer science, optics, electronics, and mechanical engineering/automation [12]. It is commonly use for inspection of manufactured goods including automobiles and semiconductor chips. Especially, machine vision is important in cases where it is difficult to make contact measurements. This is a good option for this project since braiding point is a structure pattern and hard to touch. Labview software has several algorithms that attempted to mimic human visual perception. A good example is Pattern Matching, which is actually template finding and matching. The template matching is a useful algorithms for processing images. Histogram sensing is another algorithm. Tracking a gold fish swimming in a tank is one very good applications of histogram methods. Pattern Matching can be used to precisely measure variables such as length, angle, position, orientation, etc. [13]. Optical sensors are designed for detecting the presence of object or its motion in various industrial, mobile, electronic appliances, retail automations and the analysis of human activities [14]. A USB Camera is a good optical sensor for system controlling using machine vision. It also has been commonly used in research and industry, and it is not costly.

The objective of this work is a methodology to achieve the desired braid angle as soon as possible during braiding machine startup, and to maintain that braid angle throughout the manufacturing process. In so doing, manufacturers can save on material and labor costs, since less material will now be scrapped. If the position of braiding point can be controlled, the braiding angle (the measure of product quality) will be controlled

more easily and directly. Settling time in a controls parlance (also known as setup time [1]) is greatly reduced by a simple PI control strategy with a machine vision "sensor" created for this purpose. A mathematical model of the process and plant, which likens the process to liquid level control, is developed. When incorporated with a controller and the machine vision sensor the model is experimentally validated. To our knowledge this is the first effort to automatically control the braiding process by automatically controlling the position of the braiding point.

4.2 Define of MFS based on Braiding Process

During braiding process, the braiding point is shown in red rectangle of Figure 3.2. The braiding point always oscillates slightly during the braiding process, even if it is located at its steady state. In this paper, the affect of small oscillation of braiding angle is not investigated. Instead the focus will be on how to reduce setup time of braiding process at startup, although the control strategy will prevent braiding point drift from steady state also.

In this paper, however, the stress and strain of yarns and rope are not considered, either. Comparing the LLS, the mathematical model of the MFS based on braiding process will be derived. Similar as LLS [15], the MFS is also nonlinear because of its instability of inflow and outflow. But, if the operation of the MFS is assumed near a normal operation point, the system can be linearized near operating point and mathematical model can be made linear.

4.2.1 Resistance and Capacitance of MFS

From the previous work about braiding machine, there should have linear take up velocity V and certain angular velocity of braiding motor to keep braiding process

operating [4]. These speeds are set by the operator at the beginning of a run, and not controlled. When braiding process settles down for a certain speed conditions, the braiding point reaches a steady state region. The take up speed coming from take up motor is shown in equation (1). And the braiding point will stay at the same location if speed ratio between take up speed and angular velocity satisfies the equation (2). In this case, braiding angle is determined by the velocity ratio in equation (3). Using the same figure as Figure 3.2, xyz frame is put in braiding point and x axis point to take up direction, y axis parallel to Y axis and z parallel to axis Z. The steady state position of braiding point is set as the distance between braiding point and braiding plane, H, which is analogous with head of LLS in Table 4.1. The LLS is simplified and shown in Figure 4.1. So, this steady state position is determined by braiding angle. In equations (3) and (4), the position of braiding point is really based on velocity ratio in equation (2). In Figure 4.2, it is shown the relationship from velocity right triangle that determines braiding angle, and the position right triangle that determined the braiding angle. The steady state position is determined by braiding angle in equation (4). The Figure 4.2 also shows the braiding angle based on one vertex, O, the steady state point.

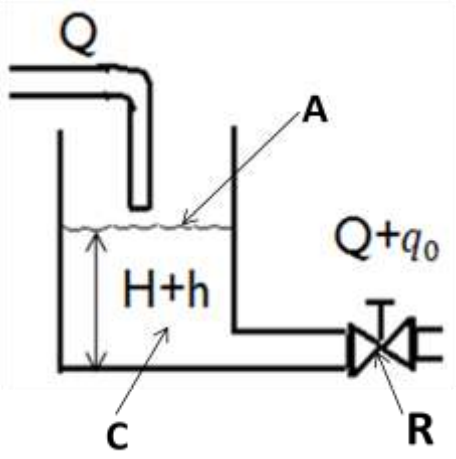

Figure 4.1 LLS comparison

$$V = r_{lc}\omega_{lc} \tag{1}$$

where, ω_{lc} is angular velocity of loading capstan of take up motor

$$\frac{\omega}{V} = \frac{\tan\theta}{r_{rope}} \tag{2}$$

$$\theta = \tan^{-1}\left(\frac{\omega r_{rope}}{V}\right) \tag{3}$$

$$H = \frac{R_c}{\tan\theta} \tag{4}$$

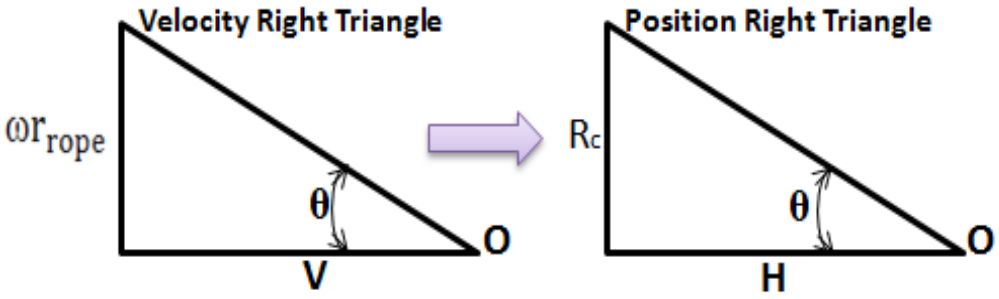

Figure 4.2 Comparison of velocity right triangle and position right triangle

In this case, the braiding process is a simple material flow system, which includes 32 same inflows (yarns) and one outflow (rope). When the outflow rate is zero in LLS and inflow rate is still in certain value, the head will rise and overflow from the tank. Meanwhile, the steady state position of braiding point will be zero when the outflow rate, V, is zero and inflow rate, braiding speed is still at certain speed. So, take up speed V is really to balance braiding speed, $\frac{\omega r_{rope}}{\tan\theta}$, which maintains the braiding process in dynamic equilibrium. If braiding point is kept at one point on the right of braiding plane in Figure 3.2, braiding speed and take up speed is needed to stay at certain constant value even if

braiding point doesn't move during braiding process. The braiding angle stays constant in this steady state condition.

Now, the resistance and capacitance of MFS is defined. Generally, the calculation for MFS should be started as mass transported. Since yarns and rope is assumed not deflected by tension, the density of yarns and their braided rope will stay same. So, the volume of materials transported is only need to be calculated. And their cross sections have relationship in equation (5). Considering the material flow coming from carriers and going through braiding convergent zone, the resistance R for MFS is defined as the change in volume difference essential to cause a unit change in flow rate. It is shown in equation (6).

$$A = A_{rope} = 32A_{yarn} \tag{5}$$

$$R = \frac{\text{change in steady state position}}{\text{change in materials flow}} = \frac{dH}{dQ} \tag{6}$$

And the capacitance of the MFS is defined to be the change in volume of transported material flow necessary to cause a unit change in the position. It is,

$$C = \frac{\text{change in materials stored}}{\text{change in steady state position}} = \frac{dVolume}{dH} = \frac{AdH}{dH} = A \tag{7}$$

4.2.2 Mathematical Modeling of Braiding Point Pattern on MFS

If the certain velocities ratio is set, the position of braiding point is set as H_0. The following parameters in steady state area can be defined,

x = small change of braiding point from its steady state in x direction, m

q_i = small change of inflow rate from its steady state in x direction, m^3/s

q_o = small change of outflow rate from its steady state in x direction, m^3/s

Since braiding point will oscillate around H_0 in real time, the small deviation of inflow rate is braiding speed multiplied by cross section area of yarns. The small deviation of outflow rate is take-up speed multiplied by cross section area of rope. So, the volume change of transported material flow is equal to net volume during the same time dt seconds. The relationship is shown in equation (8).

$$Cdx = (q_o - q_i)dt \tag{8}$$

Since x is set as small deviation from its steady state position, it has expression as equation (9). And the inflow rate and outflow rate are shown in equation (10) and (11). H is set as H_0+x, so, the equation (4) can be transformed to the equation (12). Combining equation (6), (8) and (10), the resistance can be obtained in equation (13).

$$dH = x \tag{9}$$

$$q_i = dQ_{in} = 32\frac{\omega r_{rope}}{\tan\theta}A_{yarn} \tag{10}$$

where, $A_{yarn}$is cross section area of single yarn.

$$q_o = VA_{rope} \tag{11}$$

where, $A_{rope}$is cross section area of rope.

$$\tan\theta = \frac{R_c}{H_0+x} \tag{12}$$

$$R = \frac{x}{q_i} \tag{13}$$

Substituting q_i=x/R into equation (8), the equation is obtained.

$$C\frac{dx}{dt} = q_o - \frac{x}{R} \quad \text{or} \quad RC\frac{dx}{dt} + x = Rq_o \tag{14}$$

The product of resistance and capacitance, RC, is the time constant of this MFS. Its expression is shown in equation (15). Equation (14) is a linearized mathematical model

for this braiding process when x is set as the system output. Combining equation (7), (11) and (13), equation (14) is transformed to equation (16).

$$RC = \frac{R_c}{\omega r_{rope}} \tag{15}$$

$$\frac{dx}{dt} = V - \frac{\omega r_{rope}}{\tan\theta} \tag{16}$$

Actually, the expressions of inflow rate and outflow rate can be directly substituted to equation (8) to obtain equation (16). At the steady state, the braiding point is static and the braiding speed is equal to the take up speed, which confirms the velocity ratio derivation in the previous work. Finally, the mathematical model of this MFS is obtained in equation (17) substituting equation (1) and (12) to (16).

$$\frac{dx}{dt} = r_{lc}\omega_{lc} - \frac{\omega r_{rope}(H_0+x)}{R_c} \tag{17}$$

The derived equations of MFS are summarized in Table 4.1 to compare with LLS.

This MFS is the first order differential system depending on the braiding velocity and take up velocity, which are inflow rate and outflow rate, respectively. If the inflow rate and the outflow rate can be adaptive change with braiding point, the system will be defined by them and kept in steady state. In this paper, the angular velocity of braiding motor is supposed to be a constant. Unfortunately, the operation properties of braiding motor and its horn gear system will also make the angular velocity of braiding machine slightly oscillate about a constant velocity. And the tension and material releasing process makes inflow oscillate as well. Figure 4.3 is measured angular velocity of braiding motor using encode. So, the system will oscillate in steady state area in order that braiding point locates in its steady state point. Here, the outflow rate, V, will be controlled like q_o in Fig.4.1.

MFS	LLS
Steady state position, H	Steady state head, H
Small deviation of steady state position, x	Small deviation of head from steady state, h
Resistance, $R=\frac{R_c}{32A_{yarn}\omega r_{rope}}$	Resistance $R=\frac{dH}{dQ_{out}}=\frac{h}{q_0}$
Capacitance C of tubular products, $C= A_{rope}$	Capacitance C of tank , $C=\frac{\text{change in materials stored}}{\text{change in head}}$
Steady state flow rate, Q	Steady state flow rate, Q
Small deviation of inflow rate from steady state, $q_i = 32\frac{\omega r_{rope}}{\tan\theta}A_{yarn}$	Small deviation of inflow rate from inflow rate, q_i
Small deviation of outflow rate from steady state , $q_0 = VA_{rope}$	Small deviation of outflow rate from steady state, q_0
Mathematical model, $Cdx = (q_o - q_i)dt,$ $C\frac{dx}{dt} = (q_i - \frac{x}{R}),$ $RC\frac{dx}{dt} + x = Rq_i$ The model will be , $\frac{dx}{dt} = (V - \frac{\omega r_{rope}(H_0+x)}{r_c})$	Mathematical model, $Cdh=(q_i - q_o)dt,$ $C\frac{dh}{dt} = (q_i - \frac{h}{R}),$ $RC\frac{dh}{dt} + h = Rq_i$
Time constant, $\frac{R_c}{\omega r_{rope}}$	Time constant, RC

Table4.1 Comparison of MFS based on braiding process and LLS

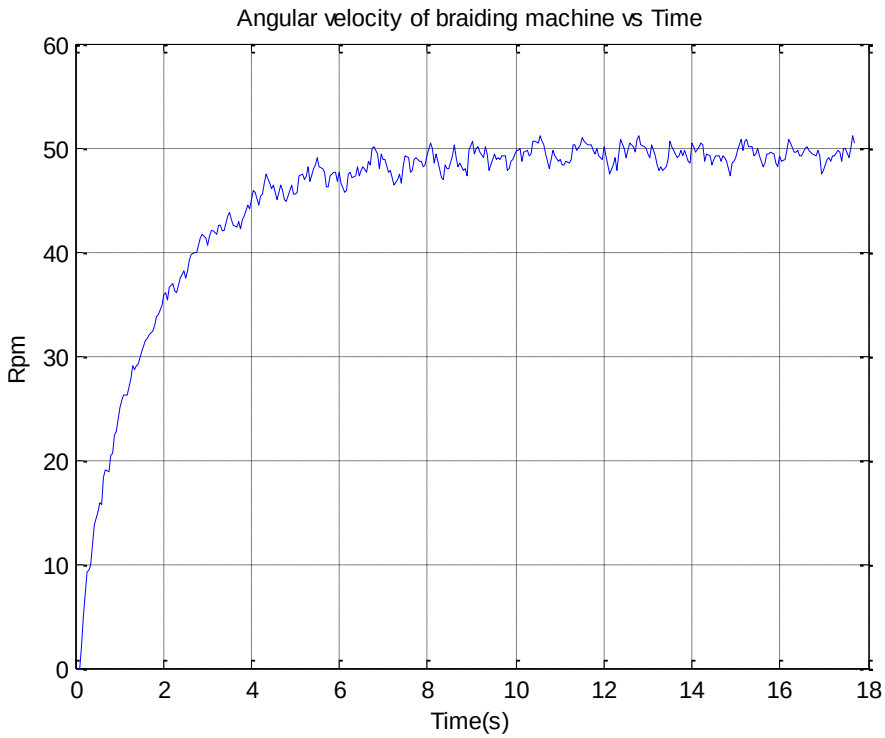

Figure 4.3 Oscillation plot of angular velocity of braiding machine acquired by encoder in Labview program.

4.2.3 Including Take Up Motor

In the definition of MFS, the take up motor is used to produce the take up speed for this system. The take up motor also includes a capstan and a gear train. Its model should be investigated, too. Since the take up velocity is always kept by certain value in steady state, angular velocity of load shaft, ω_{lc}, will be set as a variable in this paper. Tension, T_{rope}, in equation (28) of chapter 3 is transformed from load torque of an actuator.

$$T_{rope} = \frac{\tau_{lc}}{r_{lc}} \tag{18}$$

where, τ_{lc} is the load torque from an actuator.

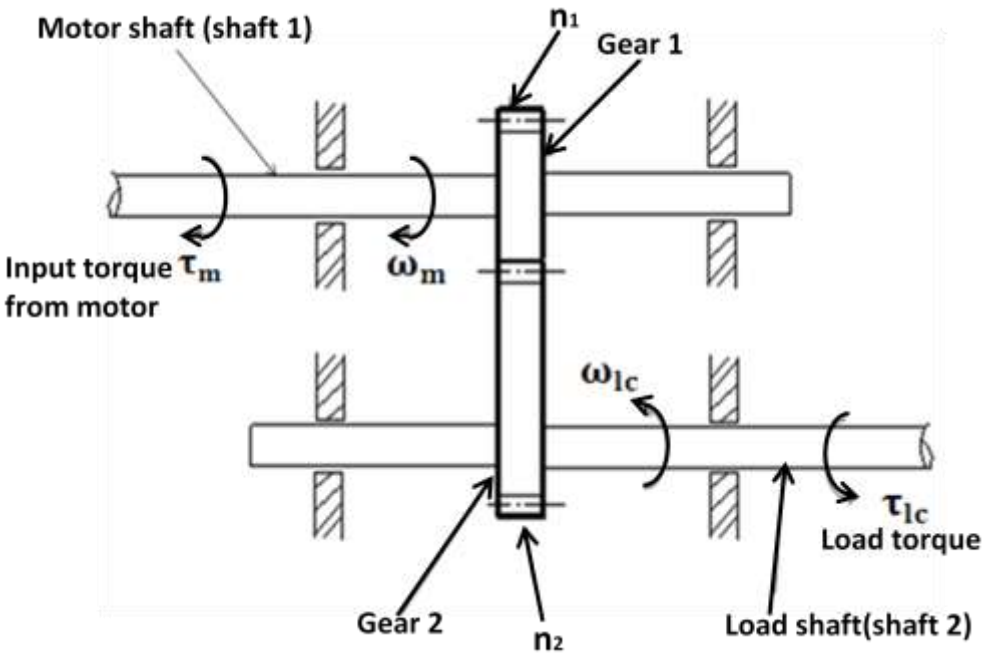

Figure 4.4 Gear train system of take up motor

Because the motor also connected with a gearhead, the load torque needs to be transformed from motor torque. All the parameters are shown in Figure 4.4. For the motor, the equation of motion is set as equation (19).

$$J_m\dot{\omega}_m + b_m\omega_m + \tau_{mg} = \tau_m \tag{19}$$

Where, J_m, $\omega_m, b_m, \tau_{mg}, \tau_m$ are moment of inertia, angular velocity, damping coefficient, load torque of motor and torque developed by the motor, respectively.

For the load shaft, a torque coming from the gearhead will drive the capstan. The equation of motion is shown in equation (20).

$$J_{lc}\dot{\omega_{lc}} + b_{lc}\omega_{lc} + \tau_{lc} = \tau_g \tag{20}$$

Where, J_{lc}, $\omega_{lc}, b_{lc}, \tau_g$ are moment of inertia, angular velocity, damping coefficient and transmitted torque from the gear in motor side, respectively. For the properties of DC motor, the relationship between motor torque and current driving motor, i_m, is also called

armature current. The relationship between armature current and motor torque is shown in equation (21). The induced voltage e_b is proportional to the angular velocity ω_m, which is shown in equation (22).

$$\tau_m = K_t i_m \tag{21}$$

Where, K_t is motor torque constant.

$$e_b = K_b \omega_m \tag{22}$$

Where, K_b is the back-emf constant.

For the armature circuit, the equation is shown in equation (23). e_m is the applied motor voltage and R_m is armature resistance.

$$R_m i_m + e_b = e_m \tag{23}$$

Also, $$\tau_{mg} = \tau_g \frac{\omega_{lc}}{\omega_m} = \tau_g \frac{n_m}{n_{lc}} \tag{24}$$

where,n_m, n_{lc} are number of teeth of gear in motor side and load shaft side, respectively. The ratio of geartrain is set as $n = \frac{n_m}{n_{lc}}$. Combining equation (19), (20) and (24), expression of τ_m by θ_m , θ_{lc} and τ_{lc} are able to be obtained in equation (25) and (26).

$$J_{meq}\dot{\omega_m} + b_{meq}\omega_m + n\tau_{lc} = \tau_m \tag{25}$$

Where, $J_{meq} = J_m + (\frac{n_m}{n_{lc}})^2 J_{lc} = J_m + n^2 J_{lc}$; $b_{meq} = b_m + (\frac{n_m}{n_{lc}})^2 b_l = b_m + n^2 b_{lc}$.

$$nJ_{lceq}\dot{\omega_{lc}} + nb_{lceq}\omega_{lc} + n\tau_{lc} = \tau_m \tag{26}$$

Where, $J_{lceq} = J_{lc} + (\frac{n_{lc}}{n_m})^2 J_m = J_{lc} + \frac{J_m}{n^2}$; $b_{leq} = b_{lc} + (\frac{n_{lc}}{n_m})^2 b_m = b_{lc} + \frac{b_m}{n^2}$.

Combining equation (21), (22), (23) and (26), function between motor voltage and T_{rope}, is derived in equation (27). Substituting the equation (28) in chapter 3 to equation (27), the expression about armature current and displacement of braiding point will be obtained by equation (28).

$$\frac{K_t}{R_m} e_m = nJ_{leq}\dot{\omega_{lc}} + nb_{lceq}\omega_{lc} + nr\tau_{lc}T_{rope} \quad (27)$$

$$\frac{K_t}{R_m} e_m = nJ_{lceq}\dot{\omega_{lc}} + (nb_{lceq} + \frac{K_t K_b}{nR_m})\omega_{lc} + nr_{lc}(32nr_{lc}T_0\cos\theta + nr_{lc}\sum_{i=1}^{32} w_i\cos\theta) \quad (28)$$

From the equation (28), the armature voltage is able to be calculated in steady state of braiding point. This voltage provides the take up speed for braiding process as needed. Since DC servo motor is able to provide for large velocity changes, the variation of armature voltage doesn't need to be considered when it is controlled during braiding process.

$$e_{m0} = (\frac{n^2 R_m b_{lceq} + K_t K_b}{nK_t})\omega_{lc0} + \frac{32nr_{lc}T_0 R_m H_0}{K_t\sqrt{H_0^2 + R_c^2}} \quad (29)$$

4.3 Controller and Simulation

4.3.1 Behavior of Plant

Based on the definition of MFS, the steady state position of braiding point is known in x direction. The time constant of MFS is $\frac{R_c}{\omega r_{rope}}$. Since the rope is made without a mandrel, the value of r_{rope} is very small and the value of R_c is relative big, the time constant in equation (15) will be big. That means it spend a long time for braiding point to settle down without control, even if the braiding point has a small offset from its steady state position, H_0. The braiding angle is not the desired value until the braiding point arrives at its steady state point. The original angular velocity of capstan is set as ω_{lc0}, which will let braiding point move to its steady state. When close to steady state, the equation can be expressed in equation (30).

$$dx = (r_{lc}\omega_{lc0} - \frac{\omega r_{rope}(H_0 + x)}{R_c})dt \quad (30)$$

In steady state, the take up velocity and braiding speed have the relationship in equation (31).

$$r_{lc}\omega_{lc0} = \frac{\omega r_{rope} H_0}{R_c} \tag{31}$$

So, the equation (30) can be transformed to,

$$\dot{x} = -\frac{\omega r_{rope} x}{R_c} \tag{32}$$

In order to find x (t), the Laplace transform of (32) is taken in two side, that is,

$$[sX(s) - x(0)] = -\frac{\omega r_{rope}}{R_c} X(s) \tag{33}$$

So, time function of x is shown in equation (34).

$$x(t) = x(0)e^{\left(-\frac{\omega r_{rope}}{R_c}\right)t} \tag{34}$$

The plots of plant behavior are shown in Figure 4.5. The left figure is showing about the initial position of braiding point is 50 mm on the right of H_0. And the right figure is 50mm on the left of H_0. It costs more than 1000 seconds to arrive the steady state of braiding point when angular velocity of braiding machine is 5 rpm and take up angular velocity is 0.0083 radian/s. And the braiding angle is calculated using the equation (12). And the plot of braiding angle changing with time is shown in Figure 4.6 when the initial position of braiding point is ±50mm. The braiding angle offset from its steady state value in most time of this period. The setup time of braiding process, therefore, is quite large and costly to a manufacturer.

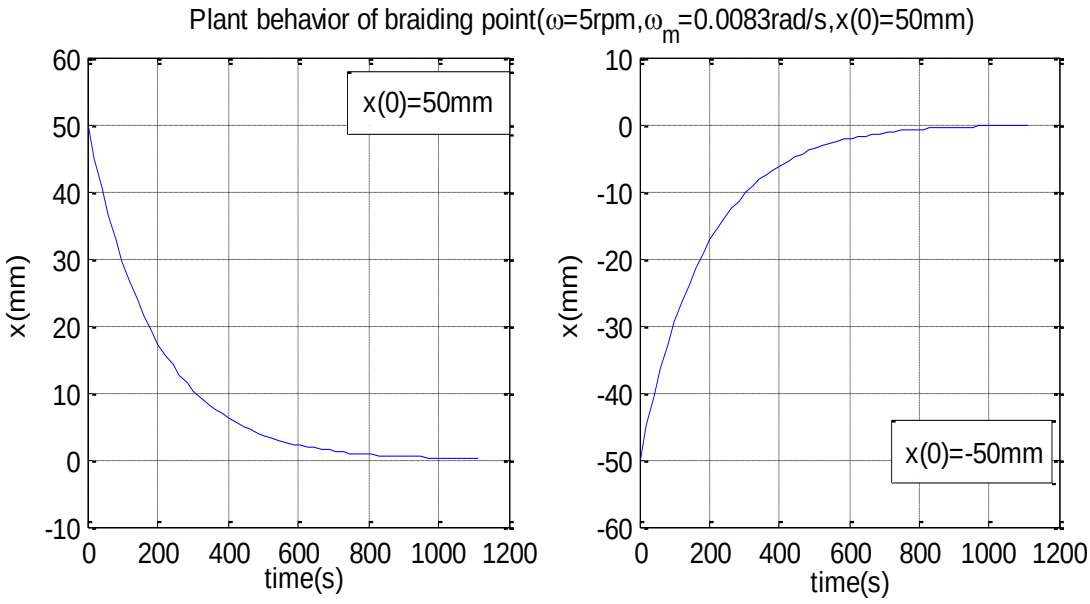

Figure 4.5 Plant behavior plots

In order to keep constant take up speed, the motor voltage should satisfy the equation (35), which transform from equation (28). Since the x(t) is so small comparing H_0, armature voltage is almost constant. In addition, the DC servo motor is able to provide angular velocity in big range and the torque almost keeps in constant value. So, how DC servo motor works doesn't need to be considered when its speed is controlled by reasonable value.

$$e_m(t) = e_{m0} - \frac{nr_l 32 T_0 R_m (H_0 + x(t))}{K_t \sqrt{(H_0 + x(t))^2 + R_c^2}} \tag{35}$$

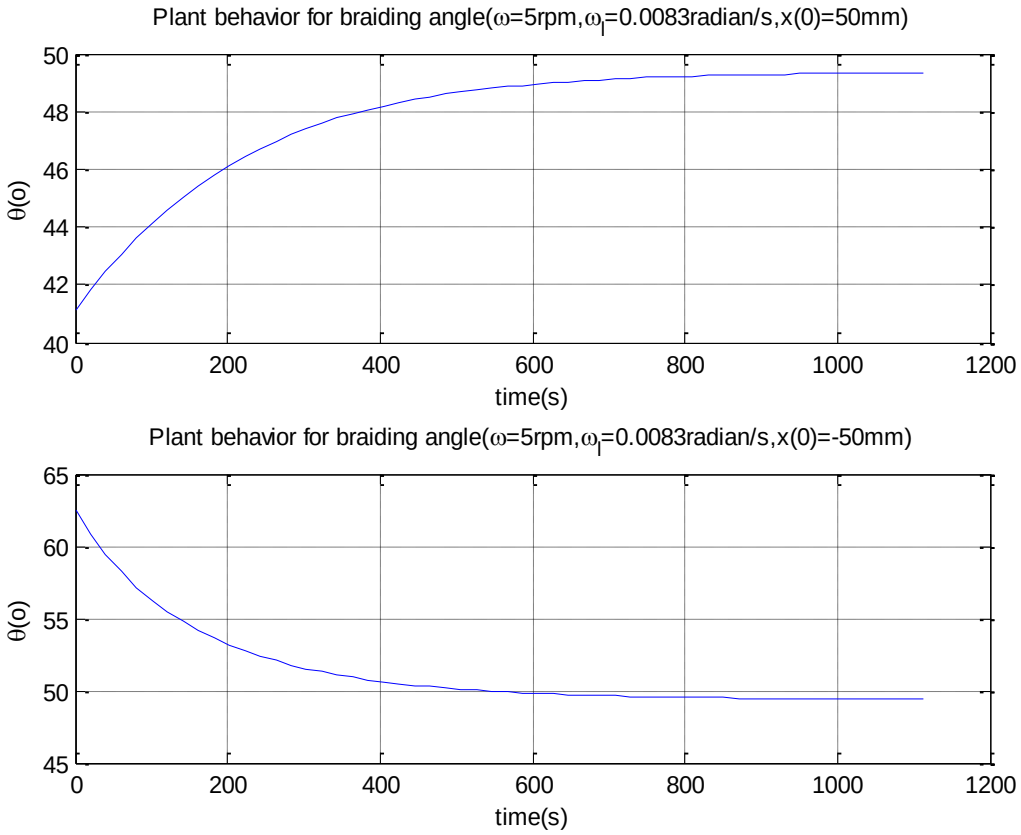

Figure 4.6 Plant behavior of braiding angle

4.3.2 PI Feedback Controller bases on MFS

In order to control the position of braiding point, the inflow rate and outflow rate should be controlled. That means two velocities should be controlled. In this paper, the take up motor is only one to be controlled. So, this MFS is one input and one output system. If the braiding point is set as offset, ±50 mm from its steady state, it will spend a long time to go back to its steady state point. In Figure 4.5, the settle time is 1113 seconds. During this period, the length of products is 2.0487m, which does not satisfy the required braiding angle. That means the required braiding angle for high quality braided products can be achieved only after this period. In order not to waste this much material,

the setup time of braiding process, which is the time between the time point of starting two motors and the time point of braiding process start to braid the products at required braiding angle, need to be reduced. And during the braiding process, the braiding point oscillates like the discussion in last chapter. This oscillation also affects the required braiding angle for high quality braided products. That means desired position (x direction) of braiding point should locate at point, H_0, which is the steady state position of braiding point and also the setpoint for control reference. In order to quickly arrive at steady state position point at the beginning and keep braiding point in steady state during process, the take up motor speed need to be controlled with an effective appropriate control strategy. The strategy chosen here is to 1) increase the angular velocity of take up motor if x is negative, and 2) if x is positive, take up motor is stopped since the rope cannot be pushed. One strategy could also be to let take up speed be certain negative value less than the braiding speed. In this paper, however, the take up motor will be held fixed when x is positive.

If only considering reducing the setup time at beginning of braiding process, a P controller might be acceptable. For reducing the error during braiding process, however, the integrate gain need to be added. So, this PI controller is actually piecewise feedback controller, input will be set as u (t) =$\omega_{lc}(x)$=ω_{lc0}-$K_p x$-$\frac{K_I}{s}x$ and u (t) =$\omega_m(x) = 0$ when x is negative and positive, respectively. Substituting these inputs into equation (34), the equation (36) and (37) can be obtained.

For $H>H_{desired}$, $x>0$. $dx = \left(-\frac{\omega r_{rope}}{\tan\theta}\right)dt = -\omega r_{tf}\frac{(H_0+x)}{R_c}dt$ (36)

For $H\leq H_{desired}$, $x\leq 0$, $dx = \left(r_{lc}\omega_{lc}(x) - \frac{\omega r_{rope}}{\tan\theta}\right)dt = (r_{lc}(\omega_{lc0} - K_p x - \frac{K_I}{s}x) - \omega r_{tf}\frac{(H0+x)}{R_c})dt$

$$dx = (-r_{lc}(K_p x + \frac{K_I}{s} x) - \omega r_{tf} \frac{x}{R_c})dt \tag{37}$$

In this case, the position of braiding point will oscillates around H_0 in real time. On the other side of H_0, the take up motor will work in different strategies. When the braiding point located in the positive side (right side in Figure 3.2), only braiding motor pull it back while simultaneously stopping take up motor, which is shown in equation (36). Otherwise, the braiding motor works with controlled take-up motor. From the above two equation, the time solutions of $x \geq 0$ are obtained in the equation (38). And state space model for $x<0$ is shown in equation (39).

For $x \geq 0$, $$x(t) = H_0(1 + e^{-\frac{\omega r_{rope}}{R_c} t}) \tag{38}$$

For $x<0$, $$\begin{cases} \begin{pmatrix} \dot{x} \\ \ddot{x} \end{pmatrix} = \begin{bmatrix} 0 & 1 \\ -r_{lc}K_I & -r_{lc}K_p - \frac{\omega r_{rope}}{R_c} \end{bmatrix} \begin{pmatrix} x \\ \dot{x} \end{pmatrix} + \begin{bmatrix} 0 \\ r_{lc} \end{bmatrix} \omega_{lc} \\ y = [1 \;\; 0] \begin{pmatrix} x \\ \dot{x} \end{pmatrix} \end{cases} \tag{39}$$

Using MATLAB code, the PI piecewise feedback controller is tuned using different PI gains. The following Figures 4.7 and 4.8 are shown the behaviors with same PI gains in different control strategies, which are continuous PI controller and piecewise PI controller uses in this paper. When $x>0$, the behavior of braiding point is much different between continuous PI controller and piecewise PI controller. That is because that only braiding motor pulls braiding point back to its steady state at constant velocity when braiding point is on the right side of its steady state. There are big overshoot in Figure 4.7, which cause braiding point to take 10 seconds to go back to its steady state. In Figure 4.8, this period only causes 6 seconds. Too much overshoot is not desired, since it leads to large positive offset of the braiding point from its steady state location. So, PI gains leading to small overshoot are preferred.

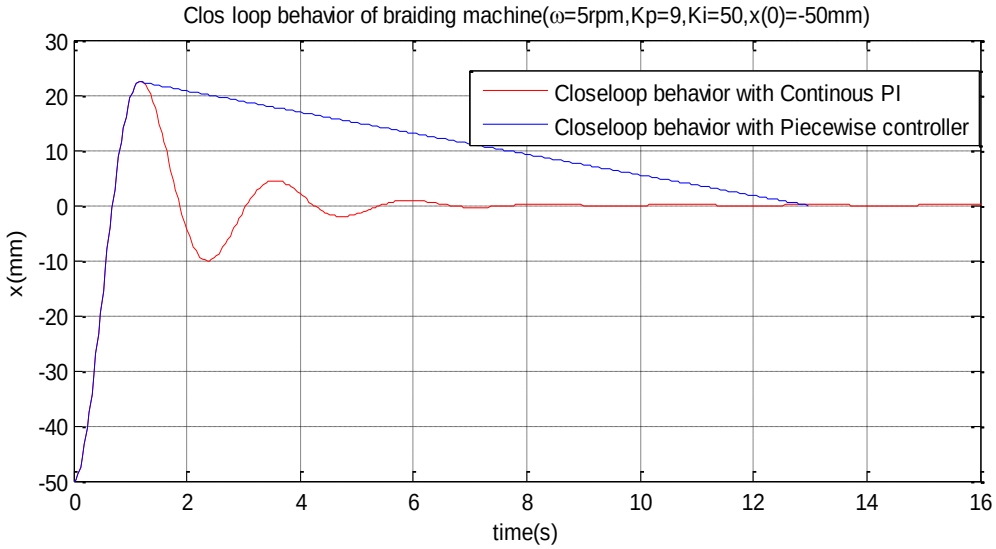

Figure 4.7 Close loop behavior using continuous PI controller and Piecewise PI controller with K_p=9, K_I=50.

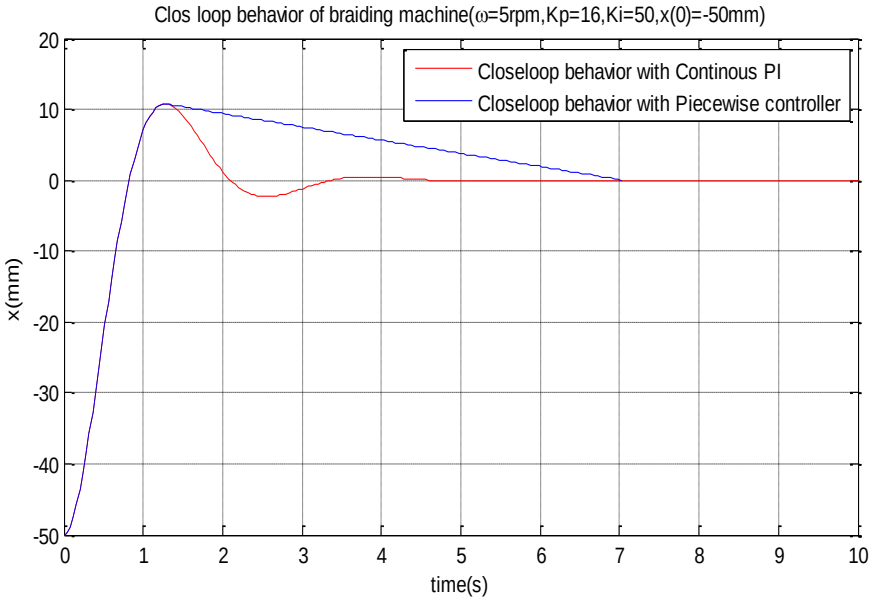

Figure 4.8 Close loop response of braiding system with PI controller and Piecewise PI controller with K_p=16, K_I=50.

4.3.3 Control Block Diagram

The basic components of MFS are depicted in Figure 4.9 using standard Laplace notation. The take up motor closes a current loop and is modeled simply as a linear transfer function G(s). The take up motor will have peak current limit, so this linear

model is not entirely accurate, however it does provide a reasonable representation for our analysis. In their most basic form, take up motor receive a voltage command that represents a desired motor current. For the purpose of this discussion, the transfer function of the current regulator or really the torques regulator can be approximated as unity for the relatively lower frequencies are interested in and therefore the following approximation is shown in equation (40).

$$G(s) = 1 \tag{40}$$

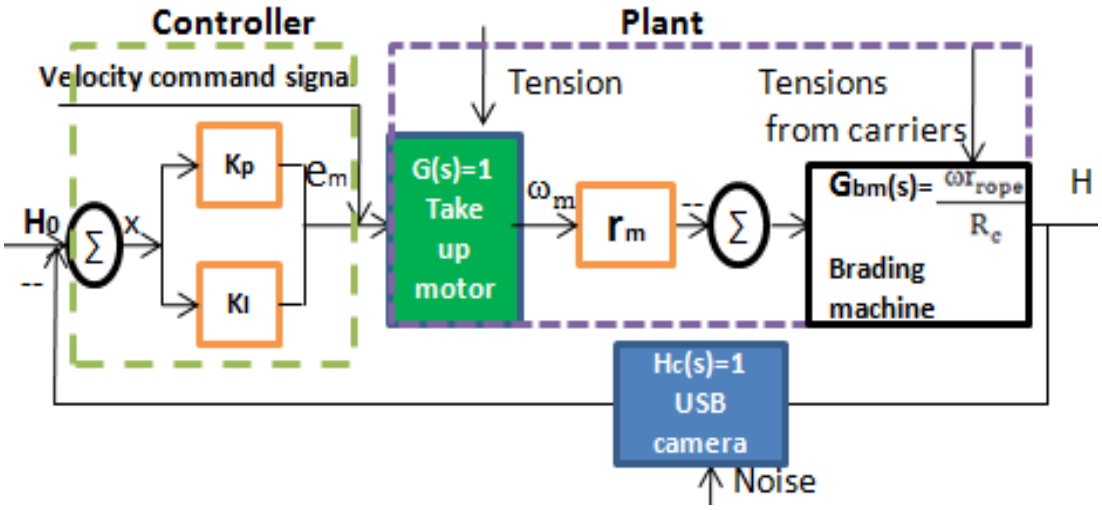

Figure 4.9 Block diagram of braiding system

4.4 Experiment Setting and Control Program

Based on the simulation and controller design in the above section, the experiment is built using separate controllable take up motor. A USB camera acquires the position data of the braiding point, the take up motor is controlled automatically by feedback of this position data.

4. 4.1 Experiment Setting Up

In this paper, motion control involves precise control of position by checking the position of braiding point from image processing loop. The motion controller calculates trajectories and completes the position/position derived loops (PI) via the encoder. The servo amplifier (drive) outputs a current proportional to an input signal-voltage received from the motion controller.

Figure 4.10 is a visual representation of the motion control hardware including some actual components and their connectivity. The NI UMI-7764 is used to provide connectivity between servo drives and PCI 7734 motion controller. All the inputs of the control system come through UMI 7764 via screw terminals such as encoder and motor current monitor signals. The USB camera acquires the position of braiding point working with Labview software, and feedback it to PC for images processing. The current camera is Philips spc 900nc/00, which acquire the images by 320x240[pixel] and 30 fps. The controlling program will compare the position with the setpoint, H_o. Then, based on the error, x, between position of braiding point and the setpoint, PCI 7344 will let Amplifier output the current to take up motor. The take up motor will have responding operation based on the current. The feedback device will monitor the angular velocity of braiding motor.

The National Instruments (NI) PCI 7344, which is a four axis motion controller including an onboard CPU with an embedded real-time operating system. And it has a Proportional Integral Derivative (PID) update rate of 62 μs per axis. This device has four general purpose analog outputs that are used for monitoring and feedback. A servo axis operates in closed-loop mode, using quadrature encoders or analog inputs to provide position feedback.

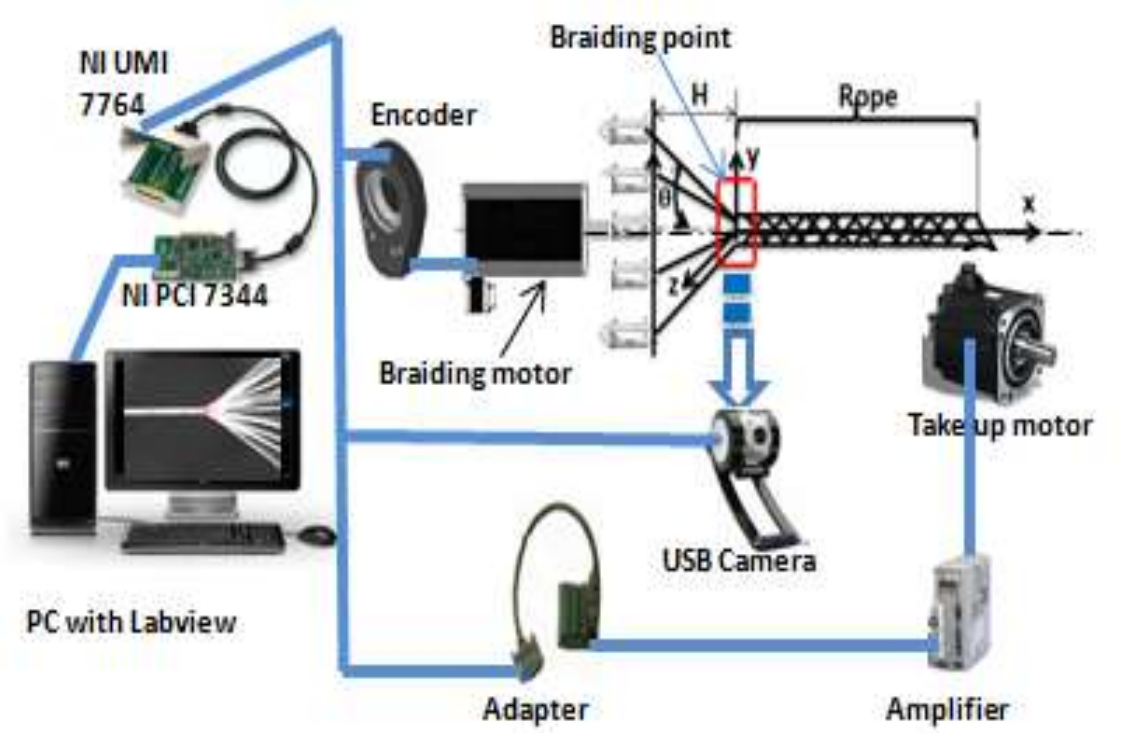

Figure 4.10 Sketch of braiding machine with controller and fabric product

4.4.2 Control Program

Labview is very powerful at image processing. Using machine vision, USB camera could be used to acquire images and PC is used to process images. Machine learning and template matching used in last chapter is really useful in this chapter.

4.4.2.1 Image Processing Loop

How to run program to acquire position using image processing loop has already been discussed before. In this chapter, the principle of machine vision used by Labview software is discussed. The Figure 4.11 is shown the block diagram of machine vision sensing loop of control program. The big gray rectangle is shown in Figure 4.11. This is

the While Loop, which is like a while loop in C/C++. At first, the program will set up some commands to initialize the camera and set up temporary memory for images and a template in PC, which locate in left side of while loop. Then the program will start to run the while loop to acquire the images. Following the signal flow, the program will acquire the images first. These images grabbed by camera are RGB images, which will be needed to convert to grayscale, 8 bit images. These images in grayscale are better to be processed by software under template matching algorithm. There are two commands, Case Structures, in command, While Loop. The two Case Structures are in two red rectangles. The commands in left case structure are set to learn template. When the template in the front panel is drawn, the background subtraction will extract the object from the image. And then the program will remember every detail including lines and dots of the template. The methods used to record information of template include drawing coordinate system, looking for object, measuring distance, overlaying and so forth. When the search button is pressed, the program will match every new acquired image with recorded information of the template. When the new image matches the template over threshold, it will draw the same rectangle in monitor window to highlight the template. The process of drawing template called draw pattern matched position, which is a subprogram shown in Figure 4.12. Simultaneously, the machine vision loop will output the position of centroid of template, which is really the braiding point pattern.

4.4.2.2 Controller for Take Up Motor

Following the controller designed in section 4.3.2, the corresponding controller is set up in program. The controller is shown in the command, Case Structure of Figure

4.13. At first, the program reads x position acquired form machine vision loop and compares it with setpoint, H_0. If condition is true, the PI controller on take up motor will speed up the take up motor. Otherwise, the PI gains will go to zero, which is false case (not shown) in Figure 4.13. In the command, Case Structure, the P gain, K_p, is 100 and I gain, K_I, is 75. The gray rectangle inside case structure is Formula Note for calculating the integrated error. Every error will be stored in shifter, which is shown in Figure A.4.1 of Appendix. And there is command called Load Velocity Override (inside case structure of Figure 4.13), which can run the take up motor in real time. But, the velocity cannot be negative for this command. If take up motor need to be turned backward, the take up motor need to be resumed. This may make the velocity has big jump. So, the take up motor isn't usually turned backward. In addition, when the command, Load Velocity Override, is used, the command, Load Velocity Filter Parameter, is also used to filter velocity when the data is to be written to a file.

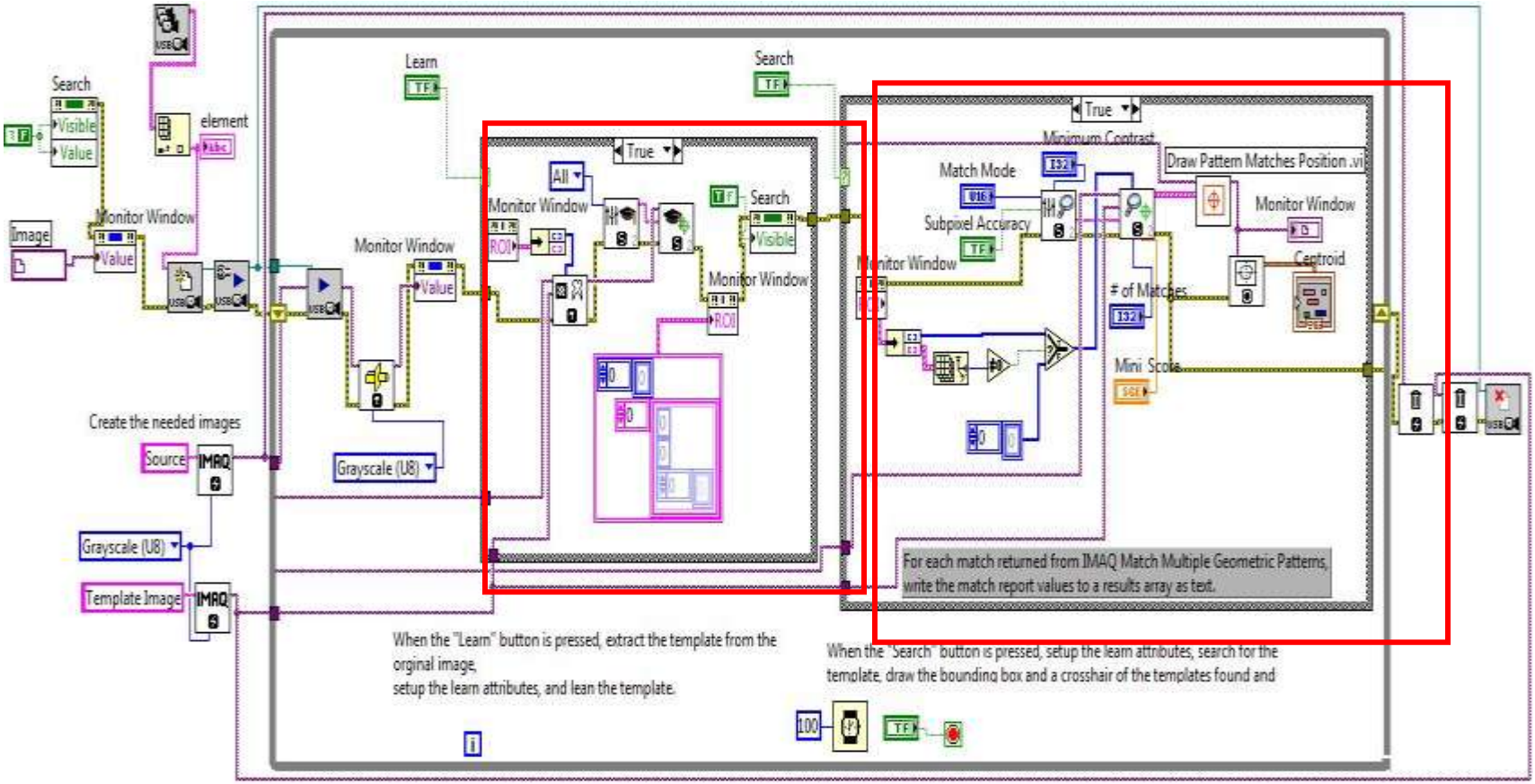

Figure 4.11 Machine vision loop

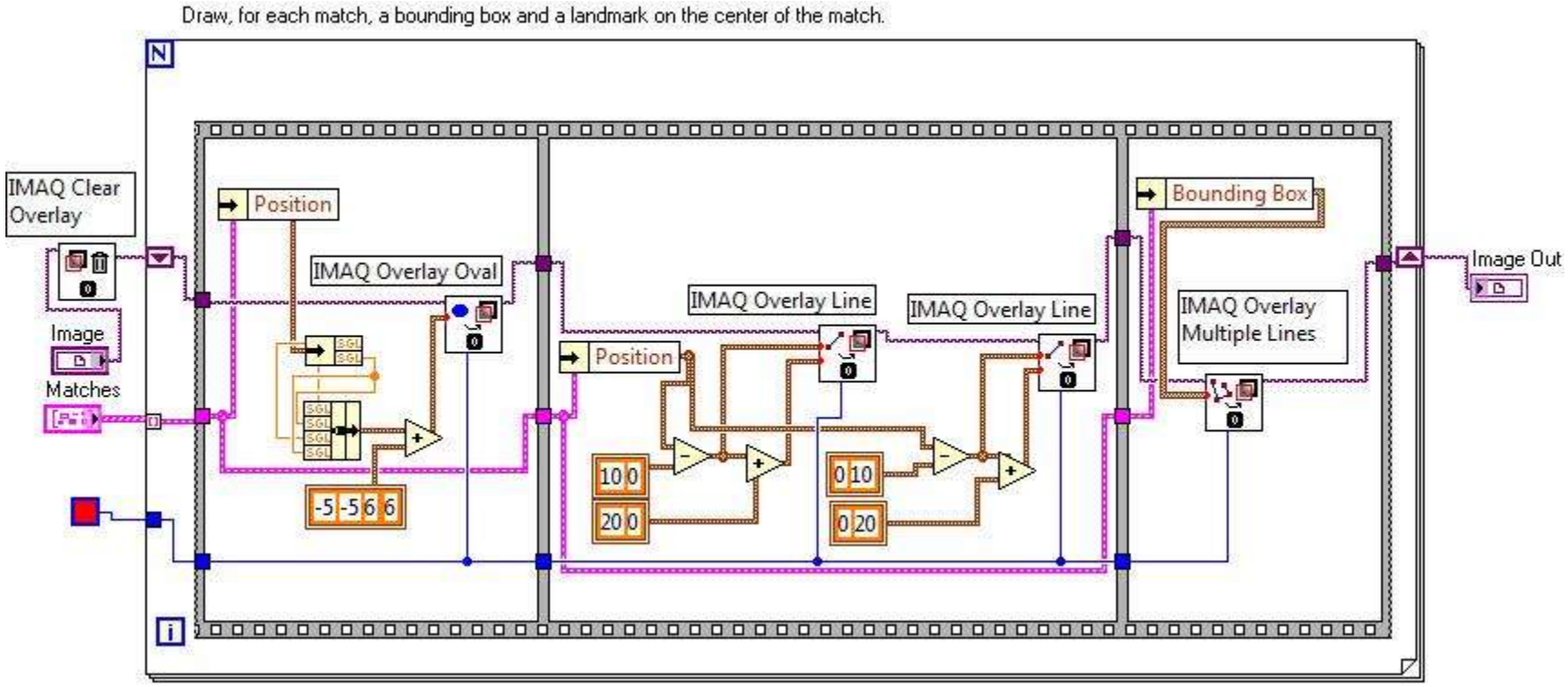

Figure 4.12 The sub-function to highlight the template

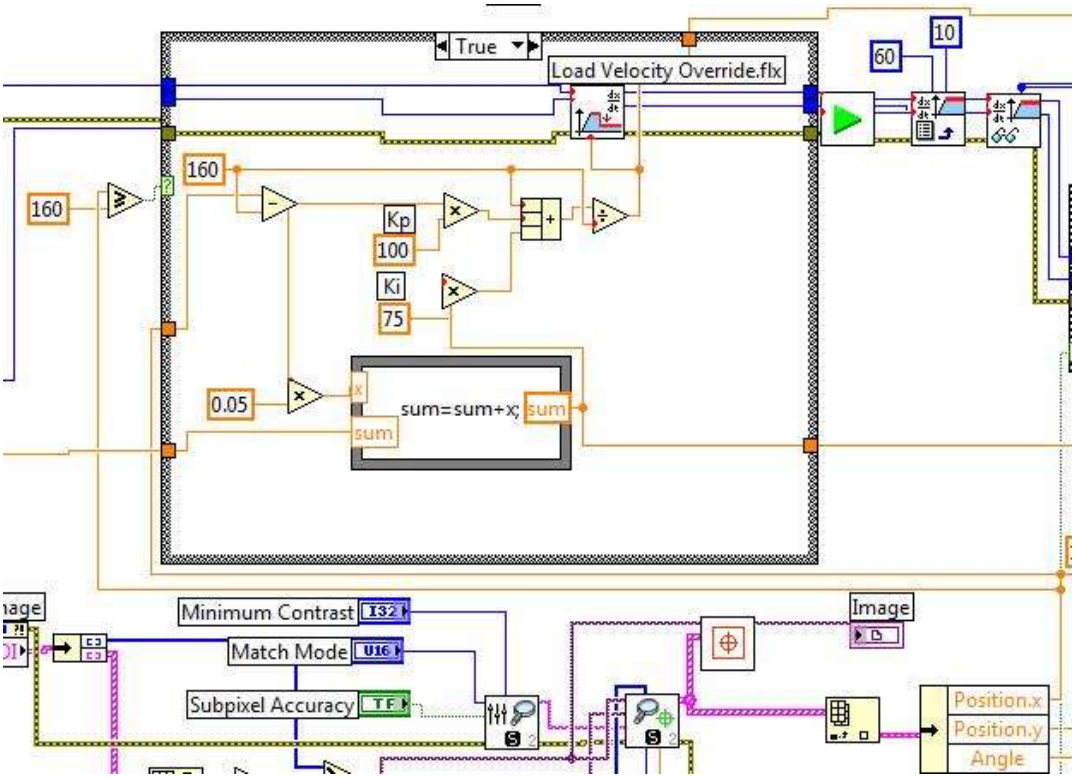

Figure 4.13 The controller of take up motor

4.4.2.3 Control Program including Image Processing Loop and Motion Control Loop

Based on the properties of USB camera used in this paper, the small delay time limit for one frame of image is 33.3 ms. In this control program, the waiting time is set as 50 ms, which is enough to let program process images and control the motion. The flow chart in Figure 4.14 shows the image processing loop and motion control loop.

The two loops are parallel. They will communicate to each other when it compares the x position of braiding point with the setpoint, H_0. With respect to the different condition, the program will operate take up motor in different strategies. At first, the controller reads x position acquired from machine vision loop and compares it with the setpoint, H_0. Every error will be stored in a shifter. A command called Load Velocity Override runs the take up motor in real time based on the error. It should be noted that the velocity

cannot be negative for this command. The take up motor is not run in reverse (if the take up motor need to be backward, it would be necessary to resume the take up motor, causing a jump in the velocity).

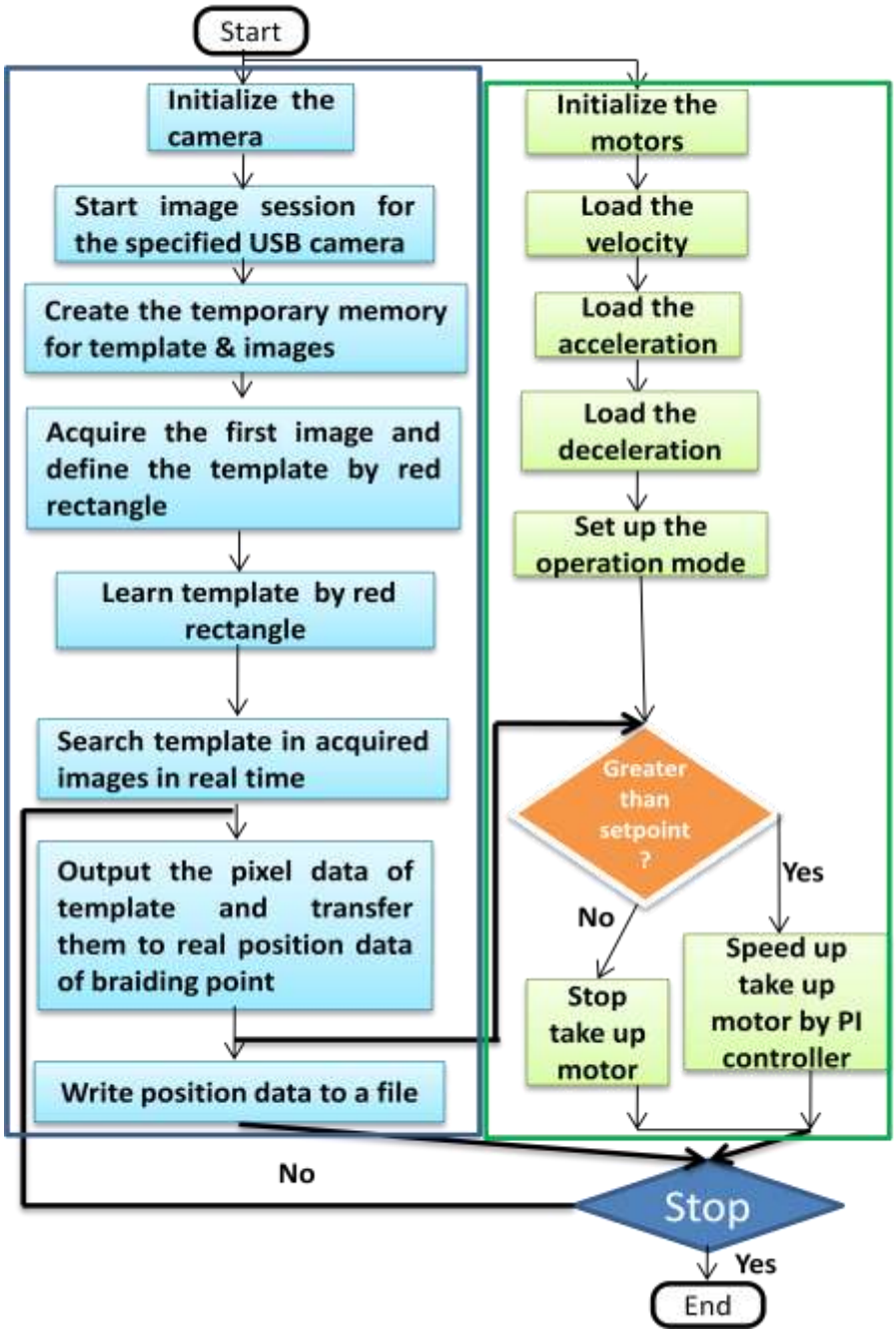

Figure 4.14 Flow chart of controlling program

Figure 4.15 is front panel of controlling program in Labview. The window in the middle is monitor window for monitoring braiding point. This monitor window is mainly for tracking braiding point, which is discussed in last chapter. In this chapter, the other controlling windows and buttons are emphasized. There are four oscilloscope windows: the window on the top left is shown X position (take up direction) of braiding point; the window in the top right is shown Z position of braiding point; and the window in the right bottom monitors the velocity of take up motor. This case is for USB camera is on the bottom of braiding point. If the camera is put on the side of braiding point, the top right wind represent Y position of braiding point. And for the right middle window, it is a window controlling the velocity of take up motor in real time. Its value is used as input for command, Load Velocity Override. In small velocity window under axis 2, the maximum velocity for command, Load Velocity Override, can be set up. Since the time of image processing loop is faster than that of motion control loop, the take up motor cannot increase its speed quickly in the small waiting time, 50 ms. In this case, the more acceleration of take up motor need to be added to fix this problem. In the appendix 2, the whole block diagram is attached as a reference.

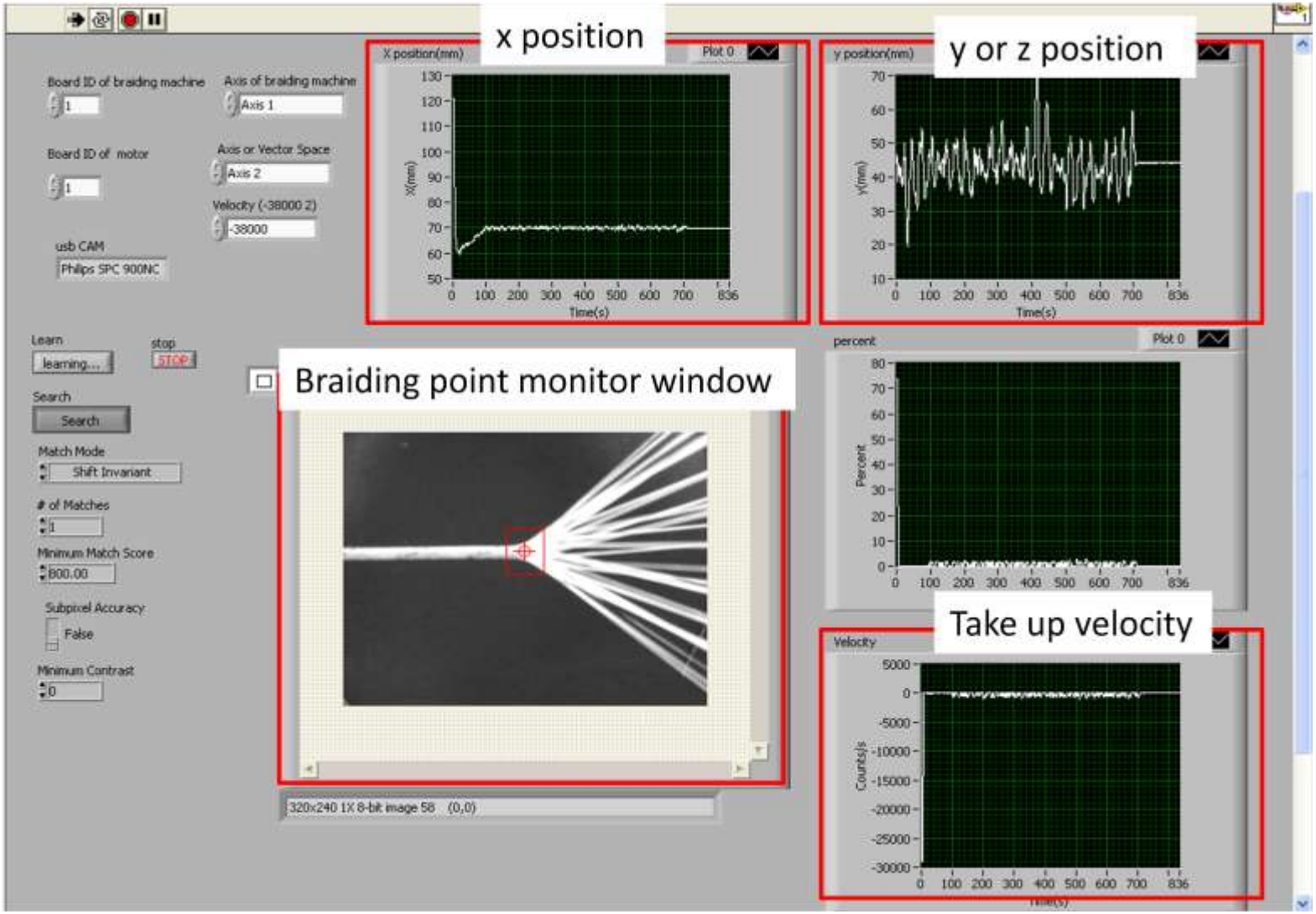

Figure 4.15 Front panel of controlling program

4.5 Correlation between Simulation and Experimental Data

In order to confirm our simulations and validate the mathematical model, numerous experiments were conducted. Simulations were correlated to the experiment, with the overall good correlation.

4.5. 1 Plant Behavior

Comparing the plant behavior in Figure 4.5, the position of braiding point is acquired without control when braiding point offset about 50mm from its steady state. For the correlating plot of the simulation and experimental data shown in Figure 4.16, they match with good accuracy. That confirms our analysis about model of MFS. The simulation plots are the plant behavior plots in Figure 4.5. So, the braiding angle of experimental data should be same as Figure 4.6 when adding some oscillations onto the position data.

4.5.2 Close Loop Behavior

The different PI gains are the next to use to tune a PI controller. Using different PI gains, the following figures are got. In Figures 4.17, the close loop behaviors was compared for simulation and experiments with K_p=10, K_I=10. The same close loop responses are compared with plant behavior in Figure 4.18. The closed loop response is almost invisible comparing the plant behavior under the same conditions. That confirms the controller on take up motor successfully reduce the setup time of braiding process. The length of material spent in plant without feedback control is 2.0487m when they settle down to steady state from ±50mm offset. And the elapsed time is 1113.1s. For a controlled braiding point, the time needed to complete this process is only 10 s in Figure

4.17 and length of material wasted is 0.0448m. That will save the material about 2 meters every time for the offset length is ±50mm for this particular application.

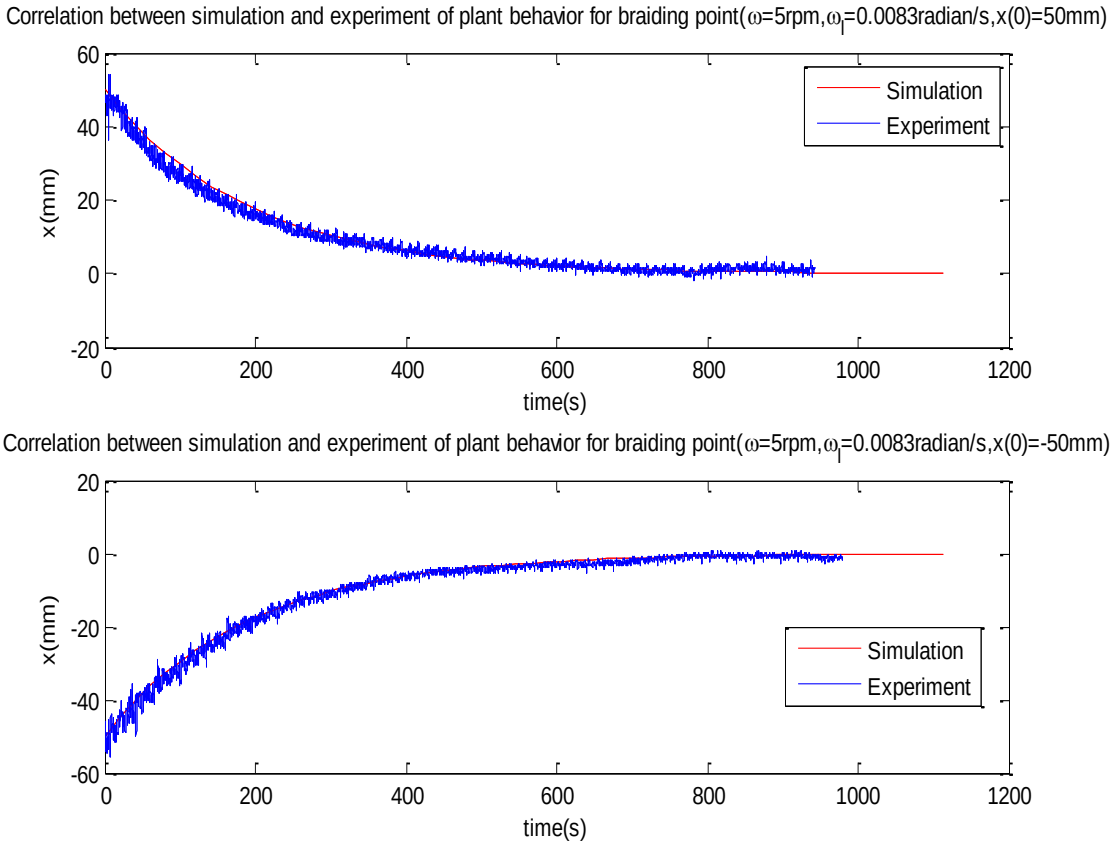

Figure 4.16 Correlation of plant behavior with initial x=±50mm

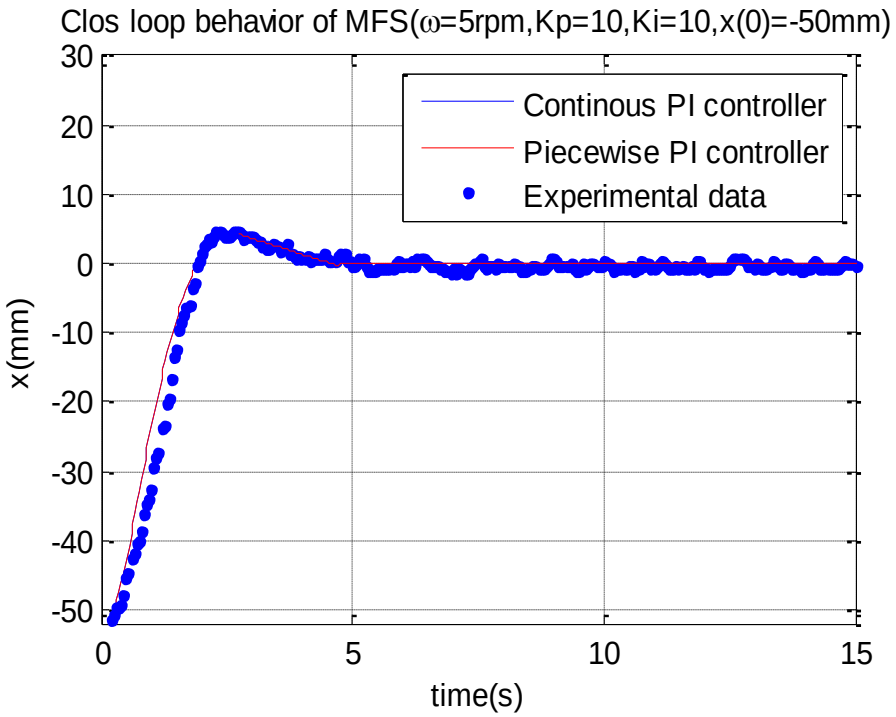

Figure 4.17 The correlation plots of close loop simulation with PI gains, K_p=10, K_I=10

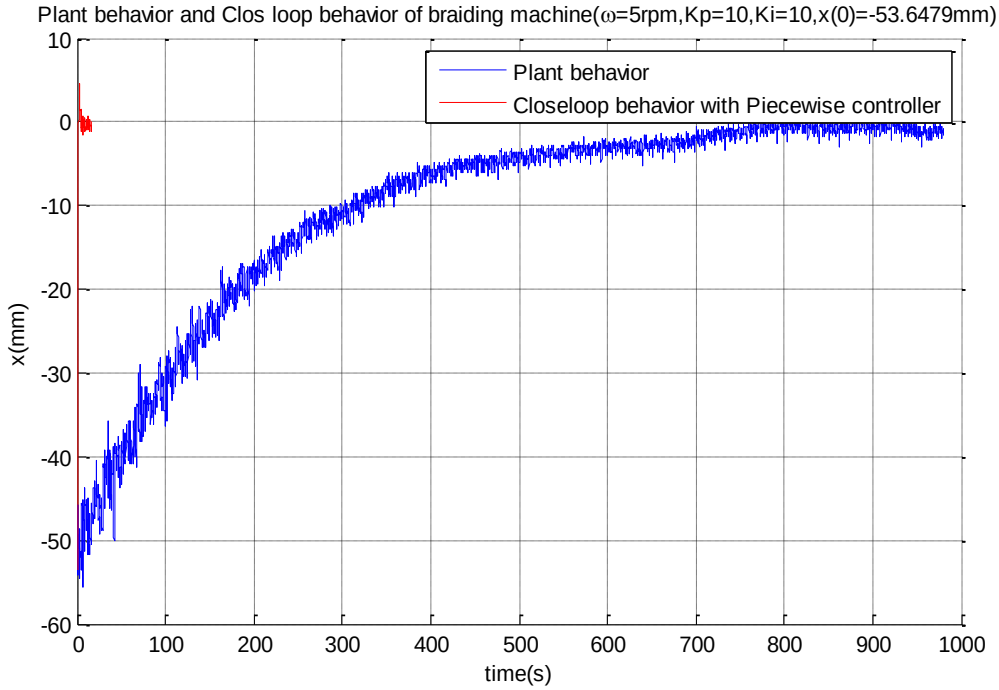

Figure 4.18 Plant behavior and the close loop response with PI gains, K_p=10,K_I=10

The following figures are showing close loop response with different PI gains. Since the waiting time is 50ms, the integrate gain, K_I, should multiply 20 in real

calculation. That's why integrate gain seems bigger than proportional gain. In Fig. 4.19, the settle time is not fast enough even if the overshoot is not big when K_p=15, K_I=140. When K_p=20, K_I=80, the settle time is small and overshoot is not so big in Fig. 4.20. In Fig. 4.21, settle time is still big because big overshoot. When K_p =40 and K_I =140, the settle time and the overshoot are both small. Since the small overshoot and fast response is preferred to get, the PI gains in Fig. 4.22 is preferred. Of course, the initial condition of braiding point will affect the response, too. The follow figures with different initial position of braiding point are shown in the bottom. Mainly, the PI gains are still important effects for response. Anyway, this controller successfully reduces the setup time of braiding process with corresponding PI gains.

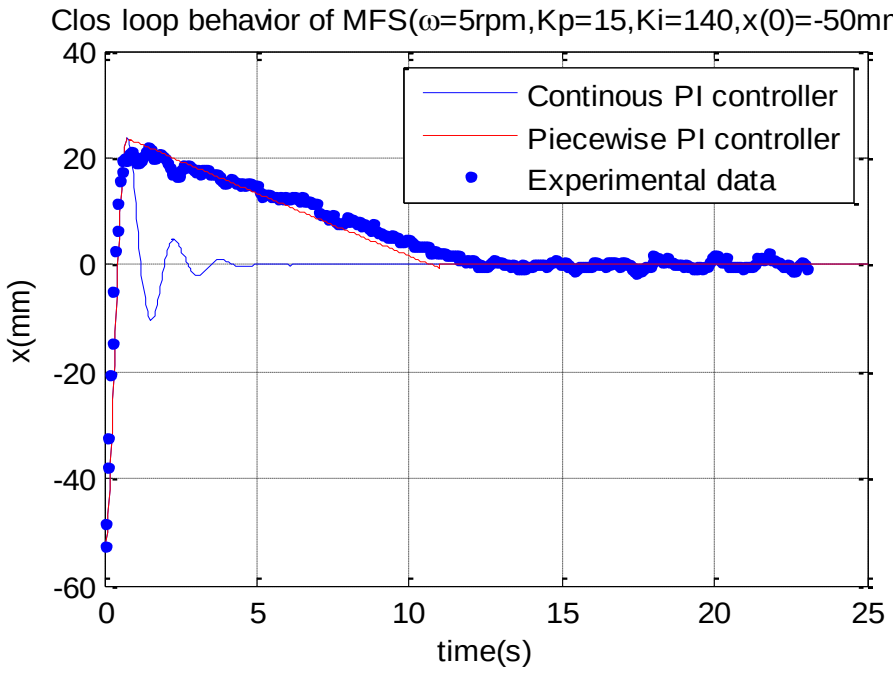

Figure 4.19 The correlation plots of close loop behavior with PI gains, K_p=15, K_I=140

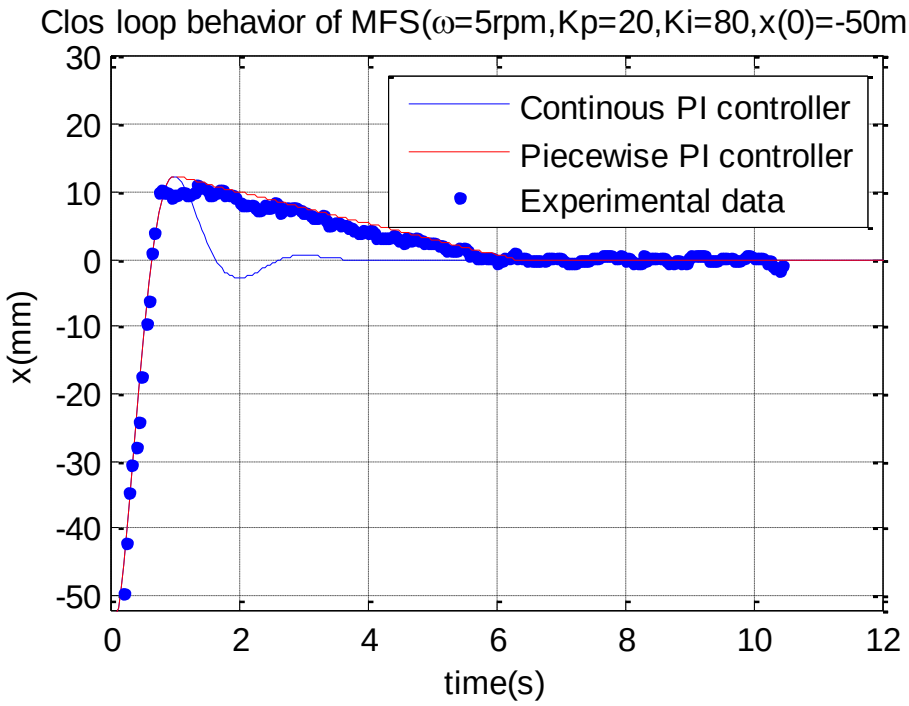

Figure 4.20 The correlation plots of close loop behavior with PI gains, K_p=20, K_I=80

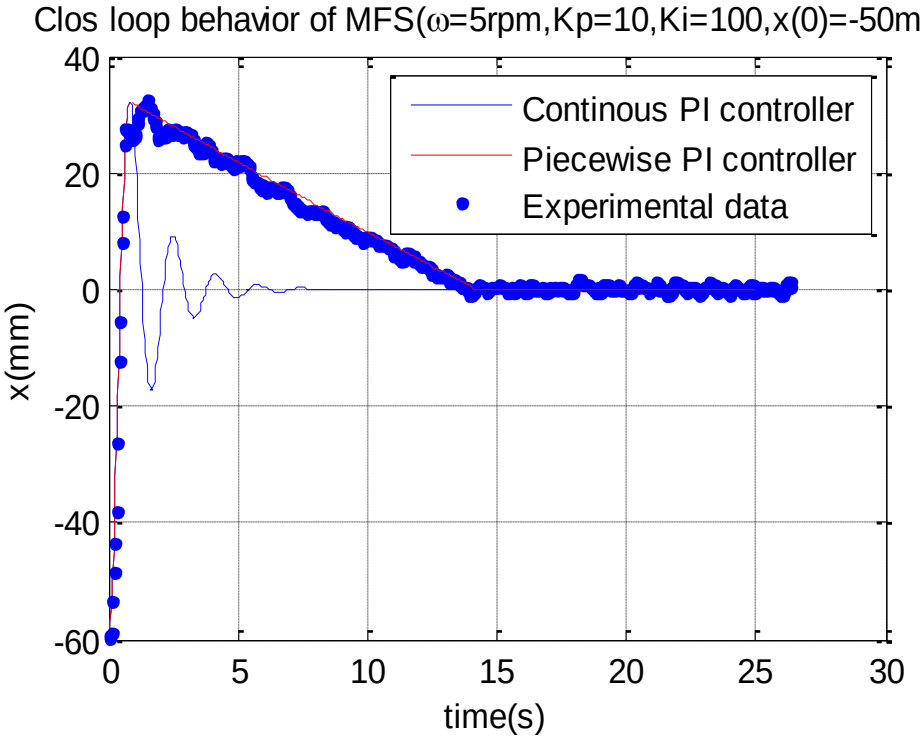

Figure 4.21 The correlation plots of close loop behavior with PI gains, K_p=10, K_I=100

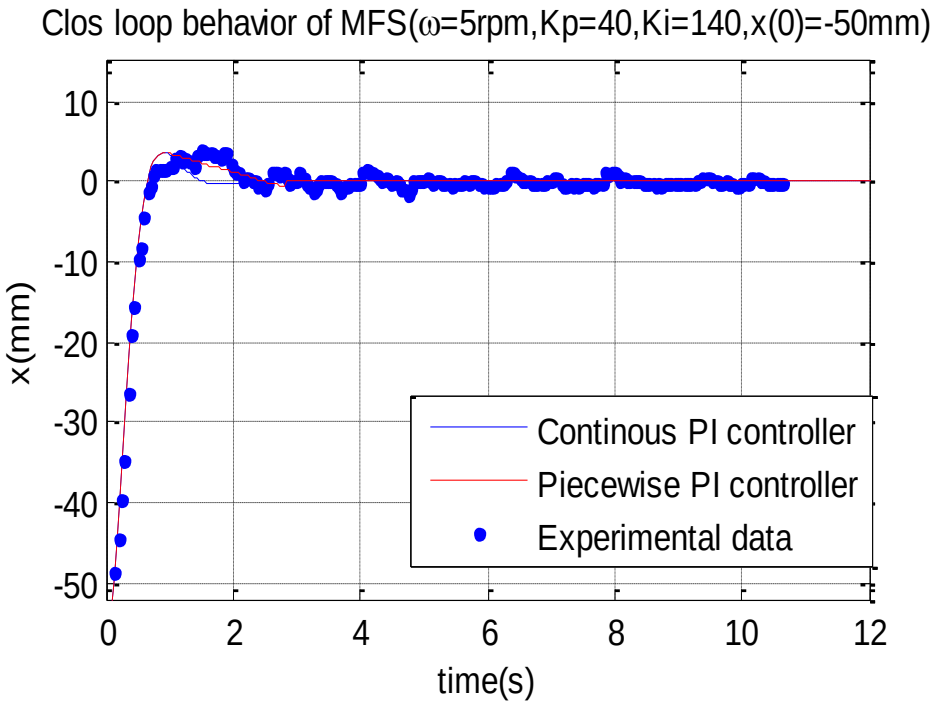

Figure 4.22 The correlation plots of close loop simulation with PI gains, K_p=40, K_I=140

4.6 Conclusion

This chapter defines the new application of MFS in braiding process. The braiding speed is considered as inflow rate and the take up speed is set as outflow rate. A mathematical model is presented that shows the plant to be a first order and nonlinear system. A unique machine vision sensor was created to measure the braid point location. It is first order linear differential system with one input and one output. Using MATLAB code, the plant behavior of system is correlated with the experimental data obtained from machine vision sensing program. The result confirms the definition of MFS.

Next, the take up motor is chosen as the only controlled actuator. Using the position feedback signals, the take up motor with piecewise PI controller is controlled. This controller reduces the braider setup time of braiding time appreciably, hence reducing waste and labor costs. Future work will extend this method to control the braiding process for braided composites that cover cylindrical mandrels of changing diameters.

4.7 List of References

[1] Burkhard Wulfhors, Thomas Gries, Dieter Veit, *Textile Technology*, pp. 201, 2006.

[2] Frank K. Ko, "Braiding," in *Engineered Materials Handbook, ASM International*, Metals Park, OH, 1987, pp. 519-528.

[3] Du, G.W., Popper, P. "Analysis of a circular braiding process for complex shapes," *Journal of the Textile Institute*, v 85, n 3, p 316-337, 1994.

[4] Zhang, Q, Beale, D., Broughton, R. (1999). "Analysis of Circular Braiding Process: Part I: Theoretical Investigation," *ASME, Journal of Manufacturing Science and Engineering*, 121: 345-350.

[5] David Branscomb, David G. Beale, *Thesis, A machine vision and sensing system for yarn defect detection, diagnosis and prevention during manufacture*.

[6] P. Potluri*, A. Rawal, M. Rivaldi, I. Porat, "Geometrical modelling and control of a triaxial braiding machine for producing 3D performs, Composites Part A," *Applied Science and Manufacturing*, Vol. 34, I 6, June 2003, Pages 481-492.

[7] Thomas A. Fischer, "Speed control apparatus and method for braiding machine," *"Braiding Machine", US Patent* #4, 716, 807, 1988.

[8] Bernhard F. Rembold, J. M. A. Tanchoco, "Material Flow Systems in Manufacturing," *Springer*, 09/30/1994.

[9] H. Hojabri, A. Hojabri, A. A. Jaafari, L. N. Farahani, "A Loop MFSDesign," *International Journal of Flexible Manufacturing Systems*, V13, Number 1, 33-48, DOI: 10.1023/A:1008144212451

[10] H. Paul, "Computer simulation of a material flow system," *Computers & Industrial Engineering*, Volume 7, Issue 1, 1983, Pages 23-32

[11] E. Wynn Berry, Jr. "Sewer System", *US Patent* # 6,698,442 B1, 2004.

[12] http://en.wikipedia.org/wiki/Machine_vision

[13] Petrovic, I., Brezak, M., Cupec, R., "Machine vision based control of the ball and beam," *Advanced Motion Control, 2002. 7th International Workshop* on pp: 573 - 577

[14] S. Bahadori, L. Iocchi, G.R. Leone, D. Nardi and L. Scozzafava, "Real-Time People Localization and Tracking Through Fixed StereoVision," *Innovations in Applied Artificial Intelligence*, vol.3533, 2005, pp.44-54.

[15] Katsuhiko Ogata, *System Dynamics* (Fourth Edition), p323, 2004

4.8 Appendices

A.4.1 MATLAB Code for State Space Model Calculation

```
%% statespacemodel.m
%Guangli Ma
clear all
clc
%Parameters defination
pi=3.1415926535897932;
load('positive50mmplantdata2');
load('negative50mmplantdata');
load('fd5rpmn200000Kp2000Ki500');
load('Kp25Ki50');
%Ki10Kp7p5(Ki=20,Kp=12);Ki50Kp10
; Ki200Kp70=Ki1Kp50;
r_tf=0.0025; r_bm=0.25; rl=0.15;
%radius of tubular fabric, brading
mchine and load shaft
omega=5*2*pi/60; V=0.0018405;
wl0=V/rl;  wl0degree=V*180/(rl*pi);
rpm=wl0*60/(2*pi);
%braiding speed %take up speed, initial
angular speed of load shaft
% theta=atan(r_tf*omega/V);
thetadegree=atan(r_tf*omega/V)*180/pi;
% braiding angle/radian
% H0=r_bm/tan(theta);
% T0= 3.50865;
T_rope=32*T0*H0/sqrt(H0^2+r_bm^2);
%the position of braiding point;
%tension of single braid and rope/N
% cos(theta);
% Parameters of Servo motor
J_m=0.000113;
J_l=0.022362059116777;
%Motor inertia/Kg/m^2 %load shaft
inertia/Kg/m^2
Kt=0.191;   Ke=0.191;  Kb=0.191;
%Torque constant/ Nm/A;
%voltage constant/ V/rad/sec;
%back-emf constant
Rm=1800;  bm=0;      bl=0;
%Resistance of motor circuit/ ohms
%damping of motor
%damping of load shaft
n=15;
%ratio of gear train
J_meq=J_m+n^2*J_l;
b_meq=bm+n^2*bl;  J_leq=J_l+J_m/n^2
;      b_leq=bl+bm/n^2;
me=18.41/1000;   K=215.75;  b=0;
%gram,me2=19.91gram; spring constant
N/m; damping;
```

```
%observer and feedback parameter
A=[-omega*r_tf/r_bm];B=rl;C=1;
plant=ss(A,[],C,[]);
[Yp,Tp,Xp]=initial(plant,50);
[Yn,Tn,Xn]=initial(plant,-50);
plantd=c2d(plant,0.05);Ad=plantd.A;
Bd=plantd.B;Cd=plantd.C;
Dd=plantd.D;[Ypd,Tpd,Xpd]=initial(pla
ntd,50);
% plot(Tpd,Xpd)

for tt=1:56
H0p(tt)=351.5+Xp(tt);
H0n(tt)=351.5+Xn(tt);
thetap(tt)=tan(250/H0p(tt));
thetadegreep(tt)=thetap(tt)*180/pi;
thetan(tt)=tan(250/H0n(tt));
thetadegreen(tt)=thetan(tt)*180/pi;
end

figure(1);
%subplot(2,1,1);
plot(Tp(44:48),Xp(44:48),'r');
subplot(2,1,1);
plot(Tp,thetadegreep);
% plot(Tp,Xp,'r');
% hold on;
plot(positive50mmplantdata2(17401:188
62,1),positive50mmplantdata2(17401:18
862,2));
%plot(positive50mmplantdata2(17201:1
8862,1),positive50mmplantdata2(17201:
18862,2));
% title('plant behavior of braiding
machine(\omega=5rpm,\omega_l=0.008
3,x(0)=50mm)');
xlabel('time(s)');ylabel('x(mm)'); grid
% title('Correlation between simulation
and experiment of plant behavior for
braiding
point(\omega=5rpm,\omega_l=0.0083ra
dian/s,x(0)=50mm)');
xlabel('time(s)');ylabel('x(mm)'); grid
% legend('Simulation','Experiment');
title('Plant behavior for braiding
angle(\omega=5rpm,\omega_l=0.0083ra
dian/s,x(0)=50mm)');xlabel('time(s)');
ylabel('\theta(o)'); grid

 subplot(2,1,2);
 plot(Tn,thetadegreen);
%  plot(Tn(44:48),Xn(44:48),'r')
%   plot(Tn,Xn,'r')
%  hold on;
plot(negative50mmplantdata(17401:188
62,1),negative50mmplantdata(17401:18
862,2));
```

```
%  title('plant behavior of braiding
machine(\omega=20rpm,\omega_l=0.06
67,x(0)=-50mm)');
xlabel('time(s)');ylabel('x(mm)'); grid
% title('Correlation between simulation
and experiment of plant behavior for
braiding
point(\omega=5rpm,\omega_l=0.0083ra
dian/s,x(0)=-50mm)');
xlabel('time(s)');ylabel('x(mm)'); grid
% legend('Simulation','Experiment');
%Braiding angle caculation
title('Plant behavior for braiding
angle(\omega=5rpm,\omega_l=0.0083ra
dian/s,x(0)=-50mm)');
xlabel('time(s)');ylabel('\theta(o)'); grid

% Length=Tp(56)*V
% Tp
%P and PI controller
Ki=0;Kp=60;                % Set PI gains
% caculate the real Ki and Kp in
experiment
%  Kie=Ki; Kpe=Kp*2;
% A2=[-omega*r_tf/r_bm-rl*Kp];
B2=rl;C=1;D=0;    % State space matrix
%[nump,denp]=ss2tf(A2,B2,C,D);
tfplant=tf(nump,denp);
%sys_Kp=ss(A2,[],C,[]);
% State space model
% [Y2,T2,X2]=initial(sys_Kp,-55.6619);
 % Close loop behavior of initial x=-
50mm
% figure(2);plot(T2,X2,'b',T2,Y2,'r');
hold on;
plot(Ki0Kp5(1:200,1),Ki0Kp5(1:200,2))
% title ('Clos loop behavior of braiding
machine(\omega=5rpm,Kp=5,Ki=0,x(0)
=-50mm)');
xlabel('time(s)');ylabel('x(mm)'); grid;
% axis([0 15 -60 15])
% legend('Experimental data using
Continous P controller','Closeloop
behavior with Continous P controller')
Ki=140;Kp=40;          % Set PI gains
% % numt=[rl*Kp rl*Ki];
dent=[1 omega*r_tf/r_bm+rl*Kp rl*Ki];
[At,Bt,Ct,Dt]=tf2ss(numt,dent);
A3n=[0 1;-rl*Ki -omega*r_tf/r_bm-
rl*Kp]; B3n=[0 rl]';C=[1 0];
 % State space model with Ki, Kp
A3n_e=[0 1;-rl*Ki -omega*r_tf/r_bm-
rl*Kp];C=[1 0];D=0;
%need change the sign of x
sys_KpKin=ss(A3n,[],C,[]);
[numb,denb]=ss2tf(A3n,B3n,C,D);sys_
KpKinb=tf(numb,denb);
```

```
sys_KpKi_D=c2d(sys_KpKinb,0.05,'t');
%Model in s domain for bode plot
% figure(3);bode(sys_KpKinb)
% title('bode plot of braiding machine
plant(\omega=5rpm,\omega_l=0.0123)');
grid
% figure(4); bode(sys_KpKinb)
% title('bode plot of close
loop(\omega=5rpm,Kp=10,Ki=40)');
grid
tn=0:0.04:25;x_i=min(Kp60Ki10(:,2))
[Y3n,T3n,X3n]=initial(sys_KpKin,[x_i,
0],tn);
% caculate position of braiding point at
x=-50mm
[n1,I]=max(Y3n);[n2,I2]=max(Y3n(88:1
20));tn2=4.04:0.01002:4.84;
%[Y3n2,T3n2,X3n2]=initial(sys_KpKin
, [-50,0],tn2);
A3p=[-omega*r_tf/r_bm];B3n=rl;C=1;
Sys_Kpequl0_3p=ss(A3p,[],C,[]);
tp=0:0.05:2.;tp2=0:0.00295:0.235;
tp3=0:0.015:4.82;
[Y3p,T3p,X3p]=initial(Sys_Kpequl0_3p
,H0*1000+n1,tp);
% [Y3p2,T3p2,X3p2]=initial
(Sys_Kpequl0_3p, H0*1000+n2,tp2);
% [Y3p3,T3p3,X3p3]=initial
(Sys_Kpequl0_3p,H0*1000+50,tp3);
%Stop take up motor, and let braiding
machine work.
Ln=length(Y3n);Lp=length(Y3p);
X3n1(1:Lp)=Y3p(1:Lp)-H0*1000;
X3n1(Lp+1:Ln-I)=0;
% X3n2=Y3p2;

figure(5)
hold on
plot(T3n,Y3n,'r');grid
axis([0 12 -60 20]);
hold on
plot(T3n(1:I),X3n(1:I),'x')
hold on
plot(Kp60Ki10(:,1),Kp60Ki10(:,2),'.')
hold on
legend('Closeloop behavior with
Continous PI','Closeloop behavior with
Piecewise controller','Experimental data
in close loop')

plot(T3n(I+1:Ln),X3n1,'x')
hold on
% plot(T3n(35)+T3p(90)-
T3n(55)+T3n(55:102),X3n(55:102))
% plot(Ki200Kp70(:,1),
Ki200Kp70(:,2),'.')
title('Clos loop behavior of braiding
machine(\omega=5rpm,Kp=40,
```

```
Ki=140,x(0)=-55.8698mm)');
xlabel('time(s)');ylabel('x(mm)'); grid;
% title('Plant behavior and Clos loop
behavior of braiding
machine(\omega=5rpm,Kp=10,Ki=10,x(
0)=-53.6479mm)');
xlabel('time(s)');ylabel('x(mm)'); grid;
% legend('Plant behavior','Closeloop
behavior with Piecewise controller')

% hold on
% plot(T3n(35)+T3p(90)-T3n(54)-
0.04+T3n2(:),X3n2(:)-H0*1000)
% hold on
% plot(T3n(35)+T3p(90)-
T3n(54)+T3n2(80)-T3n(120)-
0.12+T3n(122:177),X3n(122:177))
% axis([0 8 -53 10])
% figure(6)
% plot(T3n,X3n)
% grid
% figure(7)
% plot(T3p3,X3p3-H0*1000)
% title('Clos loop behavior of braiding
machine(\omega=5rpm,\omega_l_0=0,x(
0)=-50mm)');
xlabel('time(s)');ylabel('x(mm)');
```

A.4.2 The Block Diagram of Control Program

The loop in yellow polygon is machine vision loop. And the loop in green rectangle is motion loop.

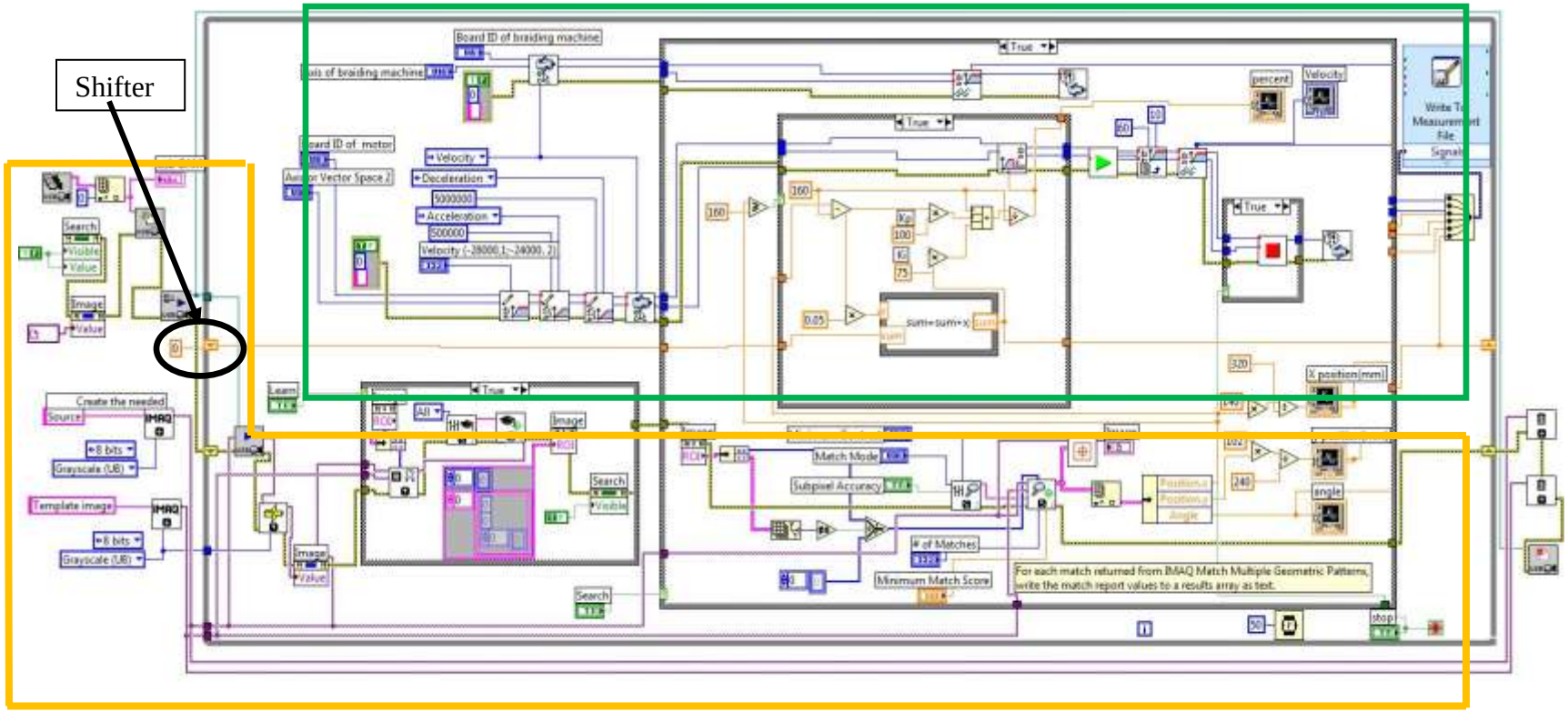

Figure A.4.1 The block diagram of control program

5 Conclusions

This dissertation systematically presented the mathematical model of a single carrier of a braiding machine and the mathematical model of the braiding process close to braiding point area. Also a MFS model of the braiding process was introduced and applied to design a controller to control take up motor speed using feedback position data from a newly-developed machine vision sensing system. These three mathematical models are created here and combined to create an integrated model of the entire braiding process. All the aforementioned mathematical models were validated experimentally.

The MFS is based on 32 carriers maypole braiding machine, and is shown to be a first order differential equation system. The steady state position of the braiding point is analogous to "head" in LLS. The braiding speed coming from braiding motor is the inflow rate and the take up speed coming from take up motor is the outflow rate. During the braiding process, this position is not constant even though the two velocities are constant. The braiding point always oscillates.

A single carrier is modeled as a mass-spring-damping system. The tension changes through six regions when the yarn is pulled and unwound from the carrier. These six regions are four linear kinematic regions including spring 1 preloading, spring 1 tensioning region, spring 2 preloading, and two spring tensioning region. The carrier will see two releasing regions, which include kinematic releasing (with spring pushing pulley 2 down) and a single degree of freedom dynamic region. This dynamic region is actually

pulley 2 impacting on the yarn. The two releasing regions strongly affect the whole braiding process. The releasing includes the releasing of tension and yarn material. These two releases affect the motion of braiding point.

Based on the releasing of yarns, the motion is analyzed and the mathematical model of the braiding process close to the braiding point area is created. Because of the tension and material releasing of yarns, the unbalance of circular tensions on the braiding point drives the braiding point to the low tension side. Since all yarns and rope are tight, the releasing of yarns makes the oscillating motion of the braiding point possible. And the releasing length of yarns mostly determines the oscillated distance of braiding point. In addition, the releasing frequency of yarns mostly defines the frequency of the oscillating braiding point. Combining with the above studies from the model of carriers, the locus of braiding point in steady state is defined as an ellipsoidal cap with base radii 9.5mm, 7.2mm and 4.6mm. Since the braiding point moves really fast, the experimental data measured from machine vision sensing loop are seen as jumps from one point to another point.

In order to reduce the setup time of braiding process, the take up motor needed to be controlled. The position of braiding point will close the motion control loop. The position is sensed by newly created machine vision system, which included image acquiring, template definition, template learning, template matching and position output. After acquiring the position of the braiding point in real time, it is compared and controlled to a desired setpoint, controlled with PI controller.

In the future, how to improve the carrier system and add the controller to braiding machine motor will be focused on.

More teeth in ratchet of spool to reduce the releasing length of material could be investigated. In this case, the base radius of ellipsoid cap would be reduced. Of course, if the tension constant can be kept and not suddenly release of material, it is possible to achieve non-oscillating motion of the braiding point.

And if the other side motion of braiding point is to be controlled, the controller needs to be added to the braiding machine motor. In this case, the braiding point can go back to its steady state quickly no matter what side it is on from the steady state position, in the x direction. The braiding angle would be better controlled. For this second control method, the USB camera can be also attached to its own DC servo motor on a rail, so that the position of the camera (and hence the monitor window) can move with the braiding point. In this case, the mandrel to change the diameter of braided products may not be needed. The position of braiding point can be quickly changed to get the different diameter of braided products. Another improvement worth investigating is to put a take up ring assembled on a DC servo motor right at the steady state position of the braiding point. Simultaneously, the braiding speed and take up speed are both monitored. By feeding backing the two speeds, the braiding point and the braiding angle will be both adaptively controlled.